UNIVERSITY OF

SOUTHERN CALIFORNIA

CIVIL ENGINEERING DEPARTMENT

Los Angeles, CA 90007

(NASA-CR-157106) FINITE ELEMENT ANALYSIS OF LAMINATED PLATES AND SHELLS, VOLUME 1 Annual Progress Report, Mar. 1977 - Mar. 1978 (University of Southern Calif.) 132 p HC A07/MF A01 CSCL 20K G3/39 N78-24577 Unclas 20792

FINITE ELEMENT ANALYSIS

OF LAMINATED PLATES AND SHELLS

PAUL SEIDE

AND

PETER N.-H. CHANG

ANNUAL PROGRESS REPORT

MARCH 1977 - MARCH 1978

Volume 1

NASA Grant No. 1401

UNIVERSITY OF SOUTHERN CALIFORNIA

CIVIL ENGINEERING DEPARTMENT

Los Angeles, CA 90007

(NASA-CR-157106) FINITE ELEMENT ANALYSIS OF LAMINATED PLATES AND SHELLS, VOLUME 1 Annual Progress Report, Mar. 1977 - Mar. 1978 (University of Southern Calif.) 132 p HC A07/MF A01 CSCL 20K G3/39

N78-24577

Unclas 20792

FINITE ELEMENT ANALYSIS

OF LAMINATED PLATES AND SHELLS

PAUL SEIDE

AND

PETER N.-H. CHANG

ANNUAL PROGRESS REPORT

MARCH 1977 - MARCH 1978

Volume 1

NASA Grant No. 1401

University of Southern California
University Park
Los Angeles, California 90007

FINITE ELEMENT ANALYSIS OF LAMINATED PLATES AND SHELLS

Paul Seide

and

Peter N.-H. Chang

Annual Progress Report

March 1977 - March 1978

Volume 1

NASA Grant No. NSG 1401

TABLE OF CONTENTS

LIST OF TABLES

LIST OF FIGURES

Figure

Figure

Figure

NOMENCLATURE

a	Length and width of a square plate
A_{α}^{i}	Coefficients defined by Equation (2.4g)
A_j	Determinant defined by Equation (2.18c), equal to twice the triangular element area
$[B_i]$	Symmetric Matrix defined by Equation (2.12d)
$[C_j]$	Matrix of element vertex coordinates defined by Equation (2.18b)
d_k	Distance from bottom reference surface to bottom of kth layer
$\{d\}_{ij}$	Displacement Vector for the jth element in the ith layer
E	Young's Modulus of Elasticity for isotropic material, psi
E_{ij}	Material modulus psi
$[E]$	Material modulus matrix
$[G]_{ij}$	Matrix defined by Equation (2.19c)
G_{ij}	Material transverse shear modulus
g_{α}, g_{β}	First fundamental quantities of shell reference surface for lines of curvature coordinates
h	Thickness of single layer plate or shell
$I^{(\mu,\lambda)}$	Integrals defined by Equations (2.13)
$[K]_{ij}$	Element Stiffness matrix for jth element of ith layer defined by Equation (2.20b)
L	Width of long layered plate
$M_{\alpha}^{i}, M_{\beta}^{i}$	Layer bending moments per unit length of layer middle surface
$M_{\alpha\beta}^{i}, M_{\alpha\beta}^{i}$	Layer twisting moments per unit length of layer middle surface
$N_{\alpha}^{i}, N_{\beta}^{i}$	Layer normal force moments per unit length of layer middle surface

$N^i_{\alpha\beta}, N^i_{\beta\alpha}$	Layer inplane shear force moments per unit length of layer middle surface
Q^i_α, Q^i_β	Layer transverse shear force moments per unit length of layer middle surface
q	Applied surface load
R	Radius of inner surface of a cylindrical shell
r, Θ, z	Cylindrical coordinates
R_α, R_β	Normal curvatures of the reference surface in the direction of the line of curvature coordinate curves
$[R]$	Matrix defined by Equation (2.19c)
R_{ij}	Components of $[R]$
S_i	Strain energy of each layer per unit reference surface area
$[T_\sigma], [T_\varepsilon]$	Transformation matrices for stress and strain components, respectively
U	Strain energy of the shell
u_α, u_β	Tangential displacements
V	Potential energy of layered shell
w	Normal displacement
W	Work of the conservative, external loadings
s, y, z	Cartesian Coordinates
α, β, ζ	Lines of curvature coordinates
$\varepsilon_\alpha, \varepsilon_\nu, \gamma_{\alpha\beta}$	Strains of line elements originally in α, β direction
$\gamma_{\alpha\zeta}, \gamma_{\beta\zeta}$	Transverse shearing strains
$\sigma_\alpha, \sigma_\beta, \tau_{\alpha\beta}$	Normal and shear stresses parallel to the shell
ν	Poisson's ratio for isotropic material

ABSTRACT

The finite element method is used to investigate the static behavior of laminated composite flat plates and cylindrical shells. The structures are composed of an arbitrary number of layers with arbitrary material properties and fiber direction within each layer. The analysis incorporates the effects of traverse shear deformation in each layer through the assumption that the normals to the undeformed layer midsurface remain straight but need not be normal to the mid-surface after deformation.

The present finite element formulation is based on assumed first order polynomial displacement functions. The nodal displacements are obtained by minimizing the corresponding potential energy to establish approximate equilibrium equations. The solution of these simultaneous equations is then the ultimate goal for the study. A digital computer program which utilizes part of the available SAP V computer program was developed to perform the required computations. The program includes a very efficient equation solution code which permits the analysis of large size problems.

To assess the behavior of the developed finite element, solutions were obtained for some laminated composite plate and cylindrical shell problems for which analytic solutions are available. The accuracy of the stress and displacement results obtained by using the developed finite element is determined for different plate and shell proportions. The rate of convergence and limitations on the use of the developed element are also discussed. The method is finally applied to the problem of stretching and bending of a perforated curved plate.

CHAPTER I

INTRODUCTION

Thin shells have become a popular subject in the field of structural mechanics in the past two decades. Numerous books and papers on their analysis have been published because of their use in such structures as aerospace structures, pressure and underwater vessels, and nuclear reactor structures subjected to both static and transient laods. The advent of advanced fiber-reinforced composite materials which has been called "the biggest technical revolution since the jet engine" (1), has led to increasing use of laminted shells.

In fiber-reinforced composites such as boron-epoxy and graphite-epoxy combinations, the fibers provide the majority of the strength and stiffness. The function of the matrix is to support and protect the fibers as well as to distribute and transmit load between the fibers. The latter function is especially important if a fiber breaks, for then load from one side of the broken fiber is transferred to the matrix and subsequently to the other side of the broken fiber and to the adjacent fibers. The matrix is of such low shearing stiffness compared to the fibers, however, that shearing deformations become important in applications involving loads normal to the structure.

In laminated structures the desirability of accounting for shear deformations in each layer has made it necessary to extend the classical analyses based upon the Kirchhoff-Love hypothesis which neglects the effects of transverse shearing deformation entirely (references 3,4) or upon the Timoshenko-Mindlin modification which deals with an average shearing deformation (references 5-11). The importance of a more rigorous analysis is indicated by the work of references 12-15 which investigates particular elasticity problems of the layered plates by means of exact analytic solutions.

For more general problems it is difficult to obtain an analytic solution, however, exact or approximate. Due to developments in computer science and digital computers, the finite element method offers the possibility of yielding numerical results for problems unsolvable by other methods. Some investigations utilizing the finite element method for laminated plates including shear deformations are already available in the literature. In references 16 and 17 the finite element model includes only average shearing deformation effects. Mau, Tong, and Pian (reference 18) provide for general laminate behavior by allowing each layer to undergo independent rotations of the normal to its undeformed middle surface in a hybrid finite element model. A modified hybrid finite element has been developed by Spilker, Chow, and Orringer (reference 19) who seek to obtain reasonable accuracy with a considerably reduced number of nodal degrees of freedom.

Because the element used is generally a rectangular plate element in these investigations, however, the solution of such problems as laminated plates with perforations for the determination of stress concentration effects around the hole cannot be readily studied. In the present investigation the stiffness matrix for a triangular curved element which has better application to these and other problems is derived and applied to various problems. The study is limited to a cylindrical shell and flat plate element which consists of a right triangle in the lines of curvature coordinate system and with the perpendicular sides oriented in the directions of the lines of curvature coordinate curves. For other shells and element shapes a numerical integration technique (reference 20) is possible.

In the study a displacement finite element model rather than the similar hybrid stress model of previous investigations is used. The motivation for this simplified model was a belief that much the same accuracy as the hybrid stress model could be obtained, with a considerable simplification of the calculations involved. This belief is borne out to some extent by a comparison of displacements and stresses for several problems solved numerically by the two finite element models, in that much the same results can be obtained, at the price, however, of a slower rate of convergence.

The finite element model is based upon a theory of layered plates and shells which retains the Love-Kirchhoff assumption of a normal deformation which is not a function of position in the shell thickness coordinate. The assumption that straight lines normal to the undeformed shell remain normal to the deformed shell is replaced by the assumption that straight lines in each layer normal to the unformed shell remain straight but rotate with respect to the normal to the deformed shell by an amount which varies from layer to layer. A similar assumption has been utilized for beams by Swift and Heller (references 21-24) and by Durocher and Solecki (references 25-26) for two and three layer plates.

The limiting case of an infinite number of infinitesimally thin layers has been shown to yield good agreement with the results of three dimensional isotropic plate theory by Boal and Reissner (reference 27). For a single layer plate the theory reduces to a form similar to that of Libove and Batdorf (reference 28) for sandwich plates.

The derivations that lead to the finite element stiffness formulation are discussed in Chapter II. A computer program based upon the results for circular cylindrical shells and flat plates is discussed in Chapter III and listed in Appendices A and B. Finally the results for several problems investigated with the present analysis are discussed in Chapter IV.

II. THEORETICAL BACKGROUND

2.1 Assumptions

The thin shell theory adopted here is associated with the following set of assumptions:

1. The shell is composed of layers of orthotropic material, the principal material directions of which do not necessarily coincide with the coordinate directions. (Fig. 2-1).

2. There is a linear distribution of tangential displacements through the thickness of each layer. The linear distribution may vary from layer to layer. (Fig. 2-2).

3. The normal displacement is constant through the entire thickness of the shell at each point on the shell reference surface, provided there are no portions of one or more interior layers missing.

The various elements of the theory are as follows.

2.2 Strain-Displacement Relations

The strain-displacement relations used are obtained from three-dimensional elasticity theory. A system of orthogonal curvilinear coordinates for points within the shell wall is defined by the coordinates α and β corresponding to the lines of curvature on the bottom surface and distance ζ along the normal to the surface. (Fig. 2-3). Then, from reference 29, the following equations can be established:

$$\varepsilon_\alpha(\zeta) = \frac{1}{(1+\frac{\zeta}{R_\beta})g_\alpha}\left[\frac{\partial u_\alpha(\zeta)}{\partial\alpha} + \frac{1}{g_\beta}\frac{\partial g_\alpha}{\partial\beta}u_\beta(\zeta) + \frac{g_\alpha}{R_\alpha}w(\zeta)\right] \tag{2.1a}$$

$$\varepsilon_\beta(\zeta) = \frac{1}{(1+\frac{\zeta}{R_\beta})g_\beta}\left[\frac{\partial u_\beta(\zeta)}{\partial\beta} + \frac{1}{g_\alpha}\frac{\partial g_\beta}{\partial\alpha}u_\alpha(\zeta) + \frac{g_\beta}{R_\beta}\bar{w}(\zeta)\right] \tag{2.1b}$$

$$\varepsilon_\zeta(\zeta) = \frac{\partial w(\zeta)}{\partial\zeta} \tag{2.1c}$$

$$\begin{aligned}\gamma_{\alpha\beta}(\zeta) &= \frac{1}{(1+\frac{\zeta}{R_\alpha})g_\alpha}\left[\frac{\partial u_\beta(\zeta)}{\partial\alpha} - \frac{1}{g_\beta}\frac{\partial g_\alpha}{\partial\beta}u_\alpha(\zeta)\right] \\ &+ \frac{1}{(1+\frac{\zeta}{R_\beta})g_\beta}\left[\frac{\partial u_\alpha(\zeta)}{\partial\beta} - \frac{1}{g_\alpha}\frac{\partial g_\beta}{\partial\alpha}u_\beta(\zeta)\right]\end{aligned} \tag{2.1d}$$

$$\gamma_{\alpha\zeta}(\zeta) = \frac{1}{(1+\frac{\zeta}{R_\alpha})g_\alpha}\left[\frac{\partial w(\zeta)}{\partial\alpha} - \frac{g_\alpha}{R_\alpha}u_\alpha(\zeta)\right] + \frac{\partial u_\alpha(\zeta)}{\partial\zeta} \tag{2.1e}$$

$$\gamma_{\beta\zeta}(\zeta) = \frac{1}{(1+\frac{\zeta}{R_\beta})g_\beta}\left[\frac{\partial w(\zeta)}{\partial\beta} - \frac{g_\beta}{R_\beta}u_\beta(\zeta)\right] + \frac{\partial u_\beta(\zeta)}{\partial\zeta} \tag{2.1f}$$

where u_α and u_β are tangential displacements, w is the normal displacement, g_α and g_β are first fundamental quantities for the lines of curvature coordinate curves on the reference surface and R_α and R_β are normal curvatures of the reference surface in the directions of the coordinate curves.

The basic assumptions in this study are those of linear tangential displacement and constant normal displacement distributions through the layer thickness. For the ith layer, then,

$$u_\alpha^i(\zeta) = u_\alpha^i(1-\frac{\zeta}{h_i}) + u_\alpha^{i+1}\frac{\zeta}{h_i} \tag{2.2a}$$

$$u_\beta^i(\zeta) = u_\beta^i(1-\frac{\zeta}{h_i}) + u_\beta^{i+1}\frac{\zeta}{h_i} \tag{2.2b}$$

$$w^i(\zeta) = w \tag{2.2c}$$

where u_α^k and u_β^k are tangential displacements of the kth interface and are functions of α and β only. The coordinate ζ is now measured in each layer from the bottom of the layer so that $0 < \zeta < h_i$. Eqs. (2.1) then become

$$\varepsilon_\alpha^i(\zeta) = \left[\varepsilon_\alpha^i \left(1-\frac{\zeta}{h_i}\right) + \varepsilon_\alpha^{i+1}\frac{\zeta}{h_i}\right]\frac{1}{A_\alpha^i(\zeta)} \quad \text{2.3a)}$$

$$\varepsilon_\beta^i(\zeta) = \left[\varepsilon_\beta^i \left(1-\frac{\zeta}{h_i}\right) + \varepsilon_\beta^{i+1}\frac{\zeta}{h_i}\right]\frac{1}{A_\beta^i(\zeta)} \tag{2.3b}$$

$$\gamma_{\alpha\beta}^i(\zeta) = \left[\frac{\gamma_\alpha^i}{A_\alpha^i(\zeta)} + \frac{\gamma_\beta^i}{A_\beta^i(\zeta)}\right]\left(1-\frac{\zeta}{h_i}\right) + \left[\frac{\gamma_\alpha^{i+1}}{A_\alpha^i(\zeta)} + \frac{\gamma_\beta^{i+1}}{A_\beta^i(\zeta)}\right]\frac{\zeta}{h_i} \tag{2.3c}$$

$$\varepsilon_\zeta^i(\zeta) = 0 \tag{2.3d}$$

$$\gamma_{\alpha\zeta}^i(\zeta) = \frac{\gamma_{\alpha\zeta}^i}{A_\alpha^i(\zeta)} \tag{2.3e}$$

$$\gamma_{\beta\zeta}^i(\zeta) = \frac{\gamma_{\beta\zeta}^i}{A_\beta^i(\zeta)} \tag{2.3f}$$

where

$$\varepsilon_\alpha^k = \frac{1}{g_\alpha}\left(\frac{\partial u_\alpha^k}{\partial \alpha} + \frac{u_\beta^k}{g_\beta}\frac{\partial g_\alpha}{\partial \beta} + \frac{g_\alpha}{R_\alpha} w\right) \tag{2.4a}$$

$$\varepsilon_\beta^k = \frac{1}{g_\beta}\left(\frac{\partial u_\beta^k}{\partial \beta} + \frac{u_\alpha^k}{g_\alpha}\frac{\partial g_\beta}{\partial \alpha} + \frac{g_\beta}{R_\beta} w\right) \tag{2.4b}$$

$$\gamma_\alpha^k = \frac{1}{g_\alpha}\left(\frac{\partial u_\beta^k}{\partial \alpha} - \frac{u_\alpha^k}{g_\beta}\frac{\partial g_\alpha}{\partial \beta}\right) \tag{2.4c}$$

$$\gamma_\beta^k = \frac{1}{g_\beta}\left(\frac{\partial u_\alpha^k}{\partial \beta} - \frac{u_\beta^k}{g_\alpha}\frac{\partial g_\beta}{\partial \alpha}\right) \tag{2.4d}$$

$$\gamma_{\alpha\zeta}^i = \frac{1}{g_\alpha}\ \frac{\partial w}{\partial \beta} + \frac{1}{h_i}\left[u_\alpha^{i+1}\left(1 + \frac{d_i}{R_\alpha}\right) - u_\alpha^i\left(1 + \frac{d_{i+1}}{R_\alpha}\right)\right] \tag{2.4e}$$

$$\gamma_{\beta\zeta}^i = \frac{1}{g_\beta}\frac{\partial w}{\partial \beta} + \frac{1}{h_i}\left[u_\beta^{i+1}\left(1 + \frac{d_i}{R_\beta}\right) - u_\beta^i\left(1 + \frac{d_{i+1}}{R_\beta}\right)\right] \tag{2.4f}$$

$$A_\alpha^i(\zeta) = 1 + \frac{d_i + \zeta}{R_\alpha} \tag{2.4g}$$

$$A_\beta^i(\zeta) = 1 + \frac{d_i + \zeta}{R_\beta} \quad . \tag{2.4h}$$

$$d_k = \sum_{j=1}^{k-1} h_j \quad , \; d_1 = 0 \tag{2.4i}$$

2.3 Material Properties

The material of each layer is assumed to be anisotropic in surfaces parallel to the reference surface of the shell. In accordance with the usual assumptions of plate and shell theory, layer strains are assumed independent of transverse stresses.

The stress-strain relations are then taken as

$$\{\sigma\} = [E]\{\varepsilon\} \tag{2.5a}$$

where $\{\sigma\}$ and $\{\varepsilon\}$ are respectively the stress and strain matrices

$$\{\sigma\} = \begin{Bmatrix} \sigma_\alpha \\ \sigma_\beta \\ \tau_{\alpha\beta} \\ \tau_{\alpha\zeta} \\ \tau_{\beta\zeta} \end{Bmatrix} \qquad (2.5b), \qquad \{\varepsilon\} = \begin{Bmatrix} \varepsilon_\alpha \\ \varepsilon_\beta \\ \gamma_{\alpha\beta} \\ \gamma_{\alpha\zeta} \\ \gamma_{\beta\zeta} \end{Bmatrix} \qquad (2.5c)$$

and E is the symmetric material constant matrix

$$[E] = \begin{bmatrix} E_{11} & E_{12} & E_{13} & 0 & 0 \\ E_{21} & E_{22} & E_{23} & 0 & 0 \\ E_{31} & E_{32} & E_{33} & 0 & 0 \\ 0 & 0 & 0 & G_{44} & G_{45} \\ 0 & 0 & 0 & G_{54} & G_{55} \end{bmatrix} \qquad (2.5d)$$

The material constants E_{11}, E_{12}... to G_{55} are generalized Young's moduli, Poisson's ratios, and shear moduli as discussed in detail in Ref. (2). For an orthotropic material with the principal material directions coinciding with the coordinate axes, Equations (2.5a) may be written as

$$\{\sigma\} = [E']\{\varepsilon\} \qquad (2.6a)$$

where

$$[E'] = \begin{bmatrix} E'_{11} & E'_{12} & 0 & 0 & 0 \\ E'_{21} & E'_{22} & 0 & 0 & 0 \\ 0 & 0 & G'_{33} & 0 & 0 \\ 0 & 0 & 0 & G'_{44} & 0 \\ 0 & 0 & 0 & 0 & G'_{55} \end{bmatrix} \qquad (2.6b)$$

The principal material directions for an orthotropic material often do not coincide with the coordinate directions, however, especially in a laminated composite structure where the orientation of material can be varied from layer to layer. Therefore it is convenient to effect a transformation of the stress-strain relations from local material axes to the overall coordinate axes. Let the angle between the global and local orthogonal layer material axes be denoted as θ (Fig. 2-4). Then

$$\{\sigma'\} = [T_\sigma]\{\sigma\} \tag{2.7a}$$

$$\{\varepsilon'\} = [T_\varepsilon]\{\varepsilon\} \tag{2.7b}$$

where

$$[T_\sigma] = \begin{bmatrix} \cos^2\theta & \sin^2\theta & \sin 2\theta & 0 & 0 \\ \sin^2\theta & \cos^2\theta & -\sin 2\theta & 0 & 0 \\ -\frac{1}{2}\sin 2\theta & \frac{1}{2}\sin 2\theta & \cos 2\theta & 0 & 0 \\ 0 & 0 & 0 & \cos\theta & \sin\theta \\ 0 & 0 & 0 & -\sin\theta & \cos\theta \end{bmatrix} \tag{2.7c}$$

$$[T_\varepsilon] = \begin{bmatrix} \cos^2\theta & \sin^2\theta & \frac{1}{2}\sin 2\theta & 0 & 0 \\ \sin^2\theta & \cos^2\theta & -\frac{1}{2}\sin 2\theta & 0 & 0 \\ -\sin 2\theta & \sin 2\theta & \cos 2\theta & 0 & 0 \\ 0 & 0 & 0 & \cos\theta & \sin\theta \\ 0 & 0 & 0 & -\sin\theta & \cos\theta \end{bmatrix} \tag{2.7d}$$

These transformations are derived in most texts on strength of materials and theory of elastiicty, for example Ref. .

Then

$$\{\sigma\} = [T_\sigma]^{-1}\{\sigma'\} = [T_\sigma]^{-1}[E']\{\varepsilon'\}$$

$$= [T_\varepsilon]^T[E'][T_\varepsilon]\{\varepsilon\} \tag{2.8}$$

and a comparison of Eqs. (2.5a) and (2.8) yields

$$[E] = [T_\varepsilon]^T [E'] [T_\varepsilon] \tag{2.9}$$

The individual elements of the transformed modulus matrix are as follows:

$$E_{11} = E'_{11} \cos^4\theta + 2(E'_{12} + 2G'_{33}) \sin^2\theta \cos^2\theta + E'_{22} \sin^4\theta \tag{2.10a}$$

$$E_{22} = E'_{11} \sin^4\theta + 2(E'_{12} + 2G'_{33}) \sin^2\theta \cos^2\theta + E'_{22} \cos^4\theta \tag{2.10b}$$

$$E_{33} = G'_{33} + \frac{1}{2}(E'_{11} + E'_{22} - 2E'_{12} - 4G'_{33}) \sin^2 2\theta \tag{2.10c}$$

$$E_{12} = E_{21} = E'_{12} + \frac{1}{4}(E'_{11} + E'_{22} - 4E'_{12} - 2G'_{33}) \sin^2 2\theta \tag{2.10d}$$

$$E_{13} = E_{31} = \frac{1}{4}(E'_{11} - E'_{22}) \sin 2\theta + \frac{1}{8}(E'_{11} + E'_{22} - 2E'_{12} - 4G'_{33}) \sin 4\theta \tag{2.10e}$$

$$E_{23} = E_{32} = \frac{1}{4}(E'_{11} - E'_{22}) \sin 2\theta - \frac{1}{8}(E'_{11} + E'_{22} - 2E'_{12} - 4G'_{33}) \sin 4\theta \tag{2.10f}$$

$$G_{44} = G'_{44} \cos^2\theta + G'_{55} \sin^2\theta \tag{2.10g}$$

$$G_{55} = G'_{44} \sin^2\theta + G'_{55} \cos^2\theta \tag{2.10h}$$

$$G_{45} = G_{54} = \frac{1}{2}(G'_{44} - G'_{55}) \sin 2\theta \tag{2.10i}$$

2.4 Principle of Minimum Potential Energy

The theorem of virtual work states that if an elastic body is in equilibrium under the action of prescribed body and surface forces, the work done by these forces in a small additional displacement is equal to the change in internal strain energy. From the theory of elasticity the internal strain energy for a layered shell is given by

$$U = \frac{1}{2}\int_{\beta}\int_{\alpha}\sum_{i=1}^{N}\int_{\zeta=0}^{\zeta=h_i}\{\sigma_i(\zeta)\}^T\{\varepsilon_i(\zeta)\}g_\alpha(\zeta)g_\beta(\zeta)\ d\zeta d\alpha d\beta \qquad (2.11a)$$

With the stress-strain relations given by Eqs. (2.5) the strain energy may be written as

$$U = \frac{1}{2}\int_{S}\sum_{i=1}^{N}\int_{\zeta=0}^{\zeta=h_i}\{\varepsilon_i(\zeta)\}^T[E_i]\{\varepsilon_i(\zeta)\}\ A_\alpha^i(\zeta)A_\beta^i(\zeta)d\zeta dS \qquad (2.11b)$$

where the surface integral is over the area of the reference surface and

$$dS = g_\alpha g_\beta d\alpha d\beta \qquad (2.11c)$$

The components of the strain matrix for each layer are given by Eqs. (2.3) and $[E_i]$ is the material modulus matrix for each layer of the form of Eq. (2.5d). Multiplication of the matrices in the integral then yields the following expression for the strain energy

$$U = \int_S \sum_{i=1}^{N} S_i dS \qquad (2.12a)$$

where S_i, the strain energy of each layer per unit reference surface area is given by

$$S_i = \frac{1}{2}\{\bar{\varepsilon}_i\}^T[B_i]\{\bar{\varepsilon}_i\} \qquad (2.12b)$$

$$\{\bar{\varepsilon}_i\} = \left\{ \begin{array}{c} \varepsilon_\alpha^i \\ \varepsilon_\beta^i \\ \gamma_\alpha^i \\ \gamma_\beta^i \\ \varepsilon_\alpha^{i+1} \\ \varepsilon_\beta^{i+1} \\ \gamma_\alpha^{i+1} \\ \gamma_\beta^{i+1} \\ \gamma_{\alpha\zeta}^i \\ \gamma_{\beta\zeta}^i \end{array} \right\} \tag{2.12c}$$

and $[B_i]$ is a symmetric matrix given by

$$
[B_i]=\begin{bmatrix}
I_{2i}(\beta,\alpha)E_{11} & \frac{h_i}{3}E^i_{12} & I_{2i}(\beta,\alpha)E_{13} & \frac{h_i}{3}E^i_{13} & I_{3i}(\beta,\alpha)E^i_{11} & \frac{h_i}{6}E^i_{12} & I_{3i}(\beta,\alpha)E^i_{13} & \frac{h_i}{3}E^i_{13} & 0 & 0 \\
 & I_{2i}(\alpha,\beta)E_{22} & \frac{h_i}{3}E^i_{23} & I_{2i}(\alpha,\beta)E^i_{23} & \frac{h_i}{6}E^i_{12} & I_{3i}(\alpha,\beta)E^i_{23} & \frac{h_i}{6}E^i_{23} & I_{3i}(\alpha,\beta)E^i_{23} & 0 & 0 \\
 & & I_{2i}(\beta,\alpha)E_{33} & \frac{h_i}{3}E^i_{33} & I_{3i}(\beta,\alpha)E^i_{13} & \frac{h_i}{6}E^i_{23} & I_{3i}(\beta,\alpha)E^i_{33} & \frac{h_i}{6}E^i_{33} & 0 & 0 \\
 & & & I_{2i}(\alpha,\beta)E_{33} & \frac{h_i}{6}E^i_{13} & I_{3i}(\alpha,\beta)E^i_{23} & \frac{h_i}{6}E^i_{33} & I_{3i}(\alpha,\beta)E^i_{33} & 0 & 0 \\
 & & & & I_{4i}(\beta,\alpha)E_{11} & \frac{h_i}{3}E^i_{12} & I_{4i}(\beta,\alpha)E^i_{13} & \frac{h_i}{3}E^i_{13} & 0 & 0 \\
 & & & & & I_{4i}(\alpha,\beta)E_{22} & \frac{h_i}{3}E^i_{23} & I_{4i}(\alpha,\beta)E^i_{23} & 0 & 0 \\
 & & & & & & I_{4i}(\beta,\alpha)E_{33} & \frac{h_i}{3}E^i_{33} & 0 & 0 \\
 & \text{SYM} & & & & & & I_{4i}(\alpha,\beta)E_{33} & 0 & 0 \\
 & & & & & & & & I_{1i}(\beta,\alpha)G_{44} & h_iG^i_{45} \\
 & & & & & & & & & I_{1i}(\alpha,\beta)G^i_{55}
\end{bmatrix}
\qquad (2.12d)
$$

where

$$I_{1i}^{(\mu,\lambda)} = \int_0^{h_i} \frac{A_\mu^i}{A_\lambda^i}\, d\zeta = R_\lambda \left[\frac{h_i}{R_\mu} + \left(1 - \frac{R_\lambda}{R_\mu}\right) \ln \frac{1+d_{i+1}/R_\lambda}{1+d_i/R_\lambda}\right] \tag{2.13a}$$

$$I_{2i}^{(\mu,\lambda)} = \int_0^{h_i} \left(1 - \frac{\zeta}{h_i}\right)^2 \frac{A_\mu^i}{A_\lambda^i}\, d\zeta = R_\lambda \left(\frac{1}{3}\frac{h_i}{R_\mu} - \left(1 - \frac{R_\lambda}{R_\mu}\right)\left\{\left[1 + \frac{R_\lambda}{h_i} \quad 1 + \frac{d_i}{R_\lambda}\right]\right.\right.$$

$$\left.\left. \ln \frac{1+d_{i+1}/R_\lambda}{1+d_i/R_\lambda} + \frac{3}{2} \quad + \frac{R_\lambda}{h_i}\left(1 + \frac{d_i}{R_\lambda}\right)\right\}\right) \tag{2.13b}$$

$$I_{3i}^{(\mu,\lambda)} = \int_o^{h_i} \frac{\zeta}{h_i}\left(1 - \frac{\zeta}{h_i}\right) \frac{A_\mu^i}{A_\lambda^i}\, d\zeta = R_\lambda \left[\frac{1}{6}\frac{h_i}{R_\mu} + \left(1 - \frac{R_\lambda}{R_\mu}\right)\left(\frac{1}{2}\right.\right.$$

$$\left.\left. + \frac{R_\lambda}{h_i}\left(1 + \frac{d_i}{R_\lambda}\right)\left\{1 - \left[1 + \frac{R_\lambda}{h_i}\left(1 + \frac{d_i}{R_\lambda}\right)\right] \ln \frac{1+d_{i+1}/R_\lambda}{1+d_i/R_\lambda}\right\}\right)\right] \tag{2.13c}$$

$$I_{4i}^{(\mu,\lambda)} = \int_0^{h_i} \left(\frac{\zeta}{h_i}\right)^2 \frac{A_\mu^i}{A_\lambda^i}\, d\zeta = R_\zeta \left(\frac{1}{3}\frac{h_i}{R_\mu} + \left(1 - \frac{R_\lambda}{R_\mu}\right)\left\{\frac{1}{2}\right.\right.$$

$$\left.\left. - \frac{R_\lambda}{h_i}\left(1 + \frac{d_i}{R_\lambda}\right)\left[1 - \frac{R_\lambda}{h_i}\left(1 + \frac{d_i}{R_\lambda}\right) \ln \frac{1+d_{i+1}/R_\lambda}{1+d_i/R_\lambda}\right]\right\}\right) \tag{2.13d}$$

If the applied forces (Fig. 2-5) are conservative the work done by these forces is given by

$$W = \int_S \left[\left(\bar{\tau}_{\alpha\zeta}^{N+1} u_\alpha^{N+1} + \bar{\tau}_{\beta\zeta}^{N+1} u_\beta^{N+1} + \bar{\sigma}_\zeta^{N+1} w\right)\left(1 + \frac{d_{N+1}}{R_\alpha}\right)\left(1 + \frac{d_{N+1}}{R_\beta}\right)\right.$$

$$\left. - \left(\bar{\tau}_{\alpha\zeta}^{1} u_\alpha^{1} + \bar{\tau}_{\beta\zeta}^{1} u_\beta^{1} + \bar{\sigma}_\zeta^{1} w\right)\right] dS$$

$$+ \int_C \sum_{i=1}^{N} \int_{\zeta=0}^{\zeta=h_i} \left[\bar{\tau}_{ns}(\zeta)u_s(\zeta) + \bar{\sigma}_n(\zeta)u_n(\zeta) + \bar{\tau}_{n\zeta}(\zeta)w\right]$$

$$\left[\left(1+ \frac{d_i \quad +\zeta}{R_s}\right)^2 + \left(\frac{d_i \quad +\zeta}{R_{ns}}\right)^2\right] dsd\zeta \tag{2.14}$$

where $1/R_s$ is the normal curvature of the reference in the direction of the boundary curve and $1/R_{ns}$ is the twist of the surface referred to surface coordinates normal and tangential to the boundary curve, while $\bar{\tau}_{ns}$, $\bar{\sigma}_n$, $\bar{\tau}_{n\zeta}$ are the applied stresses parallel, normal, and tranverse to the boundary curve, respectively.

The principle of virtual work can now be stated as follows as the principle of minimum potential energy:

Of all displacements satisfying the given boundary condition on displacement, those which satisfy the equilibrium equations make the potential energy Π_p = U-W stationary. An expression such as Π_p is called a functional to imply that Π_p is not simply a function of displacements and displacement derivatives but depends on their integrated effect.

2.5 The Finite Element Method

The principle of minimum potential energy is the basis for some procedures for obtaining approximate solutions for problems which cannot be solved analytically. The older classical procedure known as the Rayleigh-Ritz method (ref. 31) expresses the solution in terms of series of known trial functions which each satisfy geometric boundary conditions which are continuous and have continuous derivatives over the entire region of interest. The coefficients which multiply these functions in the series are determined by the condition that the potential energy be a minimum, yielding the conditions that the derivatives of the functional Π_p with respect to each of the coefficients must vanish.

The finite-element method is a variation of this procedure which seeks to define the solution in terms of different trial functions, usually polynomial expressions, for different discrete regions of the structure. Only the trial functions and, in some cases, certain of their derivatives are continuous at the common boundary of adjacent regions. Such a series of functions is said to be a piecewise continuous fit to the solution. The solution within each discrete region is expressed in terms of displacements and, if necessary, derivatives at discrete points or nodes, usually on the boundary. Thus while the form of the polynomial expression is the same for each region, the coefficients vary from region to region. The potential energy of the entire structure is then obtained in terms of these nodal quantities which take the place of the function coefficients in the classical Rayleigh-Ritz procedure. Extremalization of the potential energy then yields equations for determination of the nodal quantities (for example refs. 32 and 33).

The advantage of the finite element method over the classical Rayleigh-Ritz method is that the same discrete region functions are valid for any boundary conditions on the structure. Thus the algebraic manipulations yielding the form of the potential energy expression need be carried out only once, after which an algorithm to yield the results for regions having the same general shape but different parameters may be written for automated digital computer applications.

2.6 Finite Element Formulation

The finite element model usually chosen to represent a plate or shell structure is a series of triangles or rectangles since the analysis of the structure is reduced to that of a two-dimensional continuum. For the present problem the inclusion of shearing effects in each layer requires the analysis of a number of interacting two-dimensional continua, one for each layer interface. Thus an element consists not of a single rectangle or triangle but a number of these, one above the other, for corresponding regions on the layer interfaces. While a rectangular element shape is adequate for a structure with regular boundaries, the shape of the element is chosen to be a triangle in the α,β plane to be better adaptable for the analysis of regions with irregular boundaries, as shown in Fig. 2-1.

If the vertices of the triangle element are numbered as shown in Fig. 2-7a and the shape of the triangle is such that $\alpha_3^j>\alpha_2^j>\alpha_1^j$ and $\beta_3^j>\beta_2^j$ the corresponding strain energy U_{ij} of the j^{th} triangular element of the i^{th} layer is given by

$$U_{ij} = \int_{\alpha_1^j}^{\alpha_2^j}\int_{\beta_1^j+\frac{\beta_2^j-\beta_1^j}{\alpha_2^j-\alpha_1^j}(\alpha^j-\alpha_1^j)}^{\beta_1^j+\frac{\beta_3^j-\beta_2^j}{\alpha_3-\alpha_1}(\alpha-\alpha_1)} S_i\,dS + \int_{\alpha_2^j}^{\alpha_3^j}\int_{\beta_2^j+\frac{\beta_3^j-\beta_2^j}{\alpha_3^j-\alpha_2^j}(\alpha-\alpha_2^j)}^{\beta_1^j+\frac{\beta_3^j-\beta_1^j}{\alpha_3^j-\alpha_1^j}(\alpha-\alpha_1^j)} S_i\,dS \qquad (2.15)$$

If, however, the vertices of the triangle are numbered so that $\alpha_3^j>\alpha_2^j>\alpha_1^j$ but $\beta_3^j<\beta_2^j$ (Fig. 2-7b), the limits of integration on β are reversed.

In evaluating the strain energy of a typical triangular layer element the displacements in the j^{th} element of interface i are assumed to vary linearly within each element as

$$\begin{aligned} u_\alpha^{ij} &= a_1^{ij}\alpha + b_1^{ij}\beta + c_1^{ij} \\ u_\beta^{ij} &= a_2^{ij}\alpha + b_2^{ij}\beta + c_2^{ij} \\ w^{ij} &= a_3^{ij}\alpha + b_3^{ij}\beta + c_3^{ij} \end{aligned} \tag{2.16}$$

The coefficients may be obtained in terms of the corner displacement by means of the equations

$$\begin{bmatrix} \alpha_1^j & \beta_1^j & 1 \\ \alpha_2^j & \beta_2^j & 1 \\ \alpha_3^j & \beta_3^j & 1 \end{bmatrix} \begin{bmatrix} a_1^{ij} & a_2^{ij} & a_3^{ij} \\ b_1^{ij} & b_2^{ij} & b_3^{ij} \\ c_1^{ij} & c_2^{ij} & c_3^{ij} \end{bmatrix} = \begin{bmatrix} u_{\alpha1}^{ij} & u_{\beta1}^{ij} & w_1^{ij} \\ u_{\alpha2}^{ij} & u_{\beta2}^{ij} & w_2^{ij} \\ u_{\alpha3}^{ij} & u_{\beta3}^{ij} & w_3^{ij} \end{bmatrix} \tag{2.17}$$

yielding

$$\begin{Bmatrix} u_\alpha^{ij} \\ u_\beta^{ij} \\ w^{ij} \end{Bmatrix} = \begin{vmatrix} u_{\alpha1}^{ij} & u_{\alpha2}^{ij} & u_{\alpha3}^{ij} \\ u_{\beta1}^{ij} & u_{\beta2}^{ij} & u_{\beta3}^{ij} \\ w_1^{ij} & w_2^{ij} & w_3^{ij} \end{vmatrix} [C_j] \begin{Bmatrix} \alpha \\ \beta \\ 1 \end{Bmatrix} \tag{2.18a}$$

where

$$[C_j] = \frac{1}{A_j} \begin{bmatrix} \beta_2^j-\beta_3^j & \alpha_3^j-\alpha_2^j & \alpha_2^j\beta_3^j-\alpha_3^j\beta_2^j \\ \beta_3^j-\beta_1^j & \alpha_1^j-\alpha_3^j & \alpha_3^j\beta_1^j-\alpha_2^j\beta_1^j \\ \beta_1^j-\beta_2^j & \alpha_2^j-\alpha_1^j & \alpha_1^j\beta_2^j-\alpha_2^j\beta_1^j \end{bmatrix} \tag{2.18b}$$

$$A_j = \det \begin{vmatrix} \alpha_1^j & \beta_1^j & 1 \\ \alpha_2^j & \beta_2^j & 1 \\ \alpha_3^j & \beta_3^j & 1 \end{vmatrix} \tag{2.18c}$$

In addition the numbering system shown in Fig. 2-3 is introduced. Then a relationship between the element strain matrix $\{\bar{\varepsilon}\}_{ij}$ and the displacement matrix

$$\{d\}_{ij} = \begin{Bmatrix} u_1^{ij} \\ u_2 \\ \cdot \\ \cdot \\ \cdot \\ \cdot \\ \cdot \\ \cdot \\ \cdot \\ \cdot \\ \cdot \\ \cdot \\ \cdot \\ \cdot \\ \cdot \\ \cdot \\ \cdot \\ u_{18}^{ij} \end{Bmatrix} \tag{2.19a}$$

can be obtained as

$$\{\bar{\varepsilon}\}_{ij} = [G]_{ij}\{d\}_{ij} \tag{2.19b}$$

where

$$
[G]_{ij} = \begin{bmatrix}
\frac{1}{g_\alpha}R_{21} & \frac{1}{g_\alpha g_\beta}\frac{\partial g_\alpha}{\partial \beta}R_{11} & \frac{1}{g_\alpha}R_{22} & \frac{1}{g_\alpha g_\beta}\frac{\partial g_\alpha}{\partial \beta}R_{12} & \frac{1}{g_\alpha}R_{23} & \frac{1}{g_\alpha g_\beta}\frac{\partial g_\alpha}{\partial \beta}R_{13} & 0 & 0 \\
\frac{1}{g_\alpha g_\beta}\frac{\partial g_\beta}{\partial \alpha}R_{11} & \frac{1}{g_\beta}R_{31} & \frac{1}{g_\alpha g_\beta}\frac{\partial g_\beta}{\partial \alpha}R_{12} & \frac{1}{g_\beta}R_{32} & \frac{1}{g_\alpha g_\beta}\frac{\partial g_\beta}{\partial \alpha}R_{13} & \frac{1}{g_\beta}R_{33} & 0 & 0 \\
-\frac{1}{g_\alpha g_\beta}\frac{\partial g_\beta}{\partial \beta}R_{11} & \frac{1}{g_\alpha}R_{21} & -\frac{1}{g_\alpha g_\beta}\frac{\partial g_\beta}{\partial \beta}R_{12} & \frac{1}{g_\alpha}R_{22} & -\frac{1}{g_\alpha g_\beta}\frac{\partial g_\beta}{\partial \beta}R_{13} & \frac{1}{g_\alpha}R_{23} & 0 & 0 \\
\frac{1}{g_\beta}R_{31} & -\frac{1}{g_\alpha g_\beta}\frac{\partial g_\beta}{\partial \alpha}R_{11} & \frac{1}{g_\beta}R_{32} & -\frac{1}{g_\alpha g_\beta}\frac{\partial g_\beta}{\partial \alpha}R_{12} & \frac{1}{g_\beta}R_{33} & -\frac{1}{g_\alpha g_\beta}\frac{\partial g_\beta}{\partial \alpha}R_{13} & 0 & 0 \\
0 & 0 & 0 & 0 & 0 & 0 & \frac{1}{g_\alpha}R_{21} & \frac{1}{g_\alpha g_\beta}\frac{\partial g_\alpha}{\partial \beta}R_{11} \\
0 & 0 & 0 & 0 & 0 & 0 & \frac{1}{g_\alpha g_\beta}\frac{\partial g_\beta}{\partial \alpha}R_{11} & \frac{1}{g_\beta}R_{31} \\
0 & 0 & 0 & 0 & 0 & 0 & -\frac{1}{g_\alpha g_\beta}\frac{\partial g_\alpha}{\partial \beta}R_{11} & \frac{1}{g_\alpha}R_{21} \\
0 & 0 & 0 & 0 & 0 & 0 & \frac{1}{g_\beta}R_{31} & -\frac{1}{g_\alpha g_\beta}\frac{\partial g_\beta}{\partial \alpha}R_{11} \\
-\frac{1}{h_i}(1+\frac{d_{i+1}}{R_\alpha})R_{11} & 0 & -\frac{1}{h_i}(1+\frac{d_{i+1}}{R_\alpha})R_{12} & 0 & -\frac{1}{h_i}(1+\frac{d_{i+1}}{R_\alpha})R_{13} & 0 & \frac{1}{h_i}(1+\frac{d_i}{R_\alpha})R_{11} & 0 \\
-\frac{1}{h_i}(1+\frac{d_{i+1}}{R_\beta})R_{11} & 0 & -\frac{1}{h_i}(1+\frac{d_{i+1}}{R_\beta})R_{12} & 0 & -\frac{1}{h_i}(1+\frac{d_{i+1}}{R_\beta})R_{13} & 0 & \frac{1}{h_i}(1+\frac{d_i}{R_\beta})R_{11} & 0
\end{bmatrix}
$$

$$
\left.
\begin{array}{cccccccccc}
0 & 0 & 0 & 0 & \frac{1}{R_\alpha}R_{11} & \frac{1}{R_\alpha}R_{12} & \frac{1}{R_\alpha}R_{13} & 0 & 0 & 0 \\
0 & 0 & 0 & 0 & \frac{1}{R_\beta}R_{11} & \frac{1}{R_\beta}R_{12} & \frac{1}{R_\beta}R_{13} & 0 & 0 & 0 \\
0 & 0 & 0 & 0 & 0 & 0 & 0 & 0 & 0 & 0 \\
0 & 0 & 0 & 0 & 0 & 0 & 0 & 0 & 0 & 0 \\
\frac{1}{g_\alpha}R_{22} & \frac{1}{g_\alpha g_\beta}\frac{\partial g_\alpha}{\partial \beta}R_{12} & \frac{1}{g_\alpha}R_{23} & \frac{1}{g_\alpha g_\beta}\frac{\partial g_\alpha}{\partial \beta}R_{13} & 0 & 0 & 0 & \frac{1}{R_\alpha}R_{11} & \frac{1}{R_\alpha}R_{12} & \frac{1}{R_\alpha}R_{13} \\
\frac{1}{g_\alpha g_\beta}\frac{\partial g_\beta}{\partial \alpha}R_{12} & \frac{1}{g_\beta}R_{32} & \frac{1}{g_\alpha g_\beta}\frac{\partial g_\beta}{\partial \alpha}R_{13} & \frac{1}{g_\beta}R_{33} & 0 & 0 & 0 & \frac{1}{R_\beta}R_{11} & \frac{1}{R_\beta}R_{12} & \frac{1}{R_\beta}R_{13} \\
-\frac{1}{g_\alpha g_\beta}\frac{\partial g_\alpha}{\partial \beta}R_{12} & \frac{1}{g_\alpha}R_{22} & -\frac{1}{g_\alpha g_\beta}\frac{\partial g_\alpha}{\partial \beta}R_{13} & \frac{1}{g_\alpha}R_{23} & 0 & 0 & 0 & 0 & 0 & 0 \\
\frac{1}{g_\beta}R_{32} & -\frac{1}{g_\alpha g_\beta}\frac{\partial g_\beta}{\partial \alpha}R_{12} & \frac{1}{g_\beta}R_{33} & -\frac{1}{g_\alpha g_\beta}\frac{\partial g_\beta}{\partial \alpha}R_{13} & 0 & 0 & 0 & 0 & 0 & 0 \\
\frac{1}{h_1}(1+\frac{d_1}{R_\alpha})R_{12} & 0 & \frac{1}{h_1}(1+\frac{d_1}{R_\alpha})R_{13} & 0 & \frac{1}{2g_\alpha}R_{21} & \frac{1}{2g_\alpha}R_{22} & \frac{1}{2g_\alpha}R_{23} & \frac{1}{2g_\alpha}R_{21} & \frac{1}{2g_\alpha}R_{22} & \frac{1}{2g_\alpha}R_{23} \\
\frac{1}{h_1}(1+\frac{d_1}{R_\beta})R_{12} & 0 & \frac{1}{h_1}(1+\frac{d_1}{R_\beta})R_{13} & 0 & \frac{1}{2g_\beta}R_{31} & \frac{1}{2\rho_\beta}R_{32} & \frac{1}{2g_\beta}R_{33} & \frac{1}{2g_\beta}R_{31} & \frac{1}{2g_\beta}R_{32} & \frac{1}{2g_\beta}R_{33}
\end{array}
\right]
$$

ORIGINAL PAGE IS
OF POOR QUALITY

and the quantities R_k are the components of the matrix

$$[R]_j = \begin{bmatrix} (\beta_2^j-\beta_3^j)\alpha + (\alpha_3^j-\alpha_2^j)\beta + \alpha_2^j\beta_3^j-\alpha_3^j\beta_2^j & (\beta_3^j-\beta_1^j)\alpha + (\alpha_1^j-\alpha_3^j)\beta + \alpha_3^j\beta_1^j-\alpha_1^j\beta_3^j & (\beta_1^j-\beta_2^j)\alpha + (\alpha_2^j-\alpha_1^j)\beta + \alpha_1^j\beta_2^j- \alpha_2^j\beta_1^j \\ \beta_2^j-\beta_3^j & \beta_3^j-\beta_1^j & \beta_1^j-\beta_2^j \\ \alpha_3^j-\alpha_2^j & \alpha_1^j-\alpha_3^j & \alpha_2^j-\alpha_1^j \end{bmatrix} \qquad (2.19c)$$

Note that only the last two rows of the matrix [G] change from layer to layer. Then the layer element strain energy is given by

$$U_{ij} = \{d\}_{ij}^T [K]_{ij} \{d\}_{ij} \tag{2.20a}$$

with

$$[K]_{ij} = \int_{\alpha_1^j}^{\alpha_2^j} \int_{\beta_1^j + \frac{\beta_2^j - \beta_1^j}{\alpha_2^j - \alpha_1^j}(\alpha - \alpha_1^j)}^{\beta_1^j + \frac{\beta_3^j - \beta_1^j}{\alpha_3^j - \alpha_1^j}(\alpha - \alpha_1^j)} [F(\alpha,\beta)]_{ij} \, d\alpha d\beta + \int_{\alpha_2^j}^{\alpha_3^j} \int_{\beta_2^j + \frac{\beta_3^j - \beta_2^j}{\alpha_3^j - \alpha_1^j}(\alpha - \alpha_2^j)}^{\beta_1^j + \frac{\beta_3^j - \beta_1^j}{\alpha_3^j - \alpha_1^j}(\alpha - \alpha_1^j)} [F(\alpha,\beta)]_{ij} \, d\alpha d\beta \tag{2.20b}$$

and

$$[F(\alpha,\beta)]_{ij} = [G]_{ij}^T [B_i] [G]_{ij} g_\alpha g_\beta \tag{2.20c}$$

The element stiffness matrix $[K]_{ij}$ may be obtained in an integrated form if the components of the first and second fundamental forms have a simple variation with the lines of curvature coordinates α and β and if one has the patience to carry out the matrix multiplications and the integrations. An alternative approach is a computer program which will carry out the matrix multiplications at selected points and perform the required integrations numerically.

Similar operations will yield the work done by applied surface loads. For example, work of normal surface loading on any element is given by

$$W_j = \int_{\alpha_1^j}^{\alpha_2^j} \int_{\beta_1^j + \frac{\beta_2^j - \beta_1^j}{\alpha_2^j - \alpha_1^j}(\alpha - \alpha_1^j)}^{\beta_1^j + \frac{\beta_3^j - \beta_1^j}{\alpha_3^j - \alpha_1^j}(\alpha - \alpha_1^j)} q_j w_j dS_j + \int_{\alpha_2^j}^{\alpha_3^j} \int_{\beta_2^j + \frac{\beta_3^j - \beta_2^j}{\alpha_2^j - \alpha_3^j}(\alpha - \alpha_2^j)}^{\beta_1^j + \frac{\beta_3^j - \beta_1^j}{\alpha_3^j - \alpha_1^j}(\alpha - \alpha_1^j)} q_j w_j dS_j \tag{2.21a}$$

where

$$q_j = \bar{\sigma}_\zeta^{N+1}(1+\frac{dw}{R_\alpha})(1+\frac{dw}{R_\beta}) - \bar{\sigma}_\zeta^{1} \tag{2.21b}$$

and w_j is given by

$$w_j = \{w_{1j}\ w_{2j}\ w_{3j}\}[C_j]\begin{Bmatrix}\alpha\\ \beta\\ 1\end{Bmatrix} \tag{2.21c}$$

If q_j is assumed to vary linearly within the element as an approximation to the actual distribution, q_j is given by an expression similar to that of Eq. (2.21c). Then

$$W_j = \{q_{1j}\ q_{2j}\ q_{3j}\}\ [C_j][I_j][C_j]\begin{Bmatrix}w_{1j}\\ w_{2j}\\ w_{3j}\end{Bmatrix} \tag{2.22a}$$

with

$$[I_j] = \int_{\alpha_1^j}^{\alpha_2^j}\int_{\beta_1^j+\frac{\beta_3^j-\beta_2^j}{\alpha_3^j-\alpha_2^j}(\alpha-\alpha_2^j)}^{\beta_1^j+\frac{\beta_3^j-\beta_1^j}{\alpha_3^j-\alpha_1^j}(\alpha-\alpha_1^j)} \begin{bmatrix}\alpha^2 & \alpha\beta & \alpha\\ \alpha\beta & \beta^2 & \beta\\ \alpha & \beta & 1\end{bmatrix} g_\alpha g_\beta d\alpha d\beta$$

$$+ \int_{\alpha_2^j}^{\alpha_3^j}\int_{\beta_2^j+\frac{\beta_3^j-\beta_2^j}{\alpha_3^j-\alpha_2^j}(\alpha-\alpha_2^j)}^{\beta_1^j+\frac{\beta_3^j-\beta_1^j}{\alpha_3^j-\alpha_1^j}(\alpha-\alpha_1^j)} \begin{bmatrix}\alpha^2 & \alpha\beta & \alpha\\ \alpha\beta & \beta^2 & \beta\\ \alpha & \beta & 1\end{bmatrix} g_\alpha g_\beta d\alpha d\beta \tag{2.22b}$$

The potential energy is now given by

$$V = \sum_{i=1}^{N}\sum_{j=1}^{M} \qquad - \sum_{j=1}^{M}\Delta W_j \tag{2.22c}$$

and is expressed in terms of the displacements at the nodal points of the structure. Minimization of the potential energy with respect to each of these nodal point displacements then yields a set of linear equations for their determination. Convergence of the process to the correct solution occurs as the size of the elements become smaller with an increasing number of elements.

With the displacements known at the vertices of each triangular prism layer element, the stress distribution within each element may be obtained from the relationship

$$
\begin{bmatrix} \sigma_{\alpha}^{ij}(\zeta) \\ \sigma_{\beta}^{ij}(\zeta) \\ \tau_{\alpha\beta}^{ij}(\zeta) \\ \tau_{\alpha\rho}^{ij}(\zeta) \\ \tau_{\beta}^{ij}(\ ) \end{bmatrix} = \left[E_i\right] \begin{bmatrix} \frac{1-\zeta/h_i}{A_\alpha^i(\zeta)} & 0 & 0 & 0 & \frac{\zeta/h_i}{A_\alpha^i(\zeta)} & 0 & 0 & 0 & 0 & 0 \\ 0 & \frac{1-\zeta/h_i}{A_\beta^i(\zeta)} & 0 & 0 & 0 & \frac{\zeta/h_i}{A_\beta^i(\zeta)} & 0 & 0 & 0 & 0 \\ 0 & 0 & \frac{1-\zeta/h_i}{A_\alpha^i(\zeta)} & \frac{1-\zeta/h_i}{A_\beta^i(\zeta)} & 0 & 0 & \frac{\zeta/h_i}{A_\alpha^i(\zeta)} & \frac{\zeta/h_i}{A_\beta^i(\zeta)} & 0 & 0 \\ 0 & 0 & 0 & 0 & 0 & 0 & 0 & 0 & \frac{1}{A_\alpha^i(\zeta)} & 0 \\ 0 & 0 & 0 & 0 & 0 & 0 & 0 & 0 & 0 & \frac{1}{A_\beta^i(\zeta)} \end{bmatrix} [G]_{ij} \quad [d]_{ij} \tag{2.23}
$$

A better approximation to the transverse shear stresses $\tau_{\alpha\rho}$ and $\tau_{\beta\rho}$ can be obtained by using the equations of equilibrium of stresses within each layer as in reference 29.

2.7 Specific Results for a Right Triangle Element of a Circular Cylindrical Shell and a Flat Plate

For a right triangle element of a cylindrical shell, with α taken as the coordinate x along the generator and β as the circumferential angle Θ so that

$$g_\alpha = 1$$

$$g_\beta = R$$

$$R_\alpha = \infty$$

$$R_\beta = R$$

the matrix $[G]_{ij}$ is given by

$$
[G]_{ij} = \begin{bmatrix}
-\Delta\theta^j & 0 & \Delta\theta^j & 0 & 0 & 0 & 0 & 0 & 0 & 0 \\
0 & 0 & 0 & -\frac{1}{R}\Delta x^j & 0 & \frac{1}{R}\Delta x^j & 0 & 0 & 0 & 0 \\
0 & -\Delta\theta^j & 0 & \Delta\theta^j & 0 & 0 & 0 & 0 & 0 & 0 \\
0 & 0 & -\frac{1}{R}\Delta x^j & 0 & \frac{1}{R}\Delta x^j & 0 & 0 & 0 & 0 & 0 \\
0 & 0 & 0 & 0 & 0 & 0 & -\Delta\theta^j & 0 & \Delta\theta^j & 0 \\
0 & 0 & 0 & 0 & 0 & 0 & 0 & 0 & 0 & -\frac{1}{R}\Delta x^j \\
0 & 0 & 0 & 0 & 0 & 0 & 0 & -\Delta\theta^j & 0 & \Delta\theta^j \\
0 & 0 & 0 & 0 & 0 & 0 & 0 & 0 & -\frac{1}{R}\Delta x^j & 0 \\
-\frac{1}{h_i}R_{11} & 0 & -\frac{1}{h_i}R_{12} & 0 & -\frac{1}{h_i}R_{13} & 0 & \frac{1}{h_i}R_{11} & 0 & \frac{1}{h_i}R_{12} & 0 \\
-\frac{1}{h_i}(1+\frac{d_{i+1}}{R})R_{11} & 0 & -\frac{1}{h_i}(1+\frac{d_{i+1}}{R})R_{12} & 0 & -\frac{1}{h_i}(1+\frac{d_{i+1}}{R})R_{13} & 0 & \frac{1}{h_i}(1+\frac{d_i}{R})R_{11} & 0 & \frac{1}{2}(1+\frac{d_i}{R})R_{12} & 0
\end{bmatrix}
$$

$$
\left.\begin{array}{cccccccc}
0 & 0 & 0 & 0 & 0 & 0 & 0 & 0 \\
0 & 0 & \frac{1}{R}R_{11} & \frac{1}{R}R_{12} & \frac{1}{R}R_{13} & 0 & 0 & 0 \\
0 & 0 & 0 & 0 & 0 & 0 & 0 & 0 \\
0 & 0 & 0 & 0 & 0 & 0 & 0 & 0 \\
0 & 0 & 0 & 0 & 0 & 0 & 0 & 0 \\
0 & \frac{1}{R}\Delta x^j & 0 & 0 & 0 & \frac{1}{R}R_{11} & \frac{1}{R}R_{12} & \frac{1}{R}R_{13} \\
0 & 0 & 0 & 0 & 0 & 0 & 0 & 0 \\
-\frac{1}{R}\Delta x^j & 0 & 0 & 0 & 0 & 0 & 0 & 0 \\
\frac{1}{h_1}R_{13} & 0 & -\frac{1}{2}\Delta\theta^j & \frac{1}{2}\Delta\theta^j & 0 & \frac{1}{2}\Delta\theta^j & \frac{1}{2}\Delta\theta^j & 0 \\
\frac{1}{h_1}(1+\frac{d_1}{R})R_{13} & 0 & 0 & -\frac{1}{2R}\Delta x^j & \frac{1}{2R}\Delta x^j & 0 & -\frac{1}{2R}\Delta x^j & \frac{1}{2R}\Delta x^j
\end{array}\right] \quad (2.24)
$$

With

$$\Delta x^j = x_2^j - x_1^j \quad (2.25a)$$

$$\Delta\theta^j = \theta_3^j - \theta_1^j \quad (2.25b)$$

$$R_{11} = \Delta\theta^j (x_2^j - x) \quad (2.25c)$$

$$R_{12} = \Delta\theta^j (x - x_1^j) - \Delta x^j (\theta - \theta_1^j) \quad (2.25d)$$

$$R_{13} = \Delta x^j (\theta - \theta_1^j) \quad (2.25e)$$

In addition

$$I_{1j}(x,\Theta) = R \ln \frac{1+d_{i+1}/R}{1+d_i/R} \tag{2.26a}$$

$$I_{1j}(\Theta,x) = h_i\left(1+ \frac{d_i+ \frac{1}{2}h_i}{R}\right) \tag{2.26b}$$

$$I_{2i}(x,\Theta) = R\left[\left(1+ \frac{R+d_i}{h_i}\right)^2 \ln \frac{1+d_{i+1}/R}{1+d_i/R} - \frac{3}{2} - \frac{R+d_i}{h_i}\right] \tag{2.26c}$$

$$I_{2i}(\Theta,x) = \frac{1}{3}\, h_i \left(1+ \frac{d_i+ \frac{1}{4}h_i}{R}\right) \tag{2.26d}$$

$$I_{3i}(x,\Theta) = R \left\{\frac{1}{2} + \frac{R+d_i}{h_i} \left[1-\left(1+ \frac{R+d_i}{h_i}\right) \ln \frac{1+d_{i+1}/R}{1+d_i/R}\right]\right\} \tag{2.26e}$$

$$I_{3i}(\Theta,x) = \frac{1}{6}\, h_i \left(1+ \frac{d_i+ \frac{1}{2}h_i}{R}\right) \tag{2.26f}$$

$$I_{4i}(x,\Theta) = R\left[\frac{1}{2} - \frac{R+d_i}{h_i} \left(1- \frac{R+d_i}{h_i} \ln \frac{1+d_{i+1}/R}{1+d_i/R}\right)\right] \tag{2.26g}$$

$$I_{4i}(\Theta,x) = \frac{1}{3}\, h_i \left(1+ \frac{d_i+ \frac{3}{4}h_i}{R}\right) \tag{2.26h}$$

The stiffness matrix is given by

$$K_{ij} = \int_{x_1^j}^{x_2^j} \int_{\Theta_1^j}^{\Theta_1^j + \frac{\Delta\Theta^j}{\Delta x^j}(x-x_1^j)} R\,[G]_{ij}^T\,[B]_i\,[G]_{ij}\,dx\,d\Theta \tag{2.27}$$

while the work expression of Eq. (2.22b) is given by

$$W_j = \{q_{1j}\ q_{2j}\ q_{3j}\} \begin{bmatrix} 1/12 & 1/24 & 1/24 \\ 1/24 & 1/12 & 1/24 \\ 1/24 & 1/24 & 1/12 \end{bmatrix} \begin{Bmatrix} w_{1j} \\ w_{2j} \\ w_{3j} \end{Bmatrix} R\Delta\Theta^j \Delta x^j \tag{2.28}$$

The integrations of Eq. (2.27) have been carried out and have been incorporated in the computer program listed in Appendix A. In doing so care was taken to distinguish between the four differently oriented right triangles shown in Fig. 2-9 for which various terms in the components of the stiffness matrix change sign.

Similar results hold for a flat plate for which R is infinite while $R\ \Delta\Theta = \Delta y$. Then

$$I_{1j}(x,\Theta) = I_{1j}(\Theta,x) = h_i \tag{2.29a}$$

$$I_{2i}(x,\Theta) = I_{2i}(\Theta,x) = I_{4i}(x,\Theta) = I_{4i}(\Theta,x) = \frac{1}{3}h_i \tag{2.29b}$$

$$I_{3i}(x,\Theta) = I_{3i}(\Theta,x) = \frac{1}{6}h_i \tag{2.29c}$$

the matrix [G] becomes

$$
[G] = \frac{1}{\Delta_x^j \Delta_y^j}
\begin{bmatrix}
-\Delta y^j & 0 & \Delta y^j & 0 & 0 & 0 & 0 & 0 & 0 & 0 & 0 & 0 & 0 & 0 & 0 & 0 & 0 & 0 \\
0 & 0 & 0 & -\Delta x^j & 0 & \Delta x^j & 0 & 0 & 0 & 0 & 0 & 0 & 0 & 0 & 0 & 0 & 0 & 0 \\
0 & -\Delta y^j & 0 & \Delta y^j & 0 & 0 & 0 & 0 & 0 & 0 & 0 & 0 & 0 & 0 & 0 & 0 & 0 & 0 \\
0 & 0 & -\Delta x^j & 0 & \Delta x^j & 0 & 0 & 0 & 0 & 0 & 0 & 0 & 0 & 0 & 0 & 0 & 0 & 0 \\
0 & 0 & 0 & 0 & 0 & 0 & -\Delta y^j & 0 & \Delta y^j & 0 & 0 & 0 & 0 & 0 & 0 & 0 & 0 & 0 \\
0 & 0 & 0 & 0 & 0 & 0 & 0 & 0 & 0 & -\Delta x^j & 0 & \Delta x^j & 0 & 0 & 0 & 0 & 0 & 0 \\
0 & 0 & 0 & 0 & 0 & 0 & 0 & -\Delta y^j & 0 & \Delta y^j & 0 & 0 & 0 & 0 & 0 & 0 & 0 & 0 \\
0 & 0 & 0 & 0 & 0 & 0 & 0 & 0 & -\Delta x^j & 0 & \Delta x^j & 0 & 0 & 0 & 0 & 0 & 0 & 0 \\
\frac{-R_{11}}{h_i} & 0 & \frac{-R_{12}}{h_i} & 0 & \frac{-R_{13}}{h_i} & 0 & \frac{R_{11}}{h_i} & 0 & \frac{R_{12}}{h_i} & 0 & \frac{R_{13}}{h_i} & 0 & -\frac{1}{2}\Delta y^j & \frac{1}{2}\Delta y^j & 0 & -\frac{1}{2}\Delta y^j & \frac{1}{2}\Delta y^j & 0 \\
\frac{-R_{11}}{h_i} & 0 & \frac{-R_{12}}{h_i} & 0 & \frac{-R_{13}}{h_i} & 0 & \frac{R_{11}}{h_i} & 0 & \frac{R_{12}}{h_i} & 0 & \frac{R_{13}}{h_i} & 0 & 0 & -\frac{1}{2}\Delta x^j & \frac{1}{2}\Delta x^j & 0 & -\frac{1}{2}\Delta x^j & \frac{1}{2}\Delta x^j
\end{bmatrix}
\tag{2.30}
$$

ORIGINAL PAGE IS
OF POOR QUALITY

with

$$\Delta x^j = x_2^j - x_1^j \tag{2.31a}$$

$$\Delta y^j = y_3^j - y_1^j \tag{2.31b}$$

$$R_{11} = \Delta y^i (x_2^j - x) \tag{2.31c}$$

$$R_{12} = \Delta y^j (x - x_1^j) - \Delta x^j (y - y_1^j) \tag{2.31d}$$

$$R_{13} = \Delta x^j (y - y_1^j) \tag{2.31e}$$

and the stiffness matrix is given by

$$[K]_{ij} = \int_{x_1^j}^{x_2^j} \int_{y_1^j}^{y_1^j + \frac{\Delta y^j}{\Delta x^j}(x - x_1^j)} [G]^T [B] [G] \, dx dy \tag{2.32}$$

while the work expression is identical with Eq. (2.28) with $R\Delta\Theta^j$ replaced by Δy^j.

CHAPTER III

COMPUTER PROGRAM FOR THE ANALYSIS OF LAYERED PLATES AND SHELLS

The finite element theory of the preceeding chapter using the particular right triangular element developed for flat plates and cylindrical shells has been incorporated into the computer code listed in Appendix A for which input and output data are given in Appendix B. The code utilizes a number of subroutines taken from the SAP IV and SAP V codes (references 23-25) together with some additional subroutines devised for the present program. The SAP system codes are particularly efficient subroutines for the processing of input data, the generation of the system of equations to be solved, and the solution of an equation system of large size and bandwidth. The added subroutines deal with the input and output peculiar to laminated plates and shells.

The subroutines and their functions are as follows:

1. HEDPRT - Reads the total number of nodal points, elements, layers, and the type of analysis.
2. INPUTJ - Reads or generates the coordinates and the restraint conditions of each nodal point, reads the material properties and thickness of each layer, generates the variable number of each degree of freedom.
3. LAYSHL, AYSHL - Reads or generates the layer element type and the nodal points forming each element, calculates the element stiffness matrix, calls ADDSTF and CALBAN

4. INL - Reads or generates nodal forces.

5. CHECK - Verifies sufficiency of input data. Prints an error message if criteria not met.

6. ADDSTF - Stores layer element stiffness matrix in proper location in overall stiffness matrix, divides the stiffness matrix and load vector into blocks for storage.

7. CALBAN - Calculates bandwidth of system of equations.

8. SOLEQ - Controls input and output data from subroutine SESOL. Calls PRIND, STRESS, STRSC.

9. SESOL - Solves positive definite symmetrical system equations by Gaussian elimination.

10. ERROR - Prints error message if limit on storage requirements is exceeded.

11. STRESS, STRSC - Calculates stresses for each element.

12. PRIND - Prints out all required input and output.

The input data required for the static analysis of layered plate and shell structures is given in detail below. The nodal points should be numbered consecutively along straight, normal lines from the bottom layer to the top layer before proceeding to another nodal point on the bottom layer. The elements should also be numbered consecutively through the thickness before proceeding to another element on the bottom layer. The computations were carried out on the USC School of Engineering DEC-10 System Computer.

I. Heading Card (12A6)

Columns	Variable	Entry
1-72	HED(12)	Enter the heading information to be printed with the output

II. Master Control Card (4I5, I4, I1, 4I5, 2X, 3I1, 3I5, 5X, F10.0)

Columns	Variable	Entry
1-5	NUMNP	Total number of nodal points in the model
6-10	NELTYP	1
11-15	LL	Number of Structure load cases
16-20	N F	0
21-24	KDYN	0
25	NDYN	0
26-30	MODEX	Program execution mode 0 if problem solution wanted 1 if only data check wanted
31-35	NAD	0
36-40	KEQB	0
41-45	NIOSV	0
48		0
49	GENPRT	0 if printout of overall stiffness matrix not wanted 1 if printout of overall stiffness matrix wanted

Columns	Variable	Entry
50	ELPRT	0 if printout of element stiffness matrices not wanted
		1 if printout of element stiffness matrices wanted
51-55	IWTC	0
56-60	MINBND	0 if bandwidth minimization not wanted
		1 if bandwidth minimization wanted
61-65	IPLT	0
66-70	NRSC	0
71-80	GRAV	0

III. Structural Data (4I5)

Columns	Variable	Entry
1-5	NELTYP	13 if cylindrical shell element
		14 if flat plate element
6-10	NUME	Total number of elements
11-15	NUML	Total number of layers
16-20	NUMFX	Total number of restrained nodal points

IV. Material Properties (F5.1, F3.1, 9F8.0) (One for each Layer)

Columns	Variable	Entry
1-5	A	Angle of the layer material axes of orthotropy to global coordinate system (Equal to 0.0 if material is generally anisotropic)

Columns	Variable	Entry
6-8	H	Thickness of the layer
9-16	E_{11}	
17-24	E_{12}	
25-32	E_{13}	
33-40	E_{22}	
41-45	E_{23}	Material elastic moduli ($E_{13} = E_{23} = G_{45} = 0.0$ if material is orthotropic and properties are referred to axes of orthotropy).
49-56	E_{33}	
57-64	G_{44}	
65-72	G_{45}	
73-80	G_{55}	

V. Nodal Point Data (I3, 3F7.4) (One for each nodal point)

Column	Variable	Entry
1-3	I	Assigned number of the nodal point numbered consecutively through the structure thickness before proceeding to next node in bottom face
4-10	X(I)	X-ordinate
11-17	Y(I)	Y-ordiante
18-24	Z(I)	Z-ordinate

VI. Restrained Point Data (I3, 3I1) (One for each restrained nodal point)

Columns	Variable	Entry
1-3	N	Number of restrained nodal points
4	ID(N,1)	Restraint condition in x-translation 1 if point is restrained 0 if point is not restrained
5	ID(N,2)	Restraint condition in y-translation 1 if point is restrained 0 if point is not restrained
6	ID(N,3)	Restraint condition in z-translation 1 if point is restrained 0 if point is not restrained

VII. Radius For Shell Element (F13.3) (outfitted for flat plate analysis)

VIII. Element Load Multipliers (4F10.0)

Columns	Variable	Entry
1-10	EM(1)	0.0
11-20	EM(2)	0.0
21-30	EM(3)	0.0
31-40	EM(4)	0.0

IX. Element Data (4I5,3I1) (One for each element)

Columns	Variable	Entry	Notes
1-5	M	Element Number	(1)
6-10	I1	Vertex of the element	(2)
11-15	J1	Vertex of the element	
16-20	K1	Vertex of the element	
21	L	Layer number of the element	(2)
22	MCD	Element Code	(2)
23	ML	0 without load on the element 1 with load on the element	(3) (4)

Notes: (1) Numbered consecutively through the structure thickness before proceeding to next bottom layer element

(2) There are 4 different elements based on their orientation as shown in Fig. 2-9. In all cases

$$I2 = I1 + 1$$

$$J2 = J1 + 1$$

$$K2 = K1 + 1$$

(3) When there is no load acting on the element, input the next element data

(4) When there is any load acting on the element, input the load data (next input) before the following element data

X. Load Data (18F4.2) (One for each loaded element)

Columns	Variable	Entry
4-7	QX(I1)	Applied x-direction stress at I1
5-8	QY(I1)	Applied y-direction stress at I1
9-12	QX(J1)	Applied x-direction stress at J1

Columns	Variable	Entry
13-16	QY(J2)	Applied y-direction stress at J2
17-20	QX(K1)	Applied x-direction stress at K1
21-24	QY(K1)	Applied y-direction stress at K1
25-28	QX(I2)	Applied x-direction stress at I2
29-32	QY(I2)	Applied y-direction stress at I2
33-36	QX(J2)	Applied x-direction stress at J2
37-40	QY(J2)	Applied y-direction stress at J2
41-44	QX(K2)	Applied x-direction stress at K2
45-48	QY(K2)	Applied y-direction stress at K2
49-52	QZ(I1)	Sum of applied z-direction stresses at nodes I1 and I2
53-56	FZ(Ia)	Sum of applied z-directions concentrated forces at nodes I1 and I2
57-60	QZ(J1)	Sum of applied z-direction stresses at nodes J1 and J2
61-64	FZ(J1)	Sum of applied z-directions concentrated forces at nodes J1 and J2
65-68	QZ(K1)	Sum of applied z-direction stresses at nodes K1 and K2
69-72	FZ(K1)	Sum of applied z-direction concentrated forces and K1 and K2

XI. Load Point (I3) (One for each loaded point in every load case could be in any direction)

IV. FINITE ELEMENT ANALYSIS OF SPECIFIC PROBLEMS

A number of problems have been investigated, some to assess the accuracy and convergence properties of the finite element analysis derived and others to explore the usefulness of the analysis for problems difficult to solve by other methods. A description of the various problems and the results obtained are as follows:

4.1 Cylindrical Bending of a Wide Simply Supported Laminated Plate Subjected to Sinusoidal Surface Pressure

Pagano in Ref. 13 has given an exact plane strain elasticity solution for the problem of cylindrical bending of a layered plate subjected to normal pressure. (Fig. 4-1). The material of each layer is orthotropic and identical. The directions of the axes of orthotropy of alternating layers vary by 90°, however. The boundary conditions are those of vanishing edge normal displacement and stress. For a surface loading which varies sinusoidally, then, the displacements and stresses have sinusoidal variations as well.

To obtain an exact solution of the problem within the framework of the present theory the transverse displacement is taken in the form

$$w = W \sin \frac{\pi x}{L} \tag{4.1a}$$

while the longitudinal displacements are taken in the form

$$u_x^i = U_x^i \cos \frac{\pi x}{L} \tag{4.1b}$$

Then Eq. (2.12c) yields

$$\bar{\varepsilon}_i = \begin{Bmatrix} -U_x^i \frac{\pi}{L} \sin \frac{\pi x}{L} \\ 0 \\ 0 \\ 0 \\ -U_x^{i+1} \frac{\pi}{L} \sin \frac{\pi x}{L} \\ 0 \\ 0 \\ 0 \\ \left[\frac{\pi}{L} W + \frac{1}{h_i} (U_x^{i+1} - U_x^i)\right] \cos \frac{\pi x}{L} \\ 0 \end{Bmatrix} \tag{4.2}$$

The use of Eqs. (2.12), (2.14) and Eq. (3.2) results in the following expression for the potential energy per unit width of the layered plate

$$U = \int_0^L \sum_{i=1}^{N} S_i dx - \int_0^L qwdx$$

$$= \frac{L}{4} \sum_{i=1}^{N} \left\{ \frac{1}{3} \frac{\pi^2}{L^2} h_i E_{11}^i \left[(U_x^i)^2 + U_x^i U_x^{i+1} + (U_x^{i+1})^2 \right] \right.$$

$$\left. + G_{44}^i h_i \left[\frac{\pi}{L} W + \frac{1}{h_i}(U_x^{i+1} - U_x^i)\right]^2 \right\} - q_o W \frac{L}{2} \tag{4.3}$$

where q_o is the amplitude of the normal loading. The minimization of the potential energy with respect to the displacement coefficients U_x^i and W then yields the following set of linear equations

$$\left(\frac{1}{6}\frac{\pi^2}{L^2}E_{11}^{i-1}h_{i-1} - \frac{G_{44}^{i-1}}{h_{i-1}}\right)U_x^{i-1} + \left[\frac{1}{3}\frac{\pi^2}{L^2}(E_{11}^{i-1}h_i + E_{11}^{i}h_i) + \frac{G_{44}^{i-1}}{h_{i-1}} + \frac{G_{44}^{i}}{h_i}\right]U_x^i + \left(\frac{1}{6}\frac{\pi^2}{2}E_{11}^{i}h_i - \frac{G_{44}^{i}}{h_i}\right)U_x^{i+1} + \frac{\pi}{L}\left(G_{44}^{i-1} - G_{44}^{i}\right)W = 0 \tag{4.4a}$$

$$i=2,3,\ldots N$$

$$\left(\frac{1}{3}\frac{\pi^2}{L^2}E_{11}^{1} + \frac{G_{44}^{1}}{h_i}\right)U_x^1 + \left(\frac{1}{6}\frac{\pi^2}{L^2}E_{11}^{1}h_1 - \frac{G_{44}^{1}}{h_1}\right)U_x^2 - G_{44}^{1}\frac{\pi}{L}W = 0 \tag{4.4b}$$

$$\left(\frac{1}{3}\frac{\pi^2}{L^2}E_{11}^{N} + \frac{G_{44}^{N}}{h_N}\right)U_x^{N+1} + \left(\frac{1}{6}\frac{\pi^2}{L^2}E_{11}^{N}h_N - \frac{G_{44}^{N}}{h_N}\right)U_x^N + G_{44}^{N}\frac{\pi}{L}W = 0 \tag{4.4c}$$

$$\left(\sum_{i=1}^{N} G_{44}^{i}h_i\right)W + \sum_{i=1}^{N}G_4^i\left(U_x^{i+1} - U_x^i\right) - q_0 = 0 \tag{4.4d}$$

For a symmetric three-layer plate with

$$h_1 = h_3$$

$$E_{11}^1 = E_{11}^3$$

$$G_{44}^1 = G_{44}^3$$

the solution of Eqs. (4.4) may be written as

$$U_2 = -U_3 \quad 1\,\frac{q_o\left(\frac{L}{\pi}\right)^3}{2\Delta_1}\left[G_{44}^1G_{44}^2 - \frac{\pi^2h_1^2}{2L^2}E_{11}^1(G_{44}^1 - \frac{2}{3}G_{44}^2)\right]h_2 \tag{4.4b}$$

$$U_1 = -U_4 = -\frac{q_o\left(\frac{L}{\pi}\right)^3}{2\Delta_1}\left[G_{44}^1 G_{44}^2 (2h_1+h_2) + \frac{\pi^2 h_1 h_2^2}{6L^2} E_{11}^2 G_{44}^1 + \frac{\pi^2 h_1^2 h_2}{2L^2}\right.$$

$$\left.(G_{44}^1 - \frac{1}{3} G_{44}^2)\, E_{11}^1\right] \tag{4.5b}$$

$$W = \frac{-q_o\left(\frac{L}{\pi}\right)^4}{\Delta_1}\left[G_{44}^1 G_{44}^2 + \frac{\pi^2 h_2}{2L^2}(E_{11}^1 h_1 + \frac{1}{6} E_{11}^2 h_2)\, G_{44}^1 + \frac{\pi^2 h_1^2}{3L^2} G_{44}^2 E_{11}^1\right.$$

$$\left. + \frac{\pi^4 h_1^2 h_2}{24L^4} E_{11}^1 (E_{11}^1 h_1 + \frac{2}{3} E_{11}^2 h_2)\right] \tag{4.5c}$$

$$\Delta_1 = G_{44}^1 G_{44}^2 \left\{\frac{1}{2} E_{11}^1 \left[\frac{1}{3} h_1^3 + h_1 (h_1+h_2)^2\right] + \frac{1}{12} E_{11}^2 h_2^3\right\} + \frac{\pi^2 h_1^2 h_2}{24L^2}$$

$$E_{11}^1\ (E_{11}^1 h_1 + \frac{2}{3} E_{11}^2 h_2)(2G_{44}^1 h_1 + G_{44}^2 h_2) \tag{4.5d}$$

Direct stresses may be obtained from Eqs. (2.3) and (3.5) as

$$\sigma_x^i(\zeta) = E_{11}^i \left[\left(1 - \frac{\zeta}{h_i}\right)\frac{du_x^i}{dx} + \frac{\zeta}{h_i}\frac{du_x^{i+1}}{dx}\right] \tag{4.6}$$

Transverse shear stresses may be obtained from the solution of the equilibrium equation

$$\frac{\partial \sigma_x^i(\zeta)}{\partial x} + \frac{\partial \tau_{xy}^i(\zeta)}{\partial \zeta} = 0 \tag{4.7a}$$

yielding

$$\tau_{xy}^i(\zeta) = \tau_{xy}^i(0) - E_{11}^i \zeta \left[\left(1 - \frac{1}{2}\frac{\zeta}{h_i}\right)\frac{d^2 u_x^i}{dx^2} + \frac{\zeta}{2h_i}\ \frac{d^2 u_x^{i+1}}{dx^2}\right] \tag{4.7b}$$

together with the boundary conditions of zero shear stress at one of the surfaces. The remaining zero shear stress conditon is then automatically satisfied. For the case of three symmetric layers

$$\sigma_{x1} = -\sigma_{x3} = -\frac{\pi}{L} E^1_{11} \left[U_1 + (U_1 - U_o)\frac{\zeta_1}{h_1}\right] \sin\frac{\pi x}{L} \tag{4.8a}$$

$$\sigma_{x2} = -\frac{\pi}{L} E^2_{11} U_2 \quad \frac{2\zeta}{h_2} - 1 \quad \sin\frac{\pi x}{L} \tag{4.8b}$$

$$\tau_{xy1} = \tau_{xy3} = \frac{\pi^2 \zeta_1 E^1_{11}}{L^2} \left[U_1 = \frac{1}{2}(U_2 - U_1)\frac{\zeta'}{h_1}\right] \cos\frac{\pi x}{L} \tag{4.8c}$$

$$\tau_{xy2} = \frac{\pi^2}{2L^2} \left[E^1_{11} h_1 (U_2 + U_1) + 2E^2_{11} U_2 \zeta_2 \quad 1 - \frac{\zeta 2}{h_2^2}\right] \cos\frac{\pi x}{L} \tag{4.8d}$$

Calculated values are given in graphical form in Ref. 13 for the following beam properties:

$$E^1_{11} = 25 \times 10^6 \text{ psi}$$

$$E^2_{11} = 1 \times 10^6 \text{ psi}$$

$$G^1_{44} = 0.5 \times 10^6 \text{ psi}$$

$$G^2_{44} = 0.2 \times 10^6 \text{ psi}$$

$$h_1 = h_2 = \frac{h}{3}$$

$$\frac{L}{h} = 4,10$$

A comparison of the results of Ref. 13 and those given by the present analysis are shown in Figs. 4-2 to 4-5. It will be seen from these figures that despite the grossness of the approximations the midsurface displacements and stresses are in quite good agreement. The accuracy could be improved even further by considering each layer to be divided into a number of sublayers, each of which is analyzed on the basis of the present theory.

The finite element method using the triangular element outlined in section 2.7 was also used to solve the problem. A half-strip of the plate was divided into right triangular layer elements as shown in Fig. 4-6 where the numbering of nodes and layer elements is shown. Two numbers shown in a triangle indicates that the interface belongs to the two adjacent layer elements that are numbered. Only half of the plate strip need be used since the plate center is an axis of symmetry with $u_x = 0$. A state of plane strain was imposed by requiring that displacements u_x and w at corresponding points on both long edges of the strip be identical whicle the displacements u_y were taken equal to zero at all points. The displacements w at the top and bottom of each layer, while numbered differently in the layer element are made to be equal by assigning each the same number in the overall numbering system.

The width of the strip was taken as 1 inch and the thickness of each layer was taken as 2 inches. The plate length was defined to be 24 inches and 60 inches corresponding to length-total thickness ratios of 4 and 10, respectively. The material constants in reference 13 are given as

$$E_1 = 25 \times 10^6 \text{ psi}$$
$$E_2 = 1 \times 10^6 \text{ psi}$$
$$G_{12} = 0.5 \times 10^6 \text{ psi}$$
$$G_{23} = 0.2 \times 10^6 \text{ psi}$$
$$\nu_{12} = \nu_{23} = 0.25$$

Since

$$\nu_{12} E_2 = \nu_{21} E_1$$

the Poisson's ratio ν_{21} is equal to

$$\nu_{21} = 0.25 \times \frac{1 \times 10^6}{25 \times 10^6} = 0.01$$

so that for layers 1 and 3

$$E_{11} = \frac{E_1}{1-\nu_{12}\nu_{21}} = \frac{25 \times 10^6}{1-0.25 \times 0.01} = 25.06 \times 10^6 \text{ psi}$$

$$E_{22} = \frac{E_2}{1-\nu_{12}\nu_{21}} = \frac{1 \times 10^6}{1-0.25 \times 0.01} = 1.00 \times 10^6 \text{ psi}$$

$$E_{12} = \nu_{12}E_{22} = \nu_{21}E_{11} = 0.25 \times 10^6 \text{ psi}$$

$$E_{33} = 0.5 \times 10^6 \text{ psi}$$

$$G_{44} = 0.5 \times 10^6 \text{ psi}$$

$$G_{55} = 0.2 \times 10^6 \text{ psi}$$

while for layer 2

$$E_{11} = 1.0 \times 10^6 \text{ psi}$$

$$E_{22} = 25.06 \times 10^6 \text{ psi}$$

$$E_{12} = 0.25 \times 10^6 \text{ psi}$$

$$E_{33} = 0.50 \times 10^6 \text{ psi}$$

ORIGINAL PAGE IS OF POOR QUALITY

$G_{44} = 0.2 \times 10^6$ psi

$G_{55} = 0.5 \times 10^6$ psi

The actual half sine wave load distribution was used in determining the work expression. For a state of plane strain with w in each element given by

$$w = w_1\left(\frac{x_2 - x}{x_2 - x_1}\right) + w_2\left(\frac{x - x_1}{x_2 - x_1}\right)$$

the work expression for each triangle is then

$$W_i = \frac{1}{2} q_o \frac{L}{\pi} \left[w_1 \left(\cos \frac{\pi x_1}{L} - \frac{\sin \frac{\pi}{L} \frac{x_2 - x_1}{2}}{\frac{\pi}{L} \frac{x_2 - x_1}{2}} \cos \frac{\pi}{L} \frac{x_2 + x_1}{3} \right) \right.$$
$$\left. + w_2 \left(\frac{\sin \frac{\pi}{L} \frac{x_2 - x_1}{2}}{\frac{\pi}{L} \frac{x_2 - x_1}{2}} \cos \frac{\pi}{L} \frac{x_2 + x_1}{2} - \cos \frac{\pi x_2}{L} \right) \right] \tag{4.9}$$

where b is the width of the plate strip.

Some results obtained by solving the finite element equations with the aid of the developed computer program are shown in Figs. 4-2 to 4-5 where they are compared to the exact solution of the equations of the present theory. It will be seen that the finite element model used is capable of yielding accurate results provided a sufficiently large number of elements is used.

Also shown in the figures are the results obtained by Spilker, et al. (ref. 19), using a similar hybrid-stress finite element model which has the same displacement distribution but which utilizes an assumed stress variation in the derivation of the element stiffness matrix as well. It will be seen that the present element model yields results that are about as accurate as the somewhat more complex hybrid-stress element.

4.2 Two-Layer Angle-Ply Square Plate Under Uniform Load

As a check on the accuracy of the present finite element model when applied to laminated plates, the problem of a uniformly loaded square plate with two angle-ply layers was investigated. The fiber orientations of the layers are $+\Theta$ for one and $-\Theta$ for the other. The layers are of equal thickness, $h/2$. The plate is supported on all four edges, so that transverse displacements are not permitted to occur. Interlayer displacements normal to the edge are not permitted, but displacements parallel to the edge are unrestrained. Normal and parallel edge displacements of the top and bottom surfaces of the plate are free to occur. Material properties, dimensions and geometry are shown in Fig. 4-7. Whitney (ref. 34) has solved a similar problem with classical lamination theory in which shear deformations are neglected. Spilker, et al. (ref. 17), have solved the same problem using a simplified hybrid-stress element and have obtained good agreement with a corrected version of Whitney's results.

Due to coupling of bending and extension in the cross-ply laminated plate, there are no symmetry conditions that can be applied. Thus the entire plate must be modeled. An isotropic single layer square plate under uniform pressure was investigated first. In this case symmetry conditions permit the modeling to be limited to only one eighth of the plate. For a plate with a length-thickness ratio of 10, the finite element results converge to a value about 6% greater than the value given in ref. 31 (Fig. 4-8) when each half-length was divided into 20 equal parts, i.e. 100 elements were used for 1/8 the plate. The larger value to which the finite element solution converges is due to shear deformations which are not included in ref. 31.

For the cross-ply laminated square plate, the above results indicate that each side of the plate should be divided into 40 equal parts to achieve satisfactory convergence. Thus 3200 layer elements would be needed to model the entire plate. Results that were obtained with the side divided into 6, 8 and 10 spaces respectively (Fig. 4-9) are in accord with this conclusion. The hybrid-stress element developed by Spilker, et al. (ref. 17), provided convergent results for the angle-ply laminated plate with the side divided into 10 spaces. It is apparent, then, that a plate finite element model based upon the principal of minimum potential energy has very much poorer convergence properties.

4.3 Perforated Square Plate Under Uniform Inplane All-Round Tension

The effect of circular holes on the stress distribution in stretched plates has been the subject of many investigations. Accurate solutions are availabe for a circular hole in an infinite plate (refs. 34-37) and in an infinite strip (refs. 38-39). The effect of circular holes in a square plate has been studied less rigorously by Hengst (ref. 40) who assumed an expression for the invariant trace of the stress tensor of the form

$$\phi = \sum_{k=4}^{4} C_k r^{2k} \cos 2k\theta$$

and obtained expressions for the coefficients by minimizing the error of the expression. The investigation yields an approximate formula for the circumferential stress around the hole. For uniform tension in both directions (Fig. 4-10) the circumferential stress for various size holes is given in Table 4-1.

For the finite element solution of a plate with $r_o/a = 0.5$ the plate was modeled as shown in Fig. 4-11. The symmetry of the problem requires that only one-eighth of the plate be modeled. The displacement symmetry conditions for the problem are those of identical displacements in the x- and y-directions along the diagonal a-b and vanishing y-direction displacements along the line c-d. Along the side b-c and the circle a-d the stresses are prescribed. The symmetry condition of identical displacements is achieved by assigning the same variable number to U_x and U_y at a nodal point on the diagonal. The problem is one of generalized plane-stress with stress boundary conditions so that the results are independent of material properties and of accuracy of the model since the prescribed and calculated stress values need not be identical. The circumferential stress values along the centerline are interesting in that they decrease at first but then increase somewhat toward the loaded edge.

4.4 Perforated Square Plate Under Uniform Nodal Pressure

The square isotropic plate with a circular hole which is subjected to uniform load has been investigated by El-Hashimy in reference 41. A deflection function is assumed of the form

$$w = \frac{pa^4}{D}\left[\frac{\rho^4}{64} + C_1 + C_2\rho^2 + C_3\rho^3 \ln\frac{\rho}{\rho_i} + C_4 \ln\frac{\rho}{\rho_i}\right.$$

$$+ (A_1\rho^{-4} + B_1\rho^{-2} + A_2\rho^4 + B_2\rho^6) \cos 4\theta$$

$$\left.+ (A_3\rho^{-8} + B_3\rho^{-6} + A_4\rho^8 + B_4\rho^{10}) \cos 8\theta\right]$$

where ρ is the non-dimensional radius ratio r/a. The hole radius is $\rho_i a$. Here a is the side length of the plate. The 12 coefficients are determined by the satisfaction of the conditions of vanishing moment and effective shear force at the hole, which yields 6 equations, and by the satisfaction of conditions of simply supported or clamped edges at 3 points as indicated in Fig. 4-15. The periodicity of the solution requires that only an eighth of the plate be considered.

The finite element method of the present paper was used to analyze the plate as well. The hole size and the grid used are identical with those of the previous section. The boundary conditions are those of zero force at points on the hole, equal values of U_x and U_y and zero effective transverse shear force along the diagonal, zero values of U_y

and effective transverse shear force along the centerline, and zero transverse displacement and either zero inplane stresses displacements along the edge, corresponding to simply supported and clamped edges respectively. The number of degrees of freedom are then 648 for the simply supported plate and 576 for the clamped plate.

A comparison of the transverse displacements calculated using El-Hashimy's equations and those obtained from the finite element anlaysis is shown in Table 4-2. It will be seen that the finite element values are considerably less than those of ref. 41 although the shapes of the deflection patterns are similar. This result is attributed to the satisfaction of boundary conditions at only 3 points on the edge in El-Hashimy's solution which yields a much more flexible structure than is actually the case.

The deflections and stresses obtained from the finite element method are shown in Figures 4-16 to 4-17.

4.5 Axisymmetric Bending of a Cylindrical Shell by End Load

Having ascertained by the investigation of the previous problems that the results for flat plates obtained by means of the present finite element model are adequate, the accuracy of the theory for cylindrical shells was studied next. The first problem investigated was that of axisymmetric bending of an isotropic cylindrical shell by end load, with transverse shear deformations included. The general equations of the theory for a shell having orthotropic layers with the material axes coincident with the lines of curvature axes are given in Appendix C together with the solution of these equations for a single layer shell loaded equally at both ends by (Fig. 4-18) radial shear forces.

Since the deformations are independent of position around the cylinder, elements of any width may be used in a finite element solution. The central symmetry of the problem allows the modeling to be limited to half of the shell to be modeled. Thus a portion of the shells of length equal to one-half the total length and a width of 1 inch was divided into finite elements as shown in Fig. 4-19. To study the convergence of the procedure the number and size of the elements was varied. In some cases the size of the elements was equal. In other cases a portion of the shell nearer the load was divided into p smaller elements while the remaining portion near the center was divided into m larger elements. The maximum number of equations to be solved was limited to about 500 in the present calculations. The material of the shell was taken to be transversely isotropic with Young's modulus E equal to 1000 ksi and Poisson's ratio equal to 0.3. The transverse shear modulus was taken as 100 ksi. The thickness of the shell was assumed to be .1 inches. The inner radius was varied from 5 inches to 100 inches. The shell length varied with the shell thickness so as to maintain the value of $\sqrt[4]{3(1-\nu^2)}\,\frac{L}{\sqrt{Rh}}$ at about 6.5. In the calculations axisymmetry was imposed by requiring that the displacement u_θ be equal to zero everywhere and that u_x and w be independent of circumferential position. The boundary condition of symmetry about the center of the cylinder was imposed by making the displacement $\dot{u}_x$ and the transverse shear force equal to zero. At the loaded edge the axial stress was put equal to zero while the radial shear force was kept constant for all shells. The results of the calculations for the end deflection are given in Table 4-3 together with the values calculated for the exact theory of Appendix C.

The rate of convergence of the finite element results is shown in Fig. 4-19 where the ratio of the finite element and anlaytic maximum displacements is plotted as a function of the number of elements in the half-length of the shell. It should be noted that the number of elements shown is that of the triangular elements which is thus twice the number of linear axisymmetric cylinder elements. The results indicate that the thicker shells require less elements to achieve accurate displacements but that sufficient accuracy can be obtained within the equation limitations set.

The displacements and direct stresses obtained with the finite element analysis using the largest number elements are compared with analytic results for a long cylinder in Figures 4-21 to 4-26. The stresses were obtained by calculating the derivative of longitudinal displacements as for the beam element and combining this with the average radial displacement within the element. The very good agreement between finite element and analytic results indicates that a relatively unsophisticated element model will yield satisfactory results.

4.6 Cylindrically Curved Square Plate With a Circular Hole Under Uniform Transverse Pressure

A final problem to be treated is the effect of curvature on the deflections and stresses of a single layer square plate with a central circular hole. The developed geometry and material properties of the curved plate are similar to those of the flat plate of Section 4.4 except that the plate has a cylindrical radius of 1000 inches. Since the geometry parameter $z = (\sqrt[4]{12(1-\nu^2)}\; b^2/Rt)$ is small, the results should be similar to those for the flat plate.

One quarter of the curved plate was modeled as shown in Fig. 4-27 since the diagonal is no longer an axis of symmetry. A comparison of the radial deflections for the curved plate and those for the flat plate is given in Table 4- 4. The deflections are comparable but even a slight amount of curvature is sufficient to change the deflected shape significantly and to reduce the maximum deflection by 13%.

The distribution of stresses at the inner and outer surfaces of the curved plate are shown in Figs. 4-28 to 4-29.

CHAPTER V

CONCLUSIONS AND RECOMMENDATIONS FOR FUTURE INVESTIGATION

The results of the present investigation have indicated that the addition of shear deformations to the theory of laminated plates and shells permits the use of a simple linear displacement variation finite element model for calculations. Provided enough elements are used, accurate displacements and direct and shear stresses parallel to the layer surfaces can be obtained. Where conditions of symmetry permit the analysis to be limited to that of a small region of the structure, the elements can be made small enough while the total number of equations is kept reasonably small. However, for larger structures, the use of such a simple model in conjunction with the principle of minimum potential energy sacrifices rapidity of convergence for simplicity of calculations as compared to a similar hybrid-stress finite element model due to Mau, Tong and Pian. A linear displacement minimum potential energy element yields strains and stresses which are constant in each element and hence it does not permit the direct calculation of transverse shear and normal stresses which depend on the derivatives of the direct and shear stresses parallel to the layer surfaces. The hybrid-stress element, on the other hand, does permit the direct calculation of trnasverse shear stresses.

One would be tempted to abandon the potential energy approach were it not for the ease with wich the approach is extended to shell analysis. The extension of the hybrid-stress model is difficult, requiring the definition of a stress state within the shell wall which satisfies the equation of equilibrium and interlayer continuity conditions. Such equilibrium stress state distributions would vary with the shell geometry and would be difficult to define. Other disadvantages of the hybrid-stress model are the large amount of computer storage required to define the stress-state for each element as well as the numerous matrix inversion calculations required to obtain the combined stiffness matrix for a stack of layer elements extending through the wall thickness. These calculations increase with the number of layers. A topic for future investigation that should be pursued, therefore, is the effect of more complicated displacement variations on the accuracy and rapidity of convergence of potential energy finite element models.

The right triangle element chosen in the present investigation for ease of derivation and calculation is useful for regular structures. It is inconvenient for irregular structures, however, since it does not permit complete flexibility in the use of small triangles in a region of rapid stress variation and larger triangles in regions of slow variation. With the right triangle, the small triangle dimensions affect the size of the larger triangles. Thus the analysis should be extended to triangles of arbitrary shape.

In the absence of these extensions, the analysis technique developed in the present paper is useful but may require the solution of an extremely large number of simultaneous equations for accurate displacement and stress states in layered structures.

BIBLIOGRAPHY

1. Judge, John F., "Composite Matieral, the Coming Revolution," Airline Management and Marketing, Sept. 1969, pp. 85-91.
2. Jones, Robert M., Mechanics of Composite Materials, McGraw-Hill Book Co., 1975.
3. Dong, S.B., Pister, K.S., and Taylor, R.L., "On the Theory of Laminated Anisotropic Shells and Plates," J. Aero. Sci., Vol. 29, 1962, pp. 969-975.
4. Whitney, J.M. and Leissa, A.W., "Analysis of Heterogeneous Anisotropic Plates," Paper No. 69-APM-15, presented at ASME Applied Mechanics and Fluid Engineering Conference, Northwestern University, June 16-18, 1969.
5. Stavsky, Y., "On the Theory of Heterogeneous Plates," Doctoral Dissertation, MIT, Cambridge, Mass., 1959. Also Air Force Technical Documentary Report No. WADD-TR-60-746.
6. Reissner, E. and Stavsky, Y., "Bending and Stretching of Certain Types of Heterogeneous Aeolotropic Elastic Plates," J. Applied Mechanics, Vol. 28, 1961, pp. 402-408.
7. Yang, P.C., Norris, C.H. and Stavsky, Y., "Elastic Wave Propagation in Heterogeneous Plates," J. of Applied Mechanics, Vol. 35, No. 3. Trans. ASME Vol. 90 Series E. Sept. 1968, pp. 467-475.
8. Ambartsymyan, S.A., Theory of Anisotropic Plates, translated from Russian by T. Cheron and Edited by J.E. Ashton, Technomic Publishing Co., 1968.

9. Whitney, J.M., "The Effect of Transverse Shear Deformation on the Bending of Laminated Plates," J. of Composite Material, Vol. 3, No. 3, July 1969, pp. 534-547.

10. Wu, C.I. and Vinson, J.R., "On the Free Vibrations of Plates and Beams of Pyrolytic Graphite Type Materials," AIAA Ppaer No. 69-55, Presented at AIAA 7th Aerospace Science Meeting, New York, January 20-22, 1969.

11. Whitney, J.M. and Pagano, N.F., "Shear Deformation in Heterogeneous Anisotropic Plates," J. of Applied Mechanics, Dec. 1970, pp. 1031-1037.

12. Pagano, N.F., "Analysis of the Flexure Test of Bidirectional Composites," J. Composite Material, Vol. 1, 1967, p. 336.

13. Pagano, N.F., "Exact Solution for Composite Laminates in Cylindrical Bending," J. Composite Material, Vol. 3, July 1969, pp. 398-411.

14. Pagano, N.F., "Exact Solution for Rectangular Bidirectional Composites and Sandwich Plates," J. Composite Material, Vol. 4, No. 7, Jan, 1970, p. 20.

15. Pagano, N.F., "Influence of Shear Coupling in Cylindrical Bending of Anisotropic Plates," J. Composite Material, Vol. 4, July 1970, p. 330.

16. Pryor, C.W. and Barker, R.M., "A Finite Element Analysis Including Transverse Shear Effects for Application to Laminated Plates," AIAA J., Vol. 9, No. 5, May 1971.

17. Spilker, R.L., "A Finite Element Model for Laminated Plates Including Transverse Shear Deformation," Aeroelastic and Structures Research Lab, MIT, ASRL TR 169-1, July 1972.

18. Mau, S.T., Tong, P. and Pian, T.H.H., "Finite Element Solution for Laminate Thick Plates," J. Composite Materials, Vol. 6, April 1972, pp. 304-311.

19. Spilker, R.L., Chou, S.C., and Orringer, O., "Alternate Hybrid-Stress Elements for Analysis of Multilayer Composite Plates," J. Composite Material, Vol. 11, Jan. 1977, pp. 51-70.

20. Anon., "One Dimensional Adaptive Quadrative and Multidimensional Adaptive Quadrative, " JPL Fortran V Subprogram Directory, Edition S 13.1-1, 13.2-1, Feb. 1975.

21. Swift, G.W., and Heller, R.A., "Layered Beam Analysis, J. Eng. Mech. Div. ASCE, Vol. 100, 1974, pp. 267-282.

22. Heller, R.A., "Interlaminar Shear Stress in Sandwich Beams," Experimental Mechanics, Vol. 26, 1969, p. 413.

23. Heller, R.A., and Swift, G.W., "Solutions for the Multilayer Timoshenko Beam," Report No. VPI-E.71-12, Dept. Eng. Sci. and Mech., Virginia Polytechnic Institute and State University, Blacksbury, Va., 1971.

24. Swift, G.W., and Heller, R.A., "Laminated Beams with Arbitrary Stacking Sequence," Report No. VPI-E-72-21, Dept. Eng. Sci. and Mech., Virginia Polytechnic Institute and State University, Blackburg, Va., 1972.

25. Durocher, L.L., and Solecki, R., "Steady-State Vibrations and Bending of Transversely Isotropic Three-Layer Plates," Developments in Mechanics, Vol. 8, Proceedings of 14th Midwestern Mechanics Conference, University of Oklahoma.

26. Durocher, L.L. and Solecki, R., "Bending and Vibration of Transversely Isotropic Two-Layer Plates," AIAA J., Vol. 13, 1975, pp. 1522-1523.

27. Boal, J.L., and Reissner, E., "Three-Dimensional Theory of Elastic Plates with Transverse Inextensibility," J. Math. Phys., Vol. 39, 1961, pp. 161-181.

28. Libove, C., and Bardorf, S.B., "A General Small-Deflection Theory for Flat Sandwich Plates," NACA Rep. 899, 1948.

29. Seide, Paul, Small Elastic Deformation of Thin Shells, Noordhoff International Publishing, Leyden, The Netherlands, 1975.

30. Wang, Chi-Teh, Applied Elasticity, McGraw-Hill Book Co., Inc., New York, 1953, pp. 7-9, 17-21.

31. Timoshenko, S. and Woinowsky-Krieger, S., Theory of Plates and Shells, McGraw-Hill Book Co., 1959.

32. Cook, R.D., Concepts and Application of Finite Element Analysis, John Wiley and Sons, Inc., 1974.

33. Bathe, K. and Wilson, E.L., Numerical Methods in Finite Element Analysis, Prentice-Hall, Inc., 1976.

34. Tuzi, Z., Phil. Mag., February, 1930, p. 210.

35. Sadowsky, M., Z. angew. Math. Mech., vol. 8, p. 107, 1928.

36. Howland, R.C.J., Proc. Roy. Soc. (London), series A, vol. 148, p. 471, 1935.

37. Schulz, K.J., Proc. Nederl. Akad. van Wetenschappen, vol. 45, pp. 233,341,457, and 542, 1942, vol. 48, pp. 282 and 292, 1945.

38. Howland, R.C.J. and Stevenson, A.C., Trans. Roy. Soc. (London), series A, vol 232, p. 155, 1933.

39. Ling, C.B., Wang, P.S. and Jing, K.S., Tech. Rept. No. 9, Bur. Aeronaut. Research, Chengtu, China, Jan. 1944.

40. Hengst, H., Z. angew. Math. Mech., vol. 18, p. 44, 1938.

41. El-Hashimy, M.M., Ausgewählte Plattenprobleme, Zürich, 1956.

r_o/a	σ_θ/q
1/8	2.028498 − 0.000707 cos 4θ − 0.000000 cos 8θ
1/4	2.119101 − 0.011014 cos 4θ − 0.000010 cos 8θ
3/8	2.289766 − 0.053591 cos 4θ − 0.000237 cos 8θ
1/2	2.582663 − 0.164303 cos 4θ − 0.002353 cos 8θ

Table 4-1 Variation with Hole Size of the Circumferential Stress for a Perforated Square Plate Under Uniform Tension

	ρ \ θ	0		π/6		π/4	
		Ref. 41	Finite Element	Ref. 41	Finite Element	Ref. 41	Finite Element
Clamped Edges	0.5	14.377	5.569	15.171	5.735	15.438	6.227
	0.6	10.692	3.293	11.889	4.015	12.299	5.200
	0.8	3.679	1.247	5.769	1.867	6.567	2.635
	1.0	0.000	0.000	1.264	0.309	2.256	0.867
	$2\sqrt{3}/3$	-	-	0.000	0.000	0.450	0.363
	$\sqrt{2}$	-	-	-	-	0.168	0.000
Singly Supported Edges	0.5	85.498	38.693	87.242	39.483	87.825	39.873
	0.6	69.414	31.169	72.581	33.265	73.644	33.990
	0.8	33.876	16.011	44.113	17.952	46.650	21.831
	1.0	0.000	0.000	17.518	6.300	23.918	11.156
	$2\sqrt{3}/3$	-	-	0.046	0.000	9.934	6.877
	$\sqrt{2}$	-	-	-	-	0.000	0.000

Table 4-2 Comparison of the Transverse Displacements of a Perforated Square Plate Under Uniform Transverse Pressure ($r_o/a = 0.5$)

Edges	ρ \ θ	0		$\pi/6$		$\pi/4$	
		Ref. 41	Finite Element	Ref. 41	Finite Element	Ref. 41	Finite Element
Clamped Edges	0.5	14.377	5.569	15.171	5.735	15.438	6.227
	0.6	10.692	3.293	11.889	4.015	12.299	5.200
	0.8	3.679	1.247	5.769	1.867	6.567	2.635
	1.0	0.000	0.000	1.264	0.309	2.256	0.867
	$2\sqrt{3}/3$	–	–	0.000	0.000	0.450	0.363
	$\sqrt{2}$	–	–	–	–	0.168	0.000
Singly Supported Edges	0.5	85.498	38.693	87.242	39.483	87.825	39.873
	0.6	69.414	31.169	72.581	33.265	73.644	33.990
	0.8	33.876	16.011	44.113	17.952	46.650	21.831
	1.0	0.000	0.000	17.518	6.300	23.918	11.156
	$2\sqrt{3}/3$	–	–	0.046	0.000	9.934	6.877
	$\sqrt{2}$	–	–	–	–	0.000	0.000

Table 4-2 Comparison of the Transverse Displacements of a Perforated Square Plate Under Uniform Transverse Pressure ($r_o/a = 0.5$)

Number of Divisions	Number of Divisions	L=12.0", R=5.0"				L=16.0", R=10.0"				L=22.0", R=20.0"				L=36.0", R=50.0"				L=50.0", R=1000.0"			
		t_p	t_m	W_f	W_f/W_e %	t_p	t_m	W_f	W_f/W_e	t_p	t_m	W_f	W_f/W_e %	t_p	t_m	W_f	W_f/W_e	t_p	t_m	W_f	W_f/W_e
2	-	3.00	-	0.5780	67.0	4.00	-	0.7654	67.5	5.50	-	0.9856	64.0	9.00	-	.12622	53.4	12.50	-	1.4565	43.9
5	-	1.20	-	0.7851	91.0	1.50	-	1.0263	90.5	2.20	-	1.3556	88.1	3.60	-	1.9040	80.5	5.00	-	2.4431	73.7
10	-	0.60	-	0.8399	97.3	0.80	-	1.1021	97.2	1.10	-	1.4819	96.3	1.80	-	2,1867	92.9	2.50	-	2.9508	89.0
15	-	0.40	-	0.8514	98.7	0.53	-	1.1185	98.7	0.73	-	1.5115	98.2	1.20	-	2.2815	96.5	1.67	-	3.1225	94.3
10	20	0.15	0.225	0.8592	99.6	0.15	0.325	1.1292	99.6	0.20	0.45	1.5302	99.5	0.25	0.775	2.3332	98.7	0.40	1.05	3.2457	97.9
20	40	0.10	0.101	0.8604	99.7	0.10	0.15	1.1316	99.8	0.10	0.225	1.5353	99.8	0.15	0.375	2.3555	99.6	0.20	0525	3.2949	99.4
40	80	0.05	0.051	0.8608	99.8	0.05	0.075	1.1321	99.9	0.05	0.113	1.5365	99.9	0.08	0.185	2.3604	99.8	0.10	0.263	3.3072	99.8
W_e (with shear)		0.8629				1.1337				1.5385				2.3641				3.3141			
W_e^* (without shear)		0.7697				1.0640				1.4880				2.3314				3.2911			
W_e/W_e^* %		112.1				106.6				103.4				101.4				100.7			

Table 4-3 Comparison of Finite Element and Analytic Values of End Deflection of a Cylindrical Shell under Axisymmetric End Load

Comparison of Curved and Flat Plate Normal Deflections

θ \ ρ	0°		30°		45°		60°		90°	
	C.P.	F.P.	C.P.	F.P.	C.P.	F.P.	C.P.	F.P.	C.P.	F.P.
0.5	4.610	5.569	5.145	5.735	5.401	6.227	5.373	5.735	5.092	5.569
0.6	3.293	3.981	4.015	4.525	4.498	5.200	3.925	4.525	3.661	3.981
0.8	1.044	1.247	1.594	1.867	2.278	2.635	1.651	1.867	2.070	1.247
1.0	0.000	0.000	0.270	0.309	0.760	0.867	0.275	0.309	0.000	0.000
$2\sqrt{3}/3$	---	---	0.000	0.000	0.322	0.363	0.000	---	---	---
$\sqrt{2}$	---	---	---	---	0.000	---	---	---	---	---

C.P. - curved plate
F.P. - flat plate

Table 4-4 Comparison of Radial Deflections for Perforated Flat and Curved Plates Under Uniform Pressure

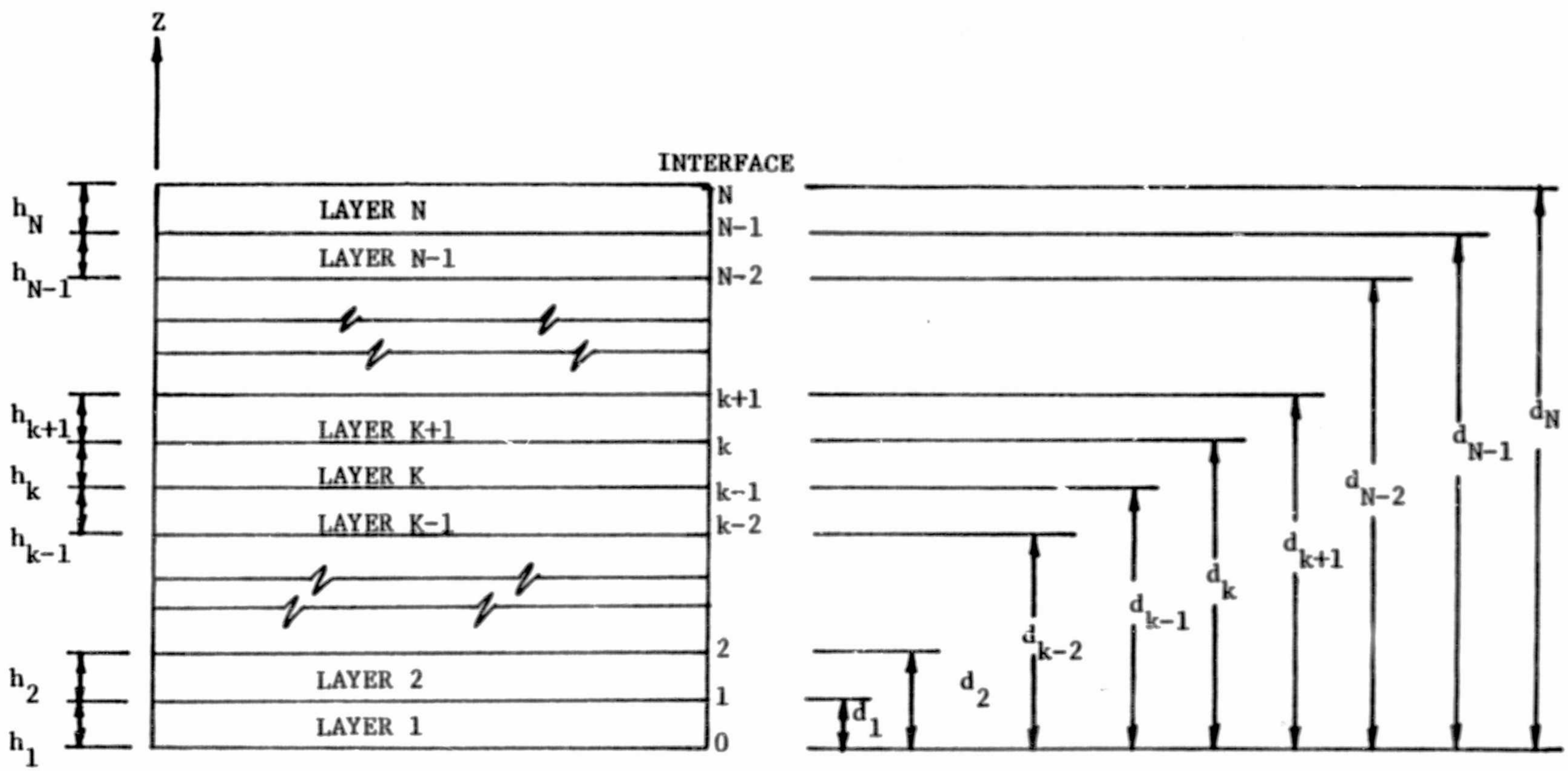

Figure 2-1 Cross-Section of a Layered Shell

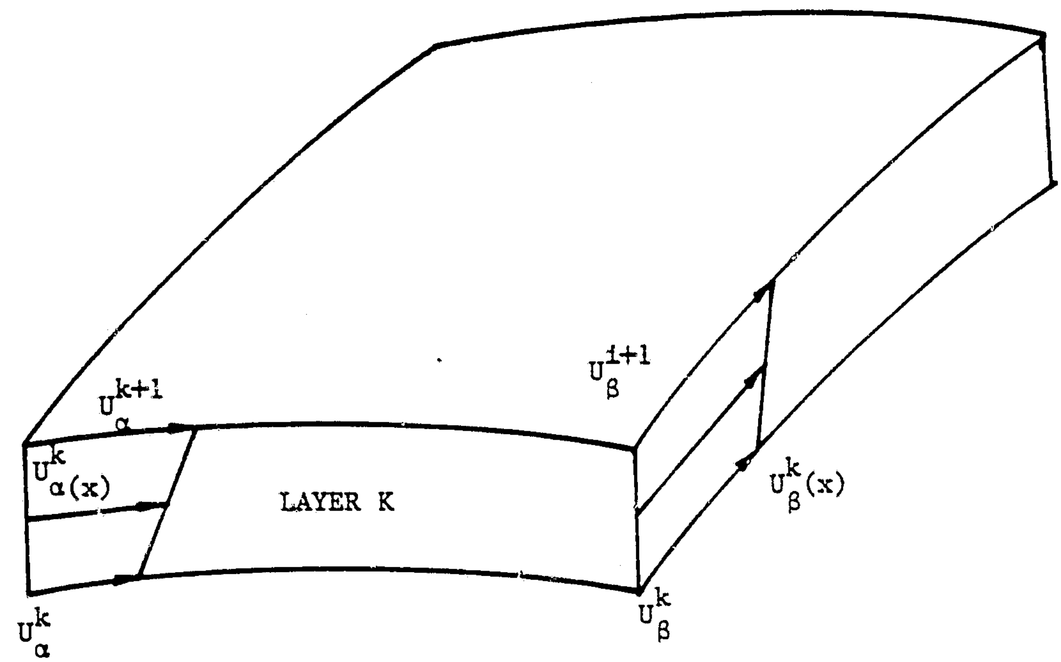

Figure 2-2 Linear Distribution of Tangential Displacements Through the Thickness of Each Layer

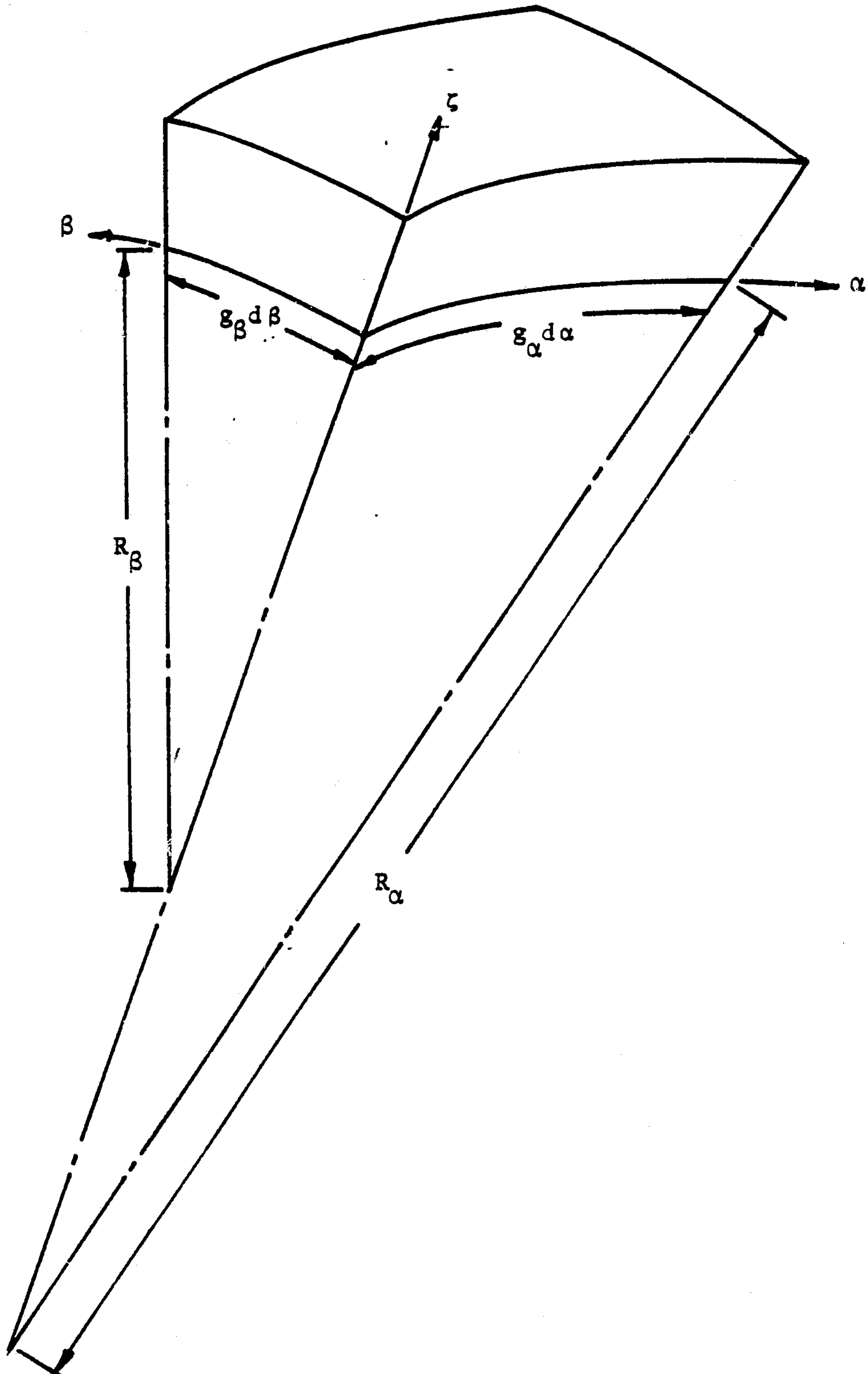

Figure 2-3 Shell Element

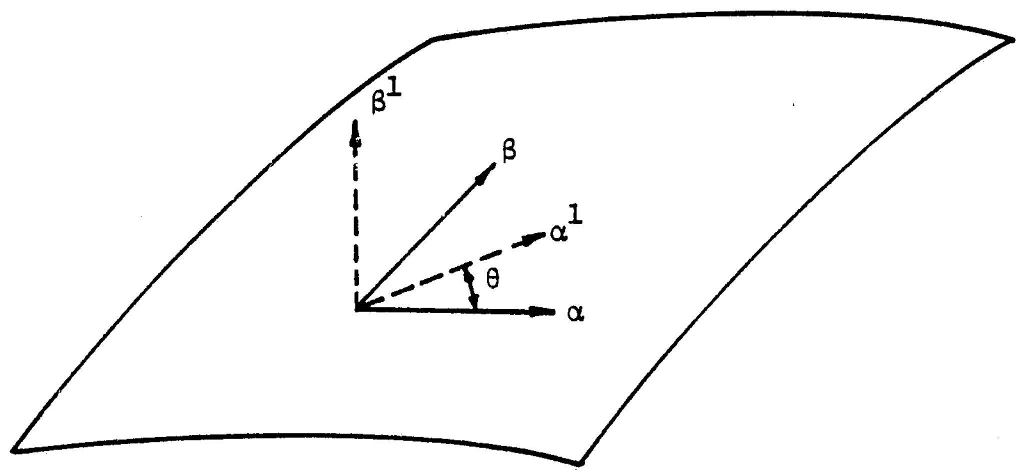

Figure 2-4 Global and Local Material Axes

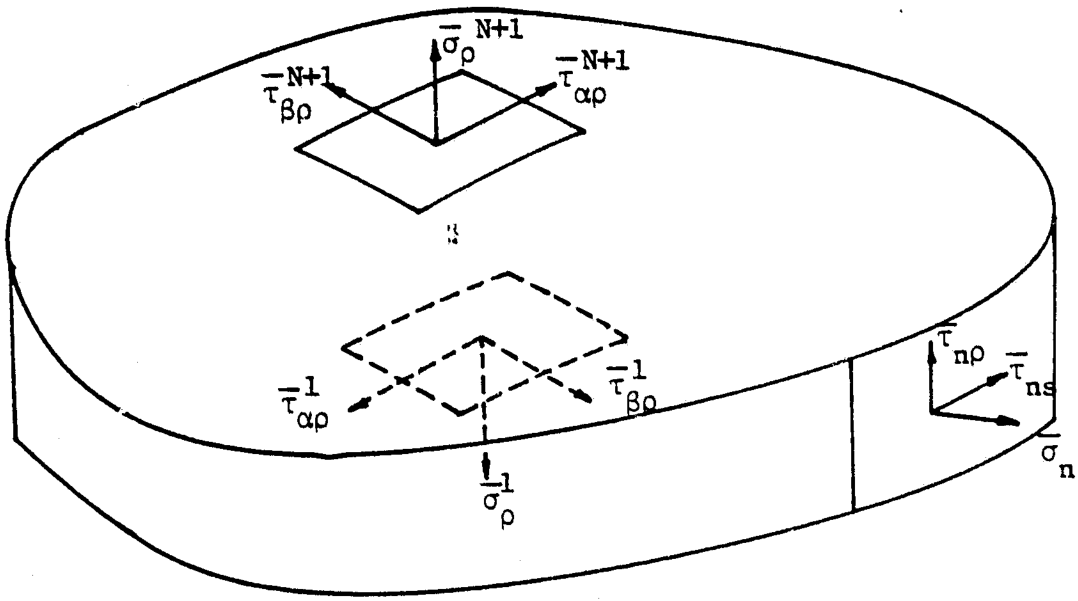

Applied Loads

Figure 2-5 Applied Surface Forces on a Shell Element

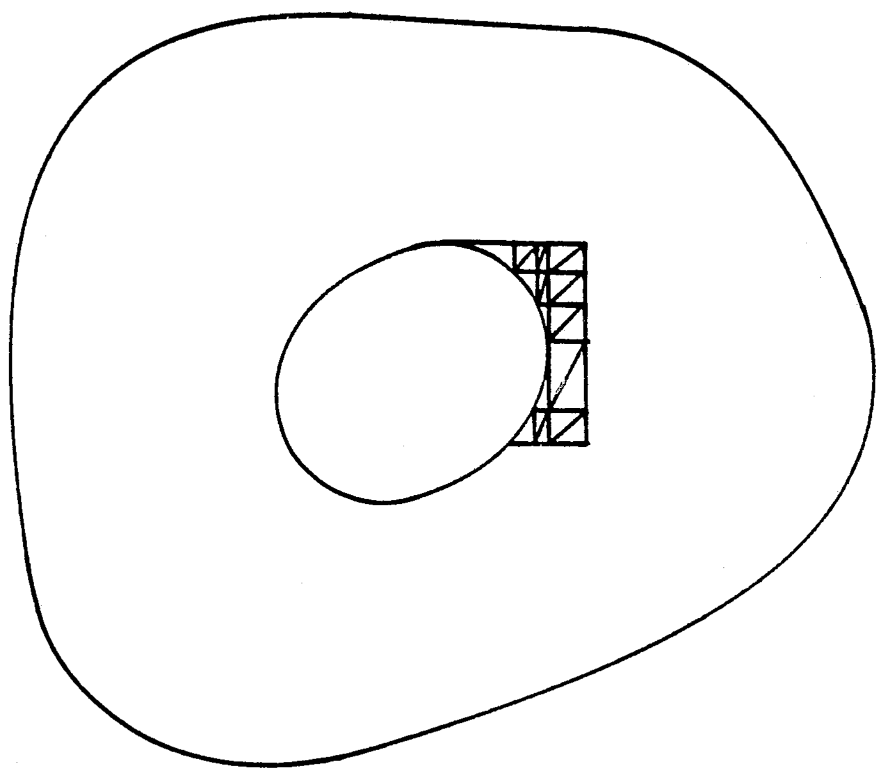

Figure 2-6 Modeling of Region with Irregular Boundary

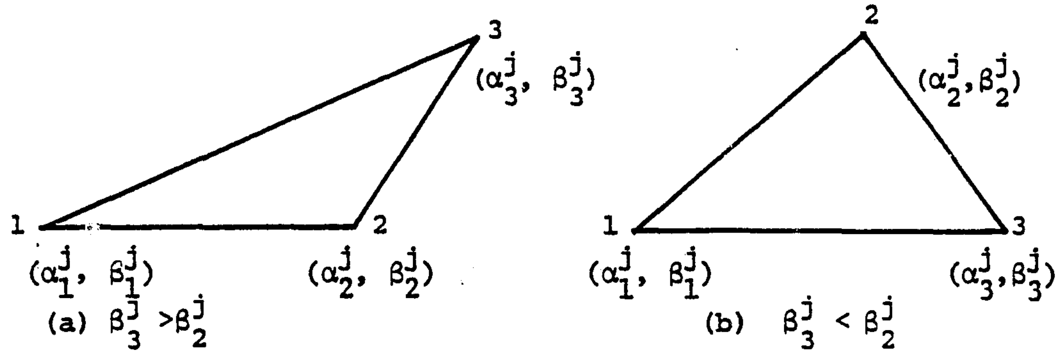

Figure 2-7

Numbering system for triangle vertices.

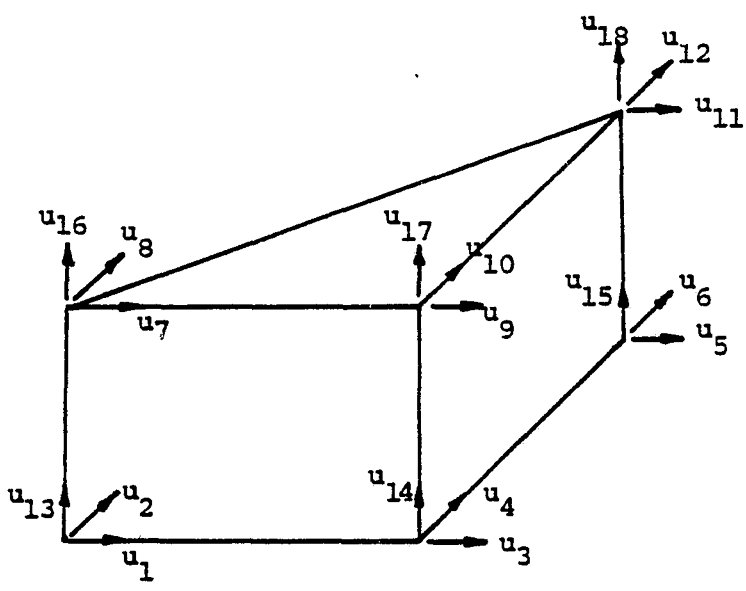

Figure 2-8

Numbering system for vertex displacements.

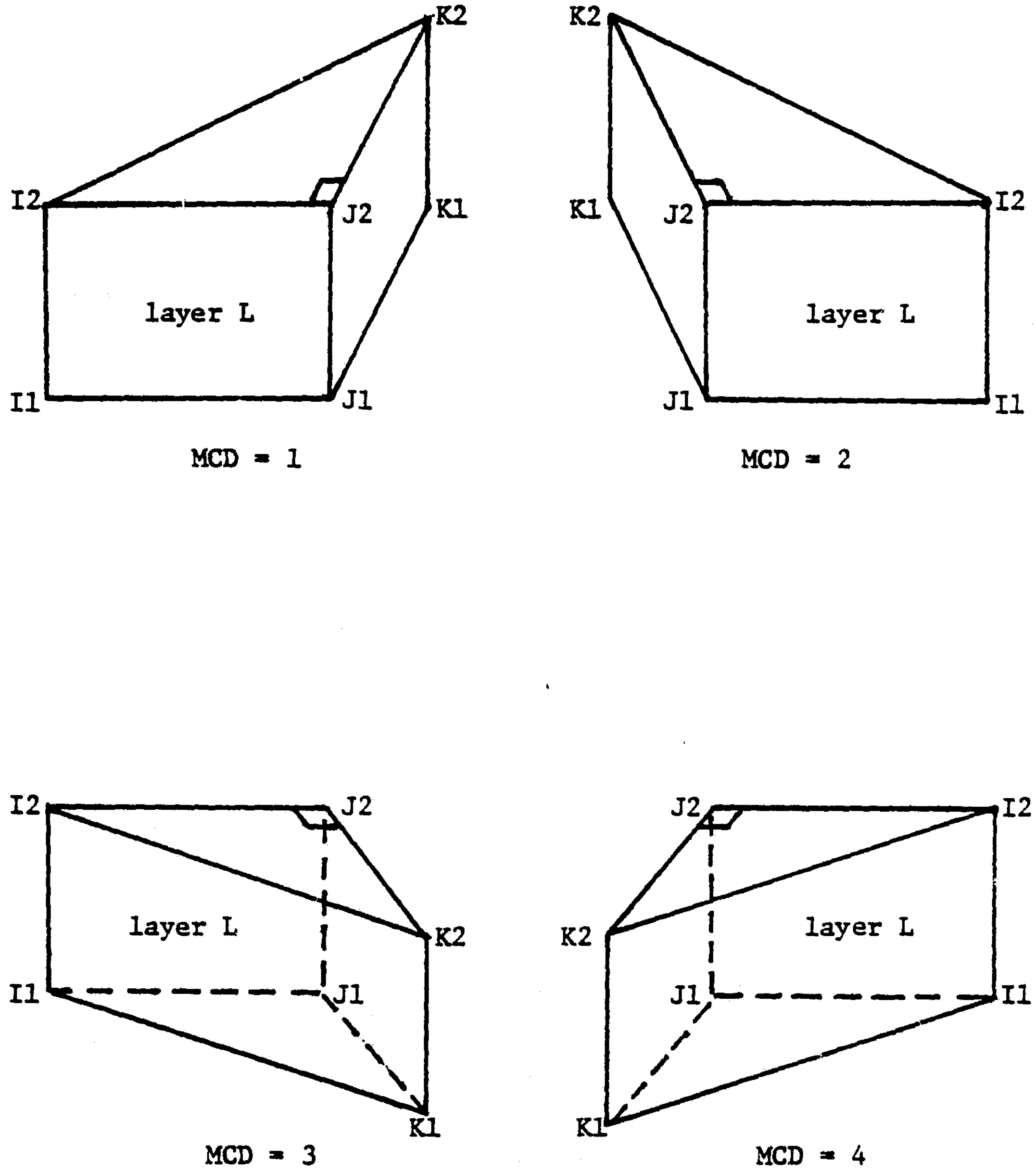

Figure 2-9 Different Element Orientations

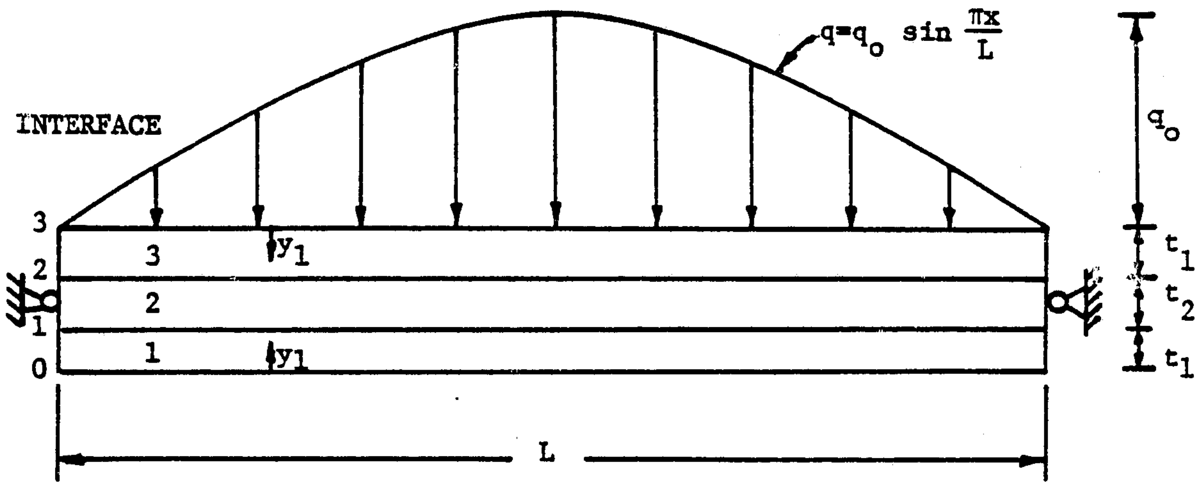

Figure 4-1 Long Laminated Plate Under Sinusoidal Surface Pressure

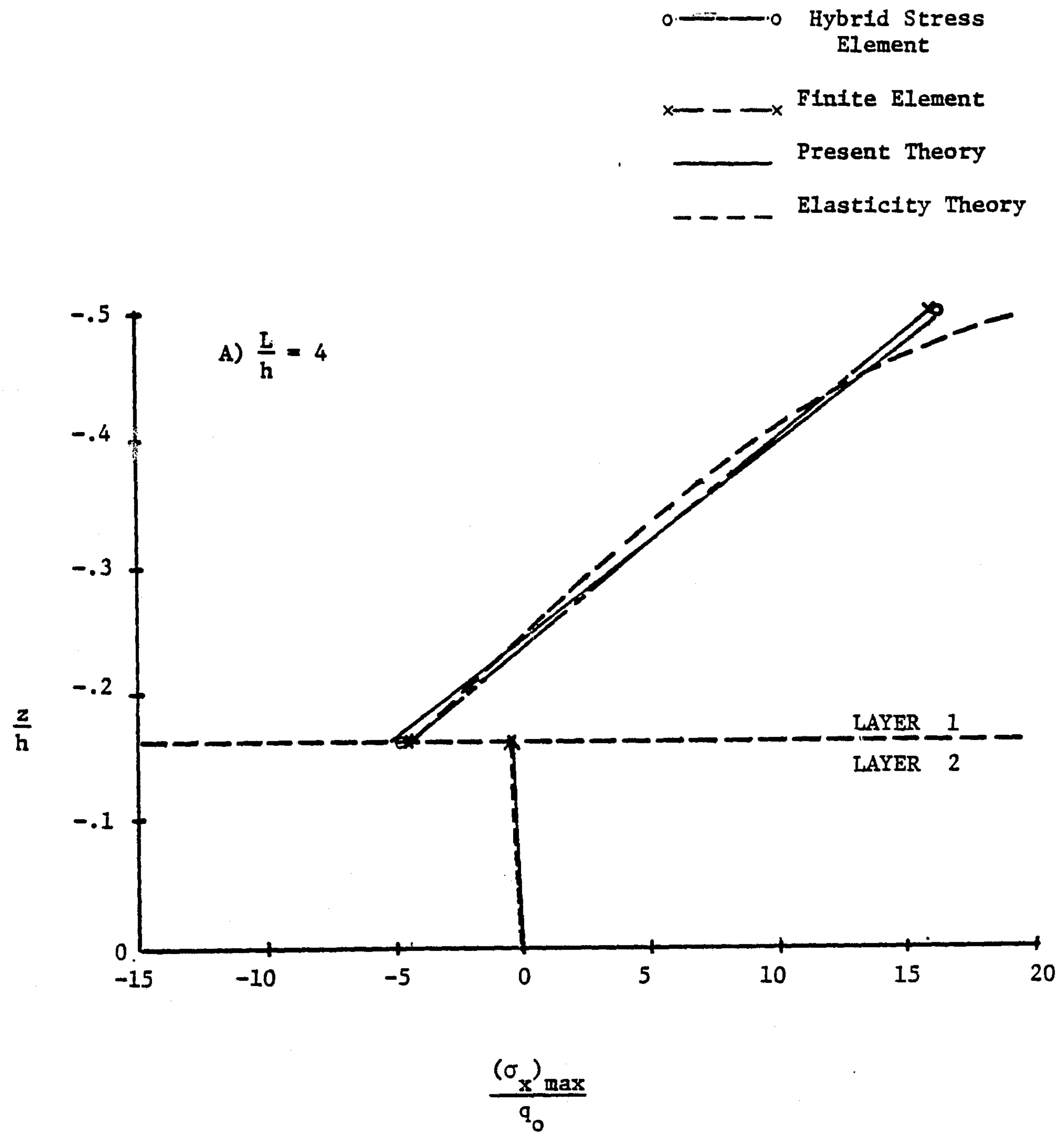

Figure 4-2a Maximum Normal Stress Distribution Through the Thickness

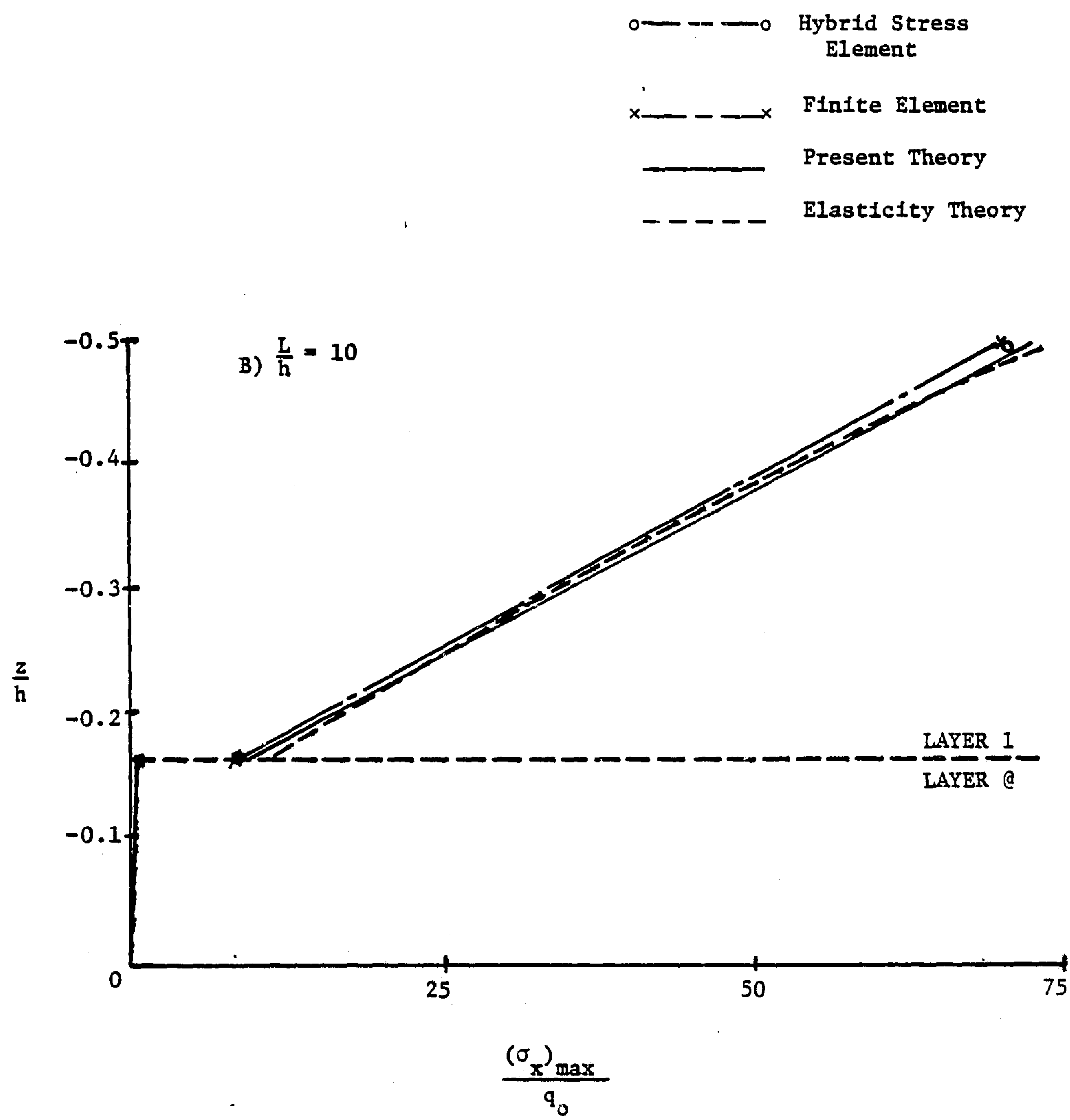

Figure 4-2b Maximum Normal Stress Distribution Through the Thickness

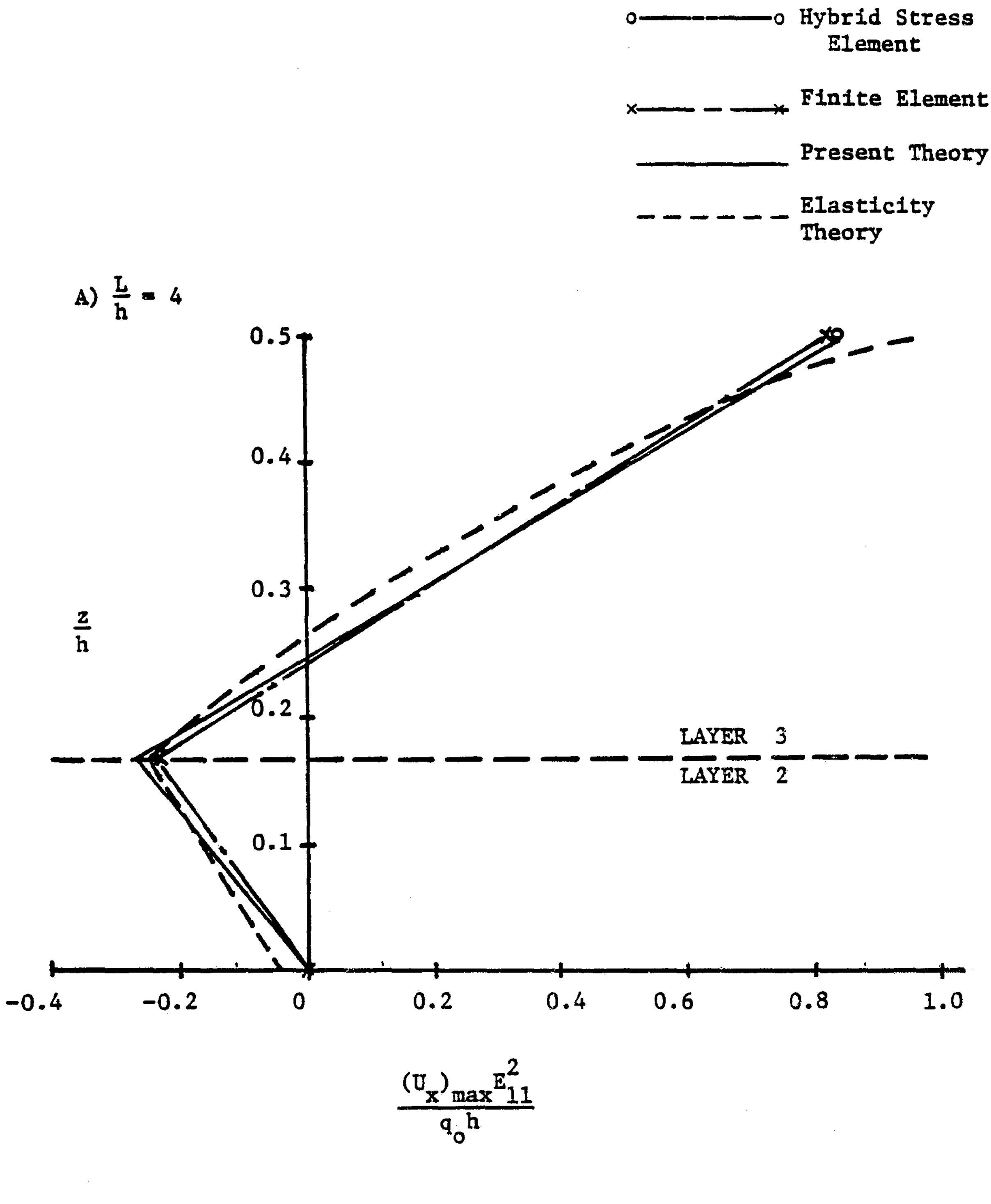

Figure 4-3a Maximum Inplane Displacement Distribution Through the Thickness

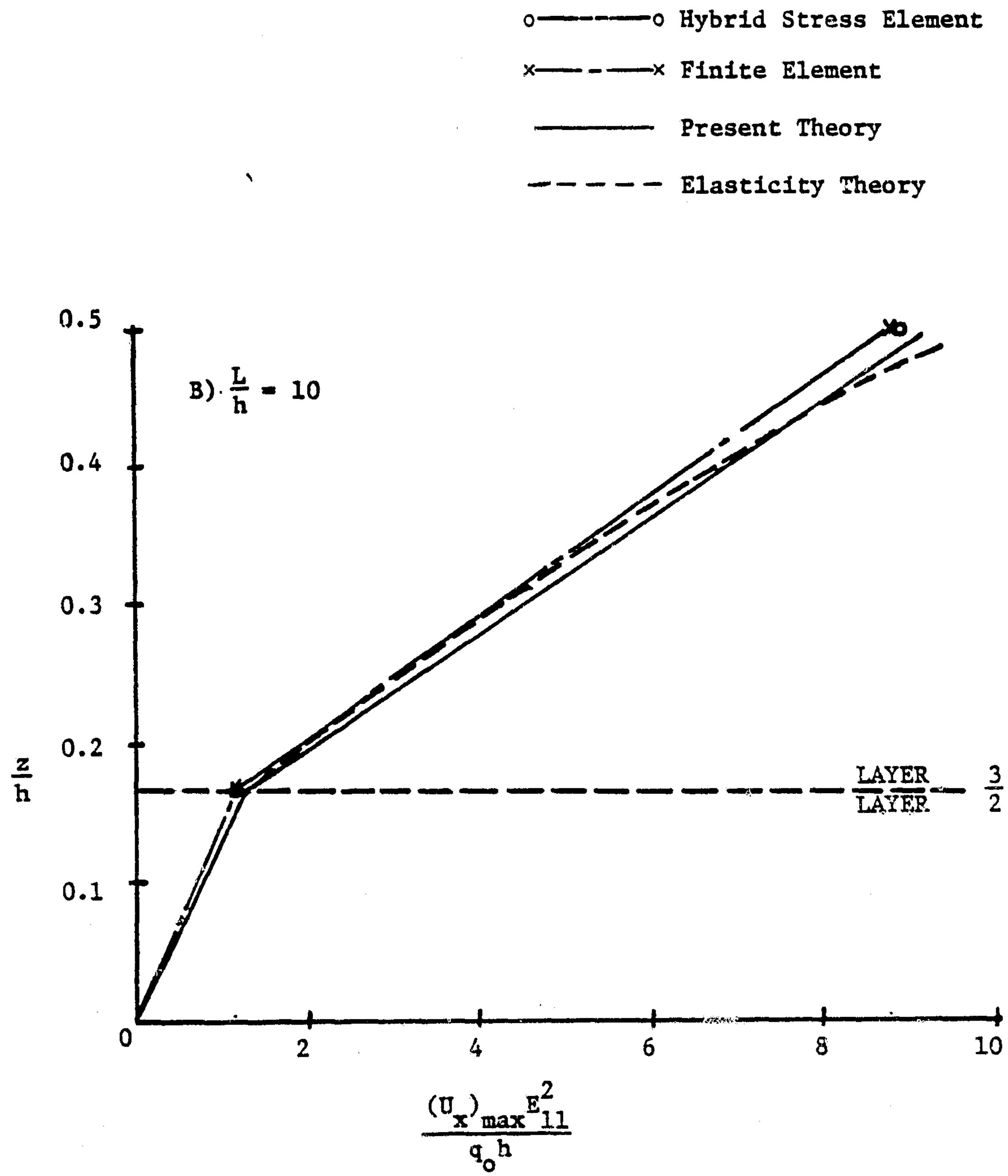

Figure 4-3b Maximum Inplane Displacement Distribution Through the Thickness

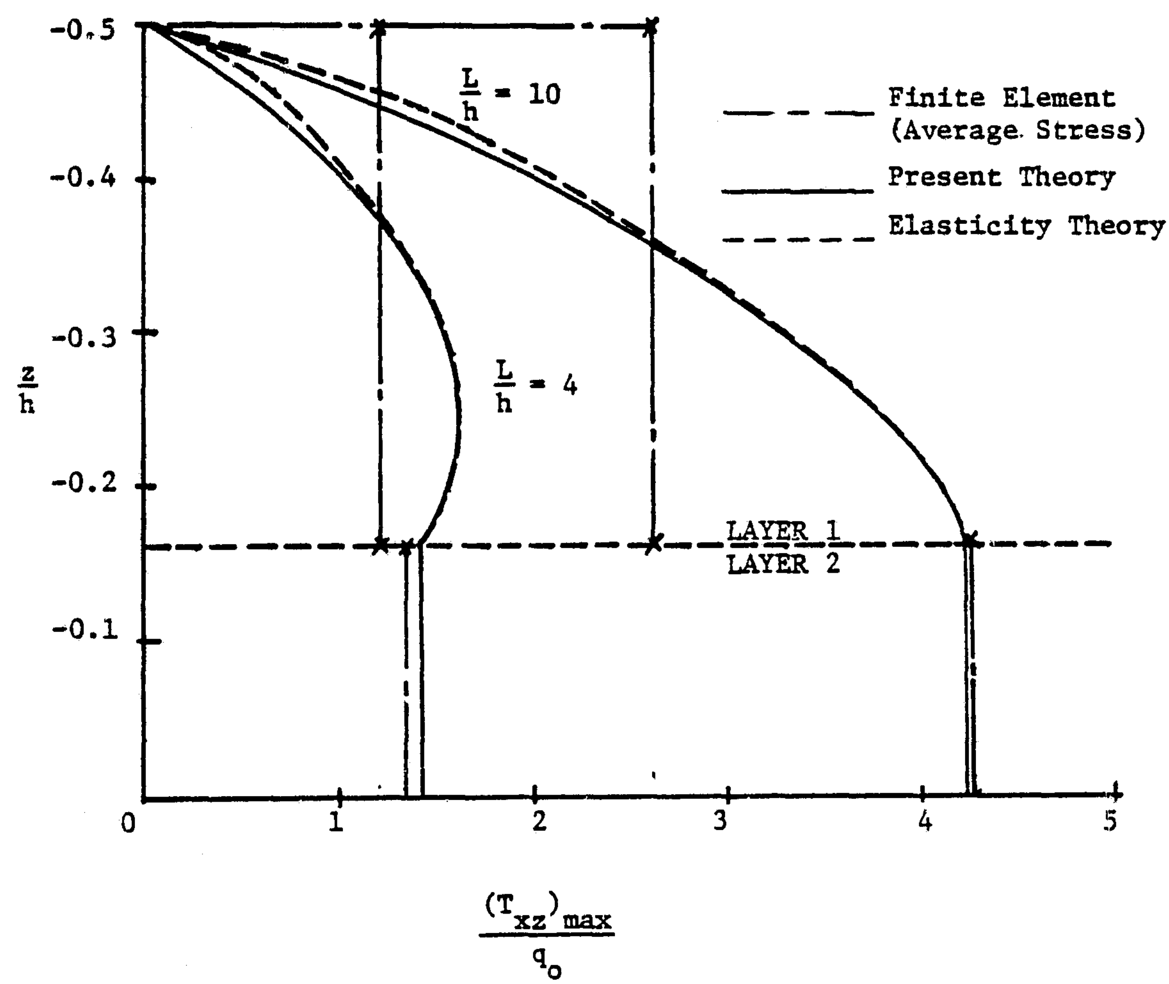

Figure 4-4 The Transverse Shear Stress Distribution Through the Thickness at the Boundary x=0

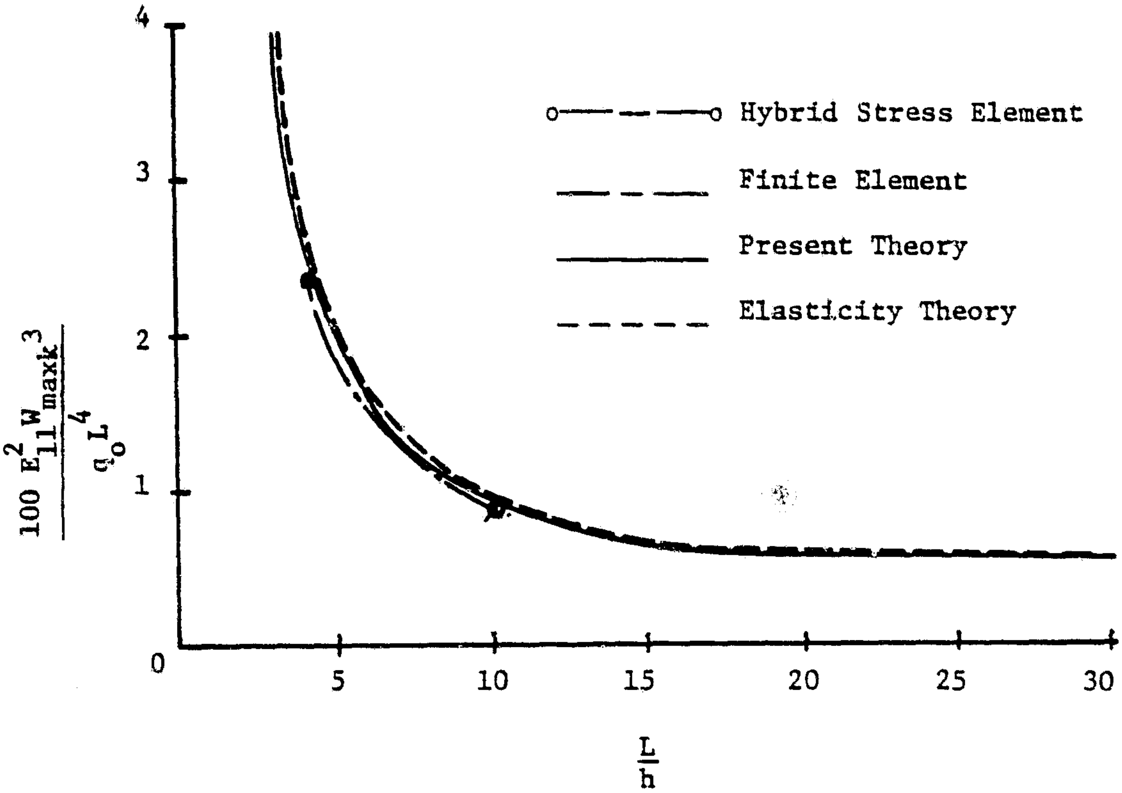

Figure 4-5 The Midplane Transverse Displacement at the Center of the Plate

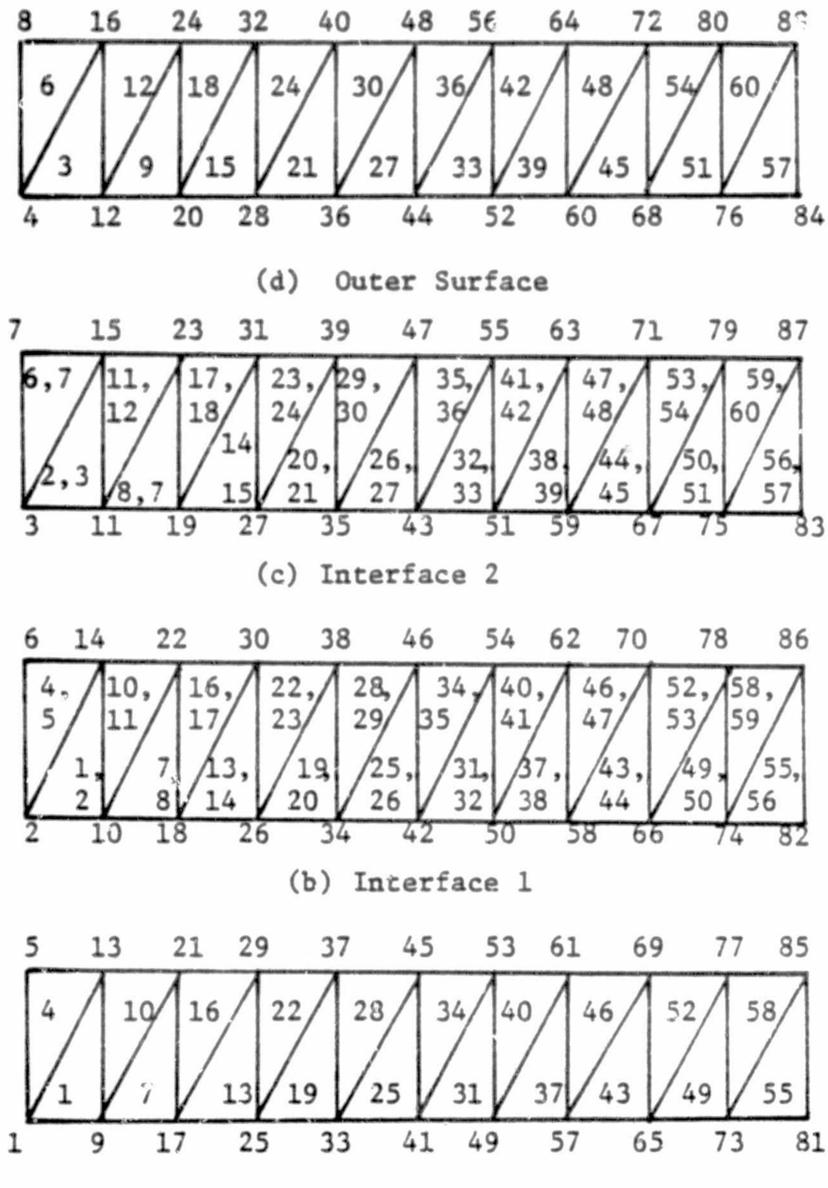

Figure 4-6 Element Numbering System for the Laminated Plate

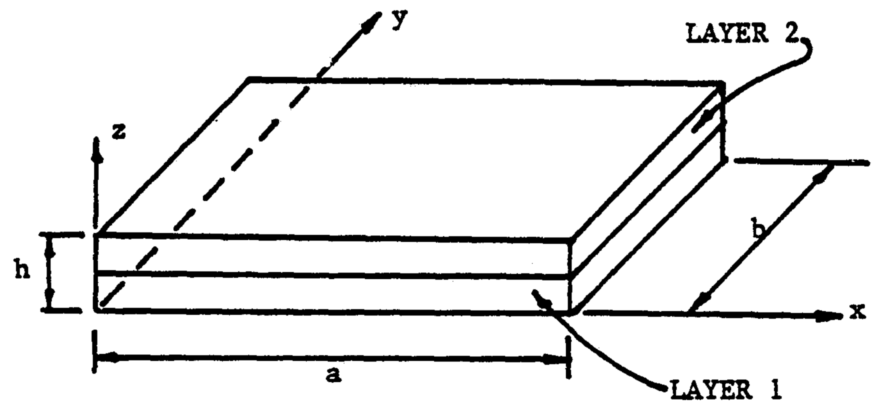

GEOMETRIC PROPERTIES: a=b=10"

MATERIAL PROPERTIES: $E_{11}=40\times10^6$ psi $E_{22}=1\times10^6$ psi

$G_{12}=G_{23}=0.5\times10^6$ psi

$\nu_{12}=\nu_{23}=0.25$

FIBER ORIENTATIONS: $-\theta$ in layer 1; $+\theta$ in layer 2

LOADING: Uniform transverse load, q_o= 100 psi

BOUNDARY CONDITIONS: Simply supported on all four sides

FINITE ELEMENT MESH: MxM square elements in entire plate

Figure 4-7 Laminated Plate Under Uniform Transverse Pressure

C-2

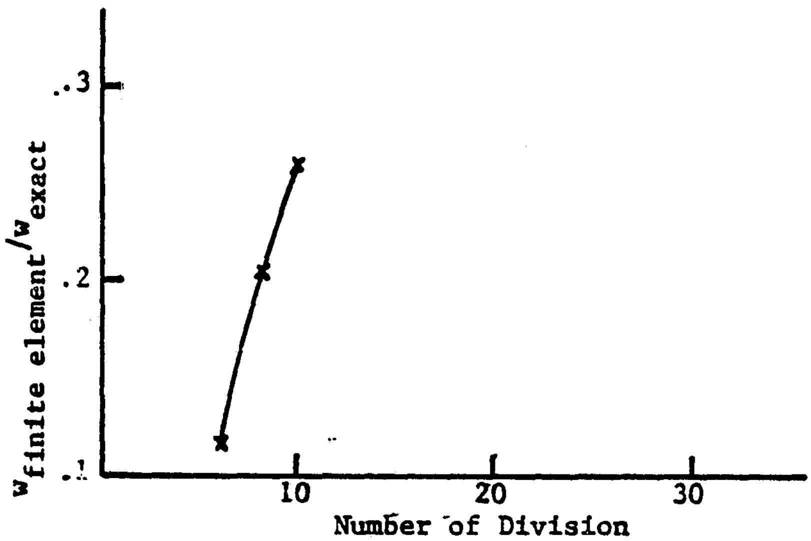

Figure 4-8 Convergence Rate for a Square Plate

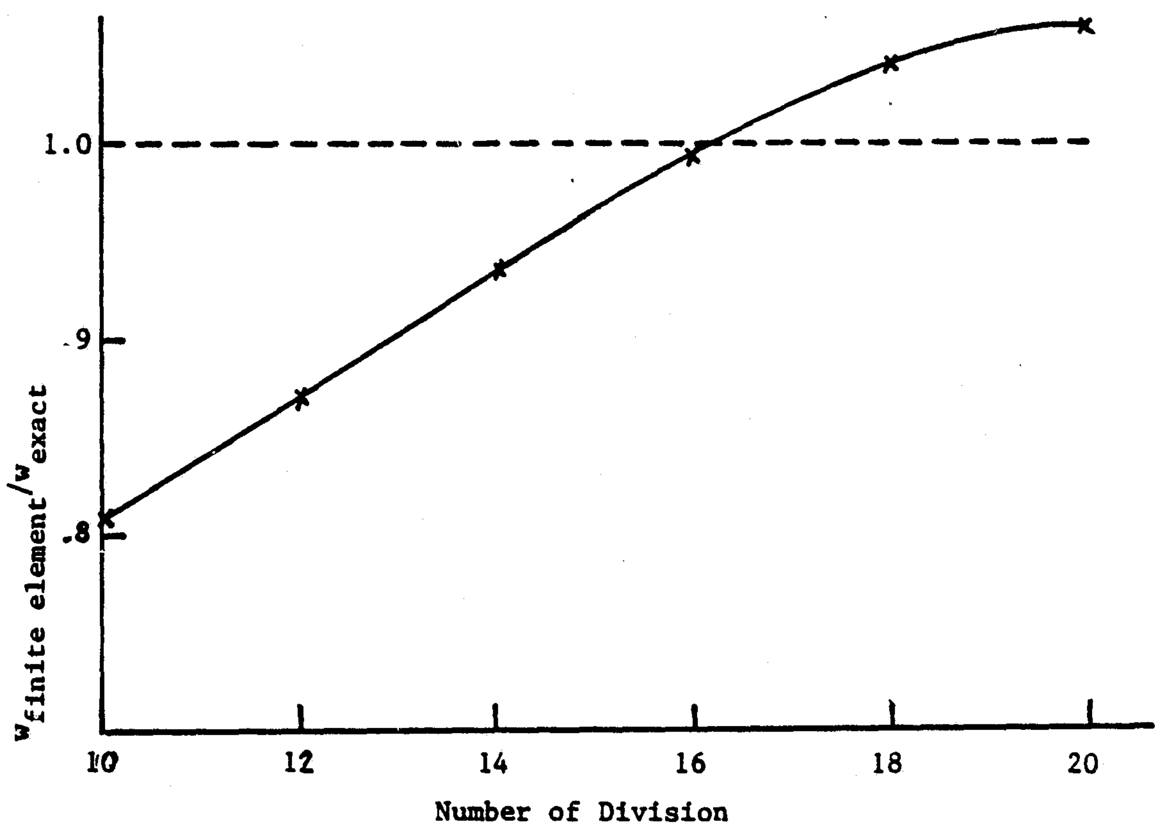

Figure 4-9 Convergence Rate of a Square Laminated Plate

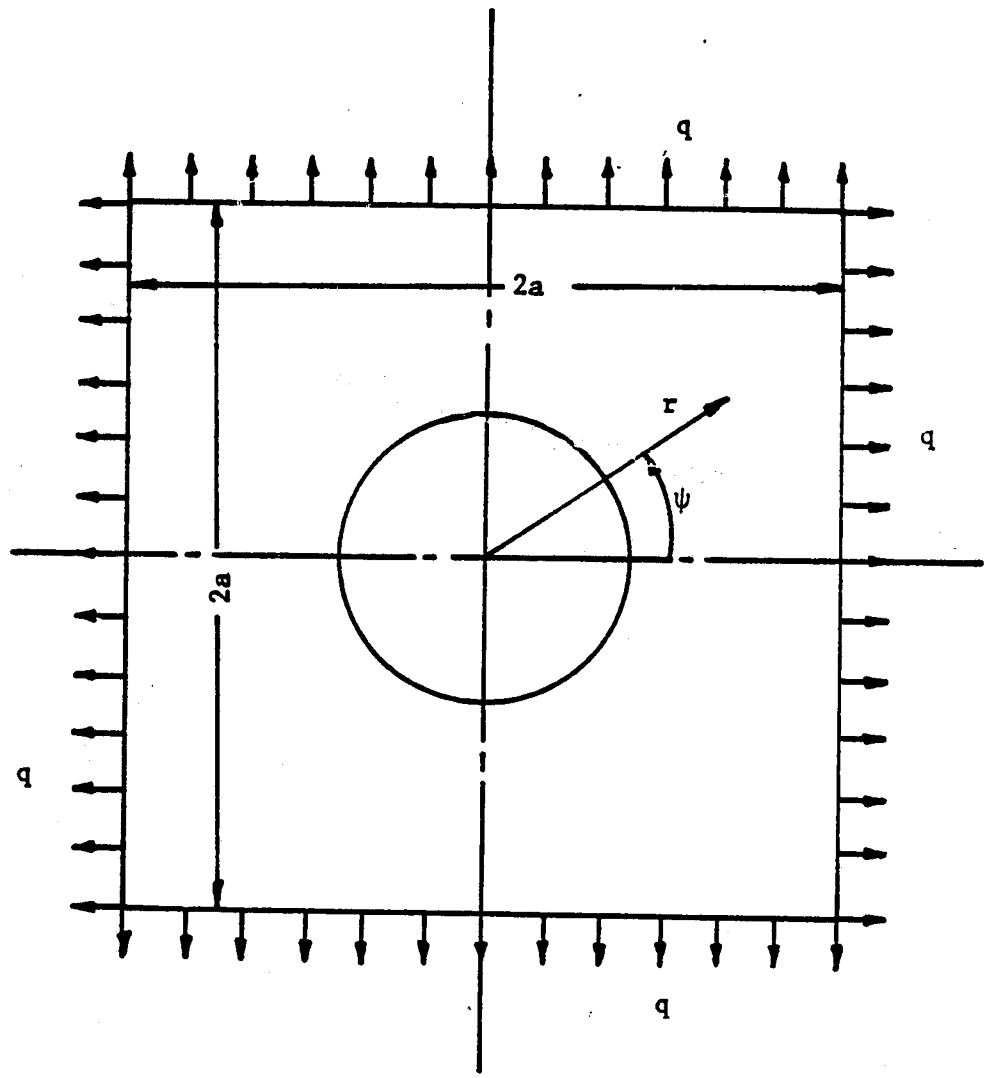

Figure 4-10 Perforated Square Plate Under Uniform Tension

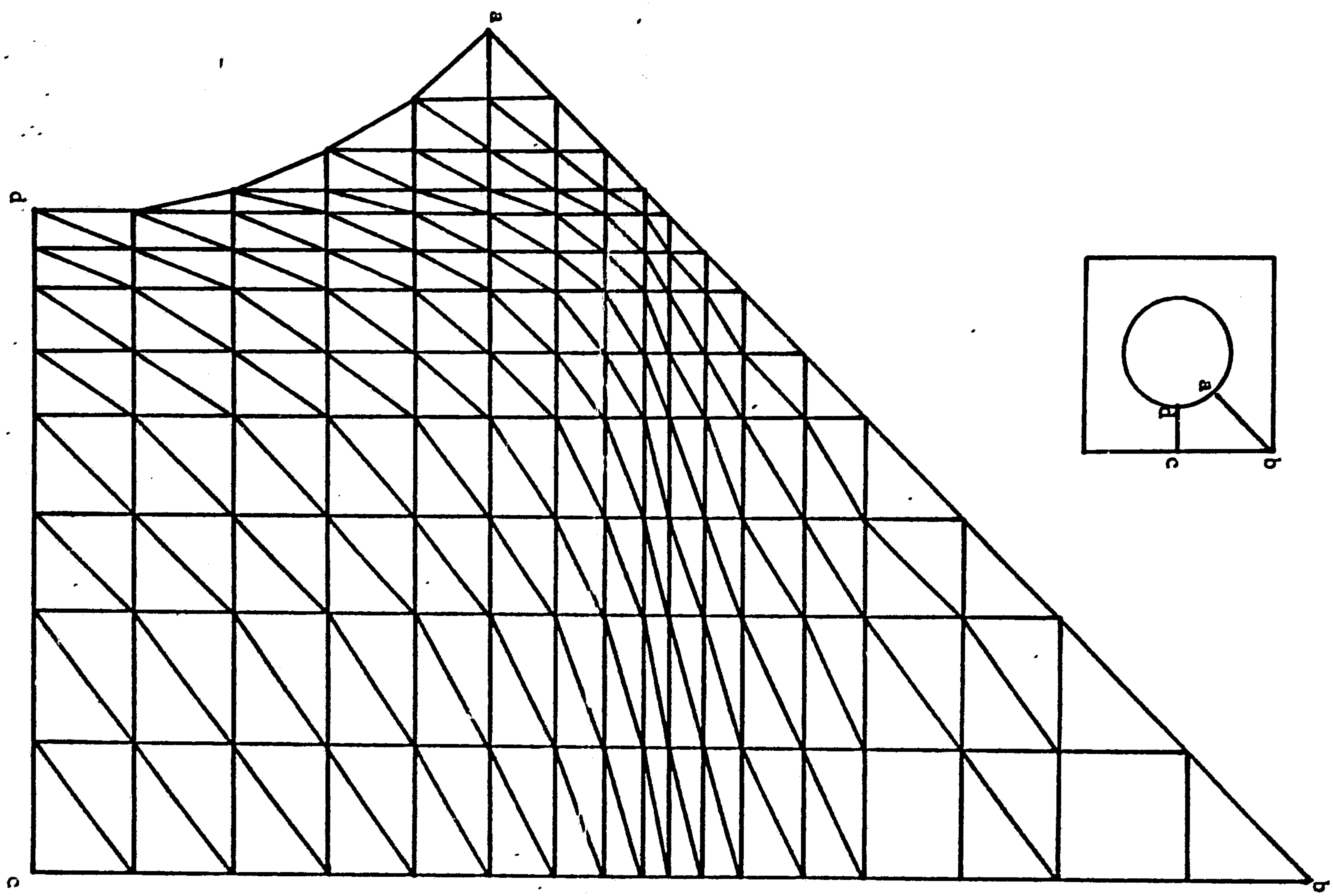

Figure 4-11 Finite Element Model

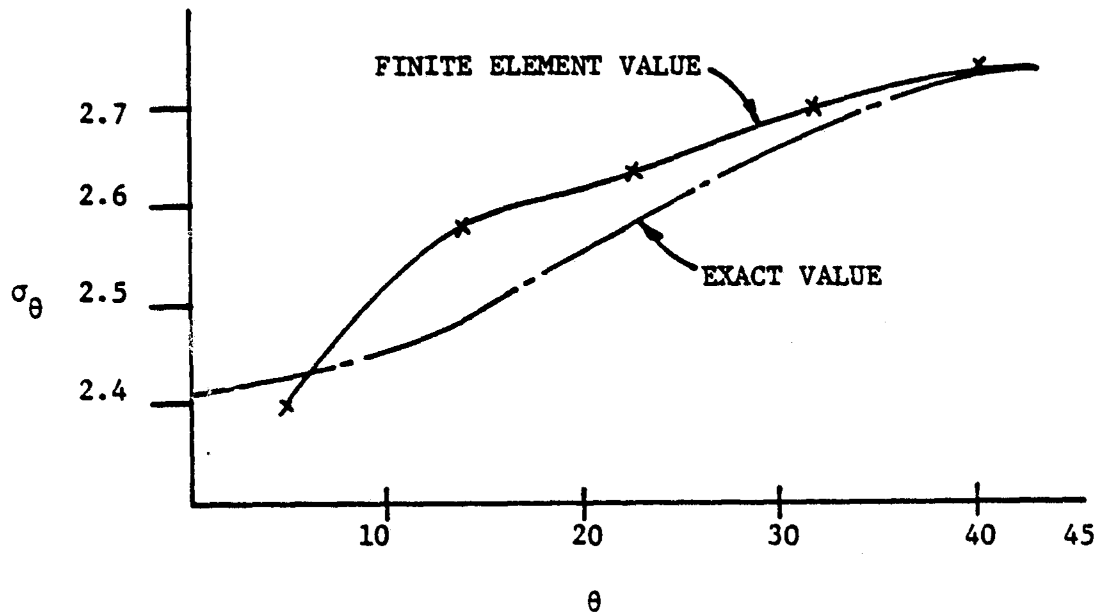

Figure 4-12 Comparison of Finite Element and Analytic Values of Circumferential Stress Around the Hole

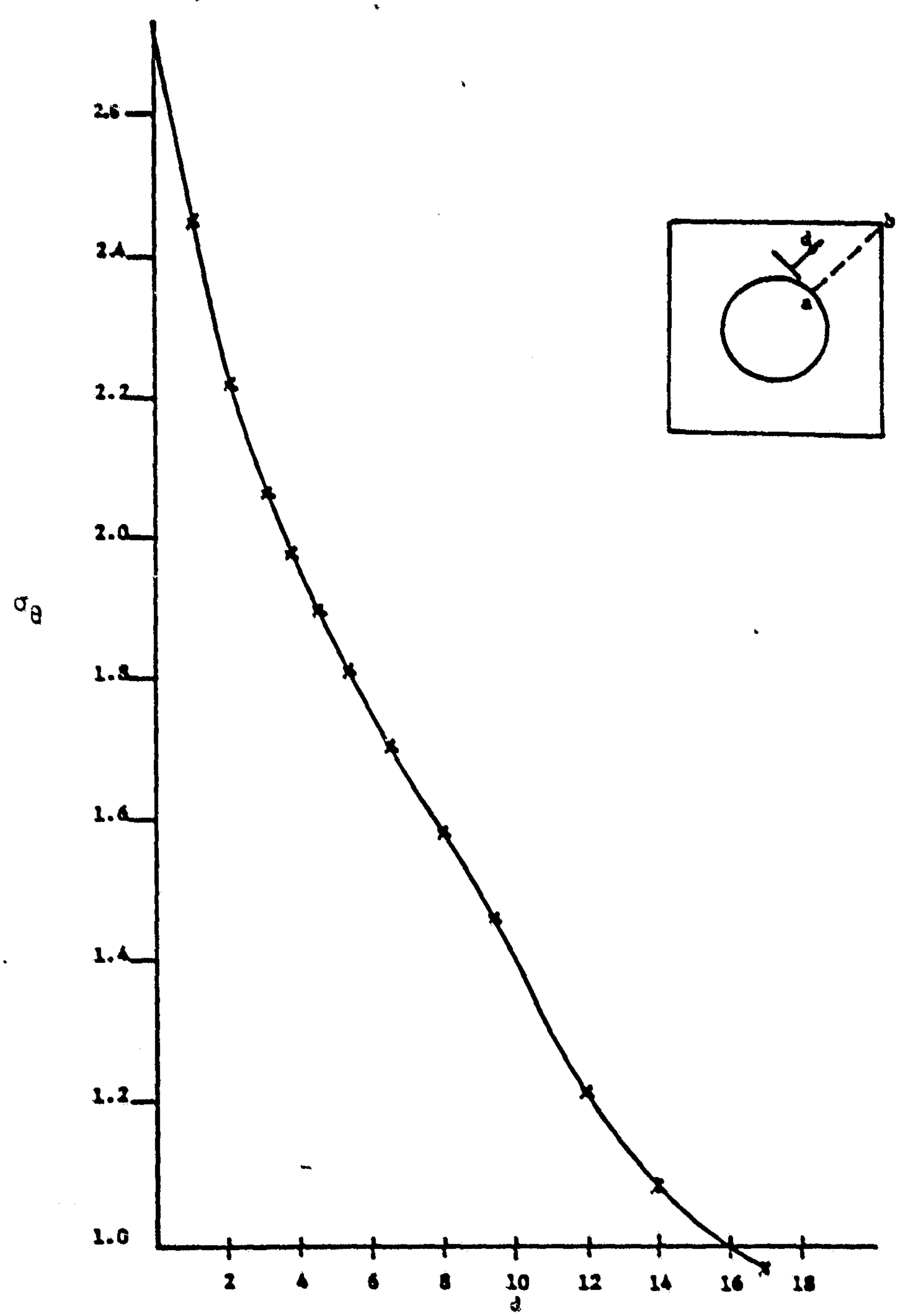

Figure 4-13 Comparison of Finite Element and Analytic Values of Circumferential Stress Along the Diagonal

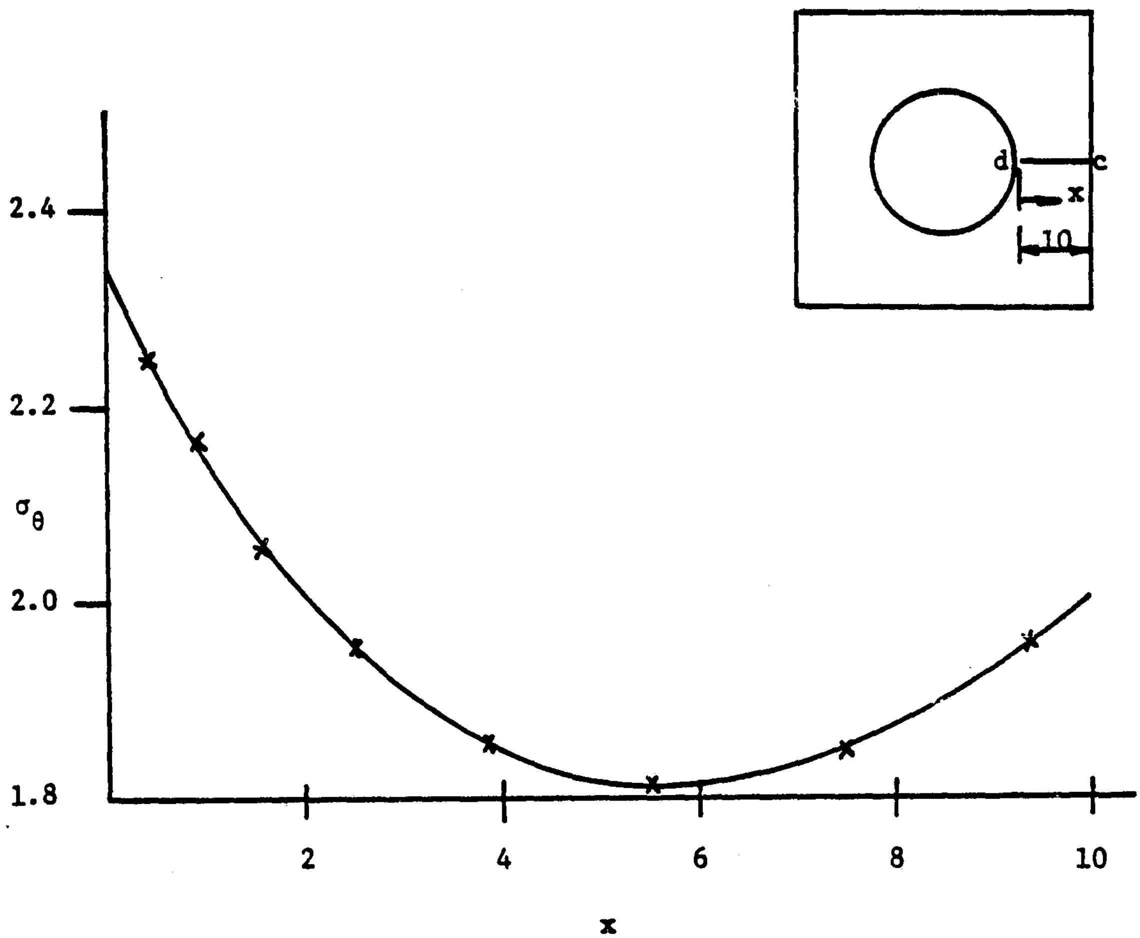

Figure 4-14 Comparison of Finite Element and Analytic Values of Circumferential Stress Along the Axis

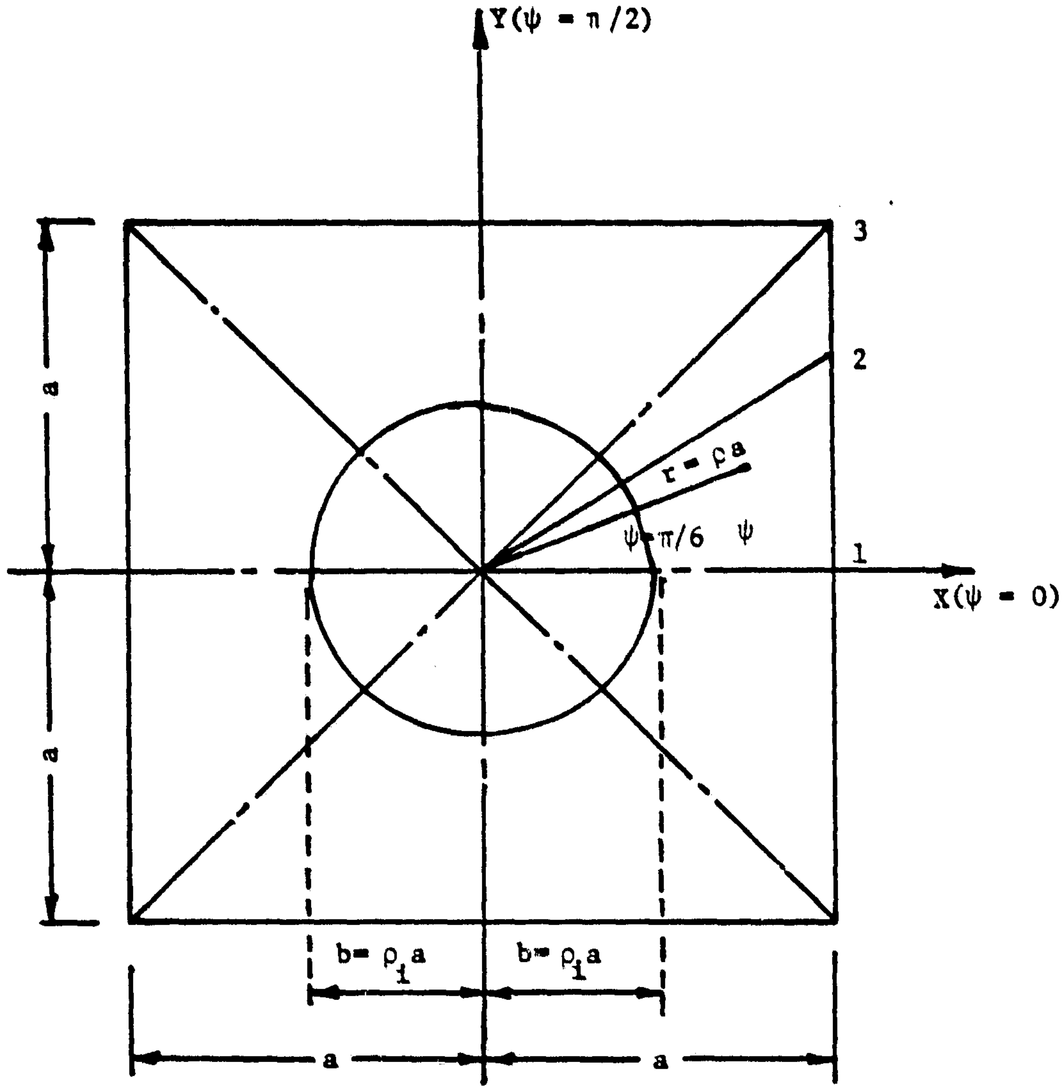

Figure 4-15 Perforated Square Plate Under Uniform Transverse Pressure

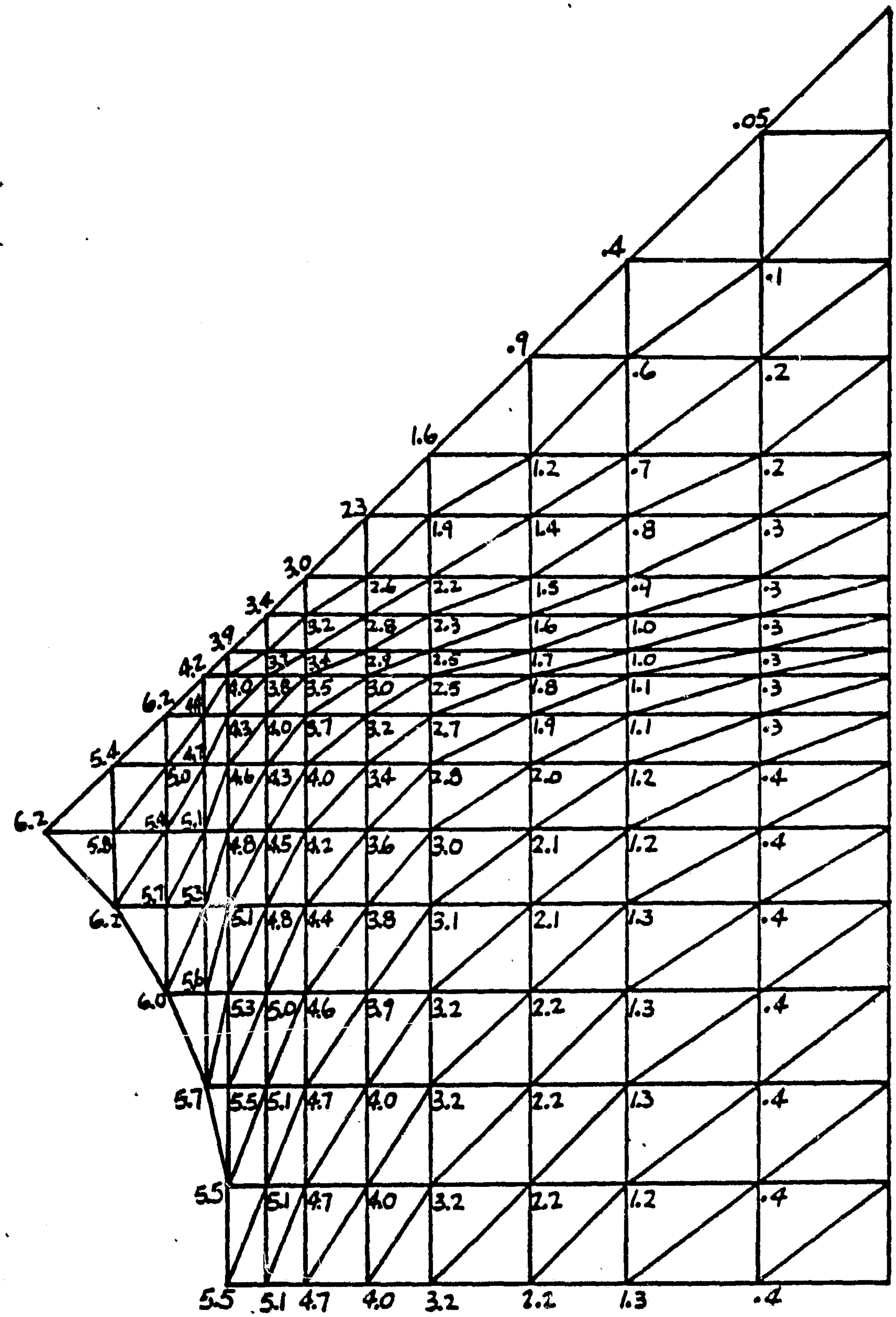

Figure 4-16 Deflection Distribution for a Perforated Square Plate with Clamped Edges

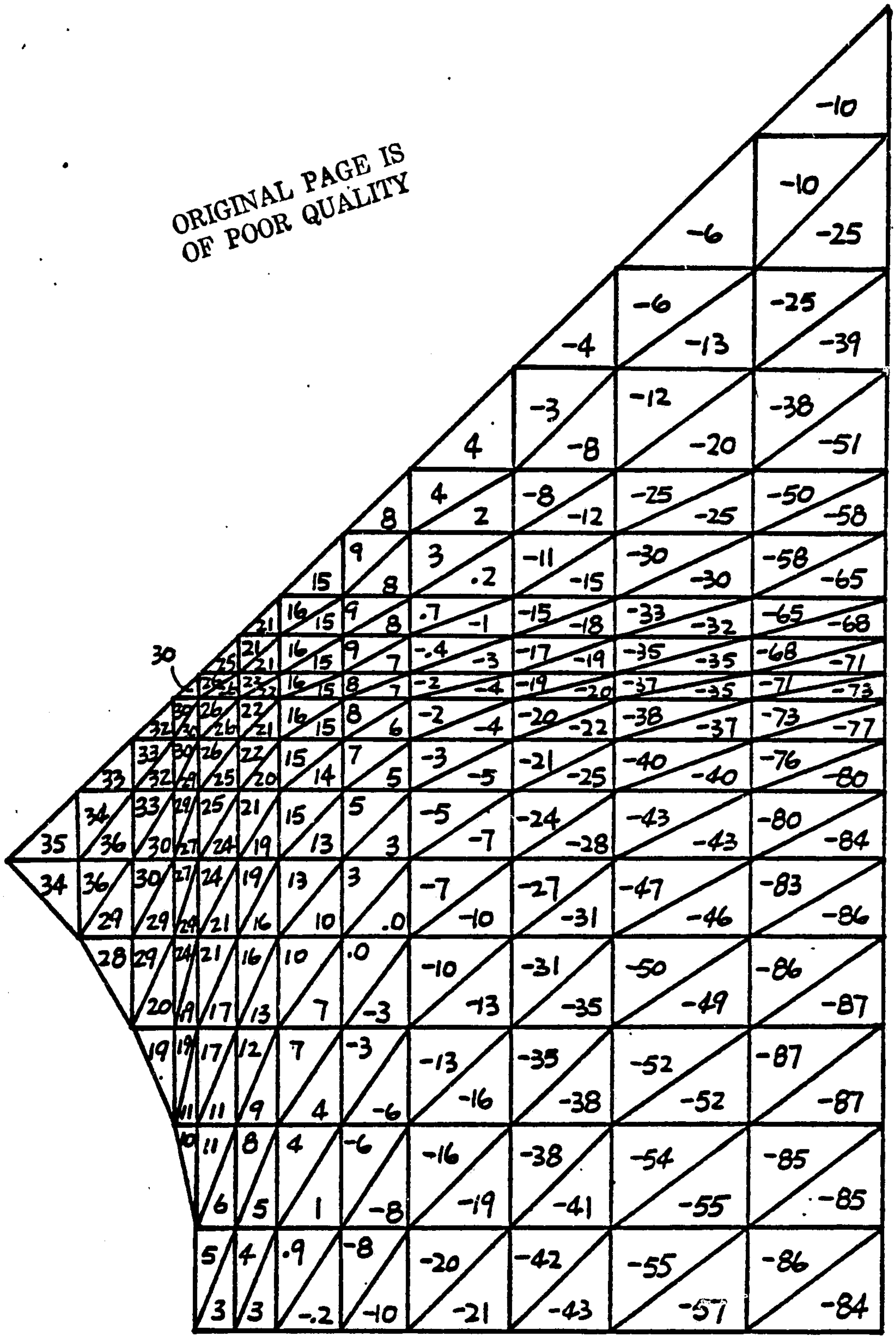

Figure 4-17a Distribution of Stresses σ_x in a Perforated Square Plate with Clamped Edges

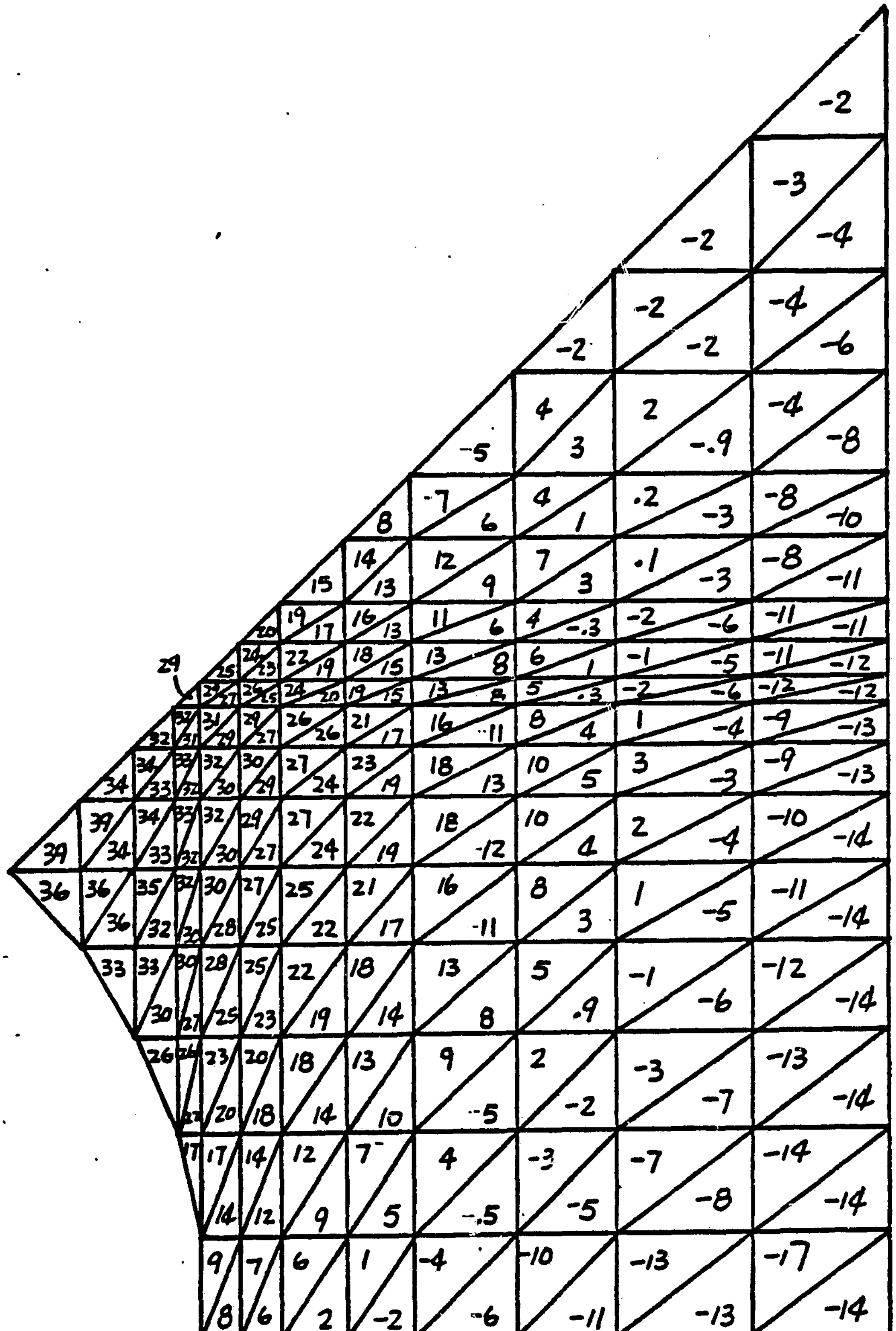

Figure 4-17b Distribution of Stresses σ_y in a Perforated Square Plate with Clamped Edges

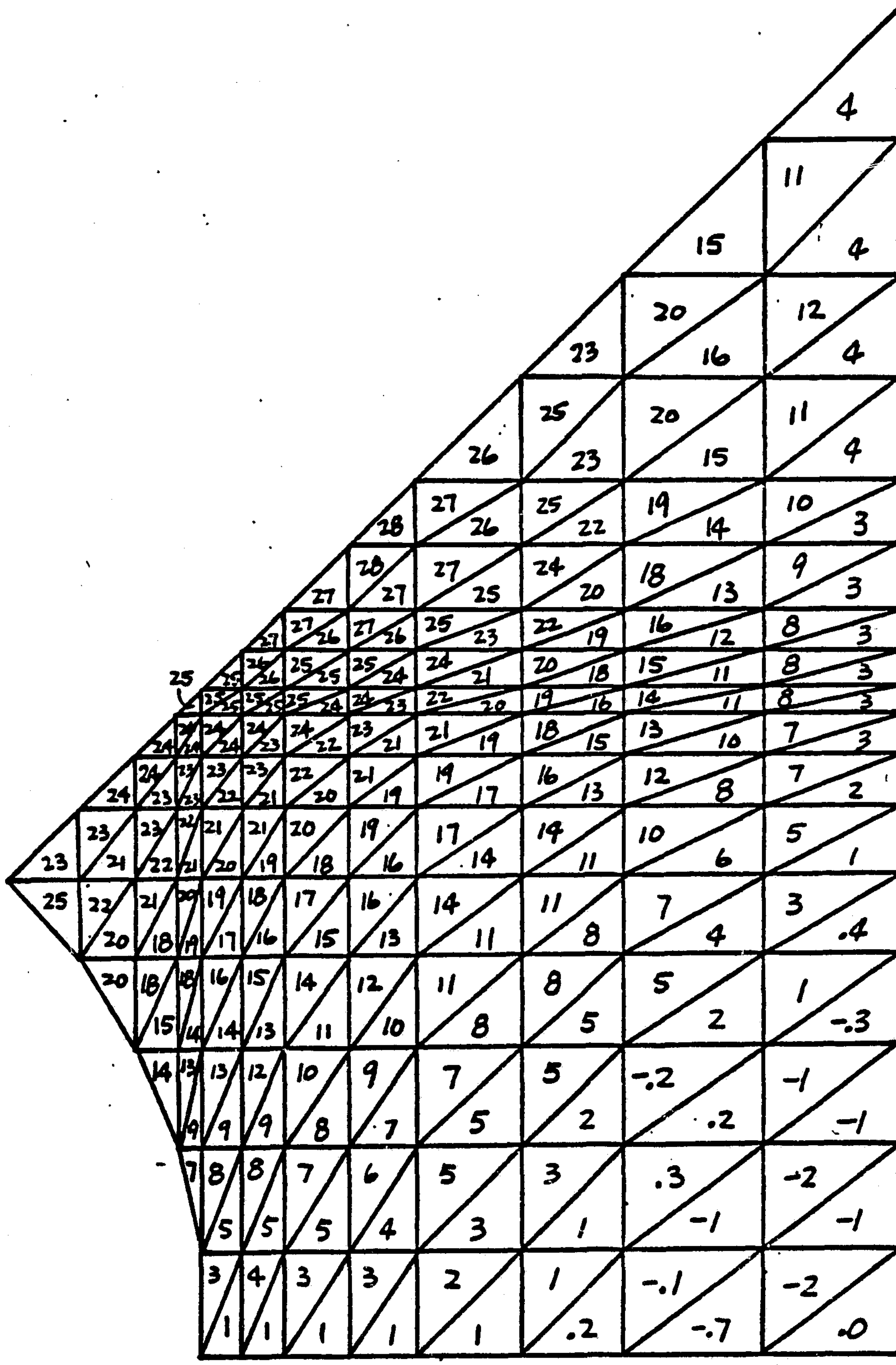

Figure 4-17c Distribution of Stresses τ_{xy} in a Perforated Square Plate with Clamped Edges

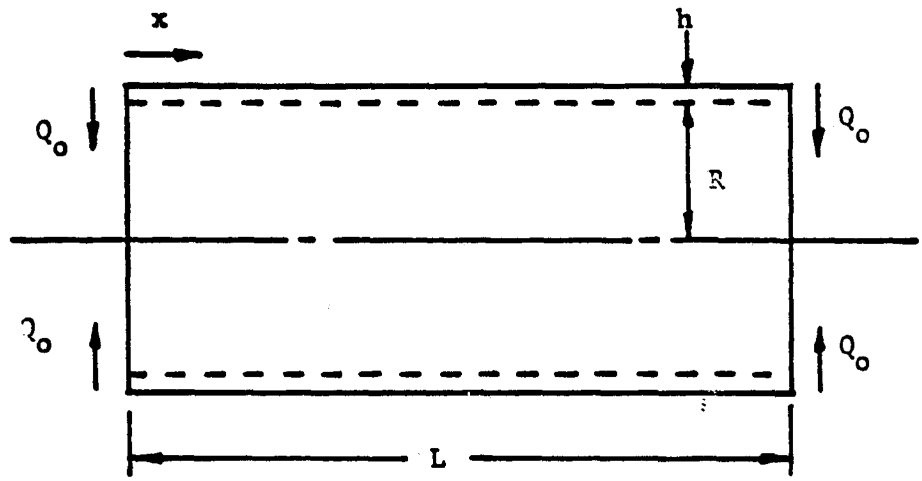

Figure 4-18 Cylindrical Shell Under End Load

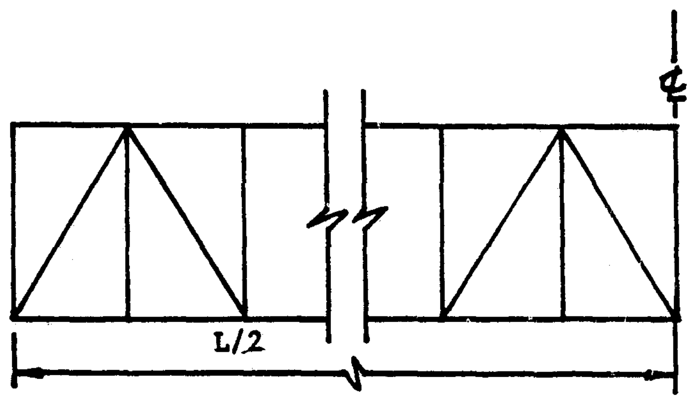

Figure 4-19 Finite Element Model for Cylindrical Shell Under End Load

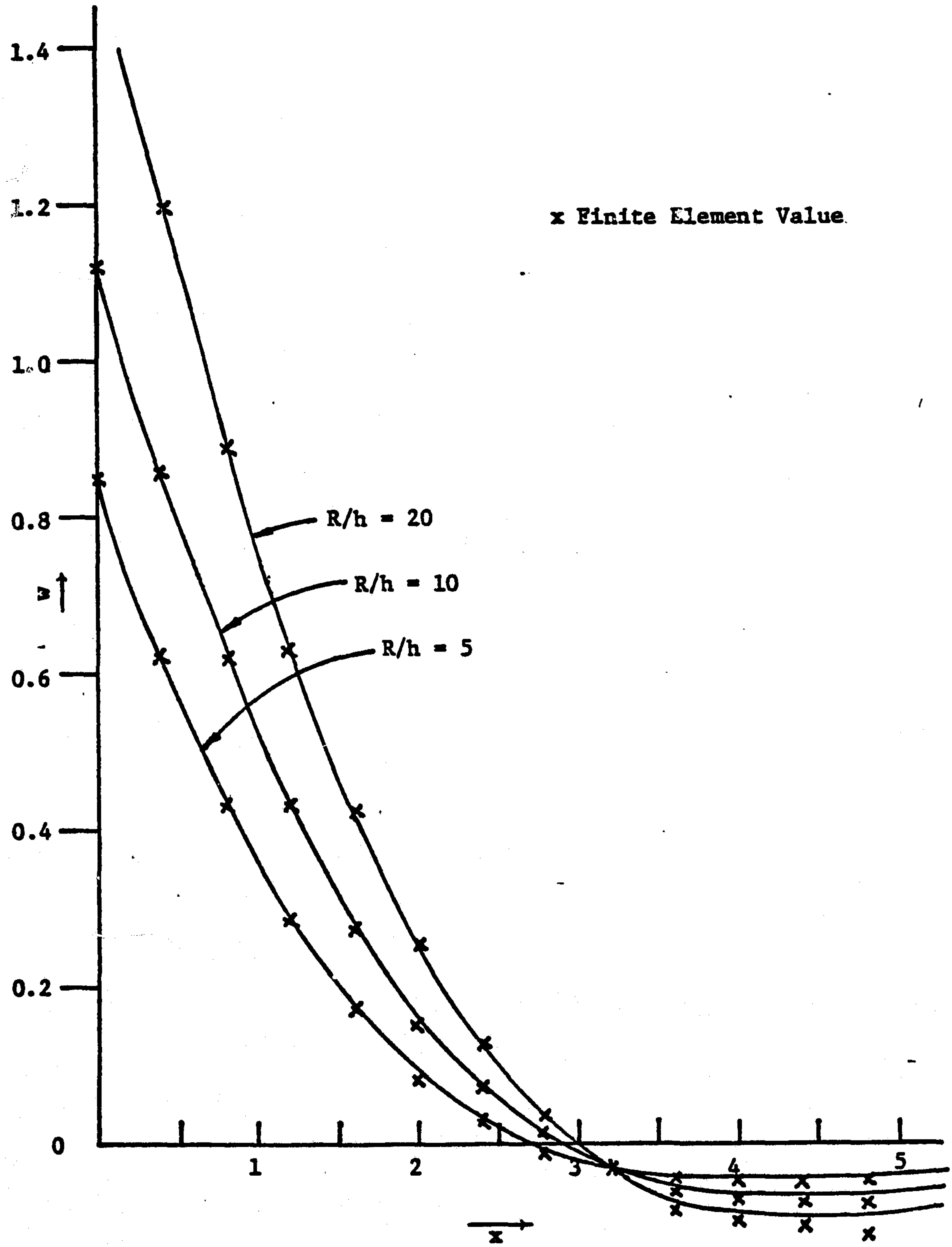

Figure 4-20a Convergence Rate of Finite Element Solution for End Displacement

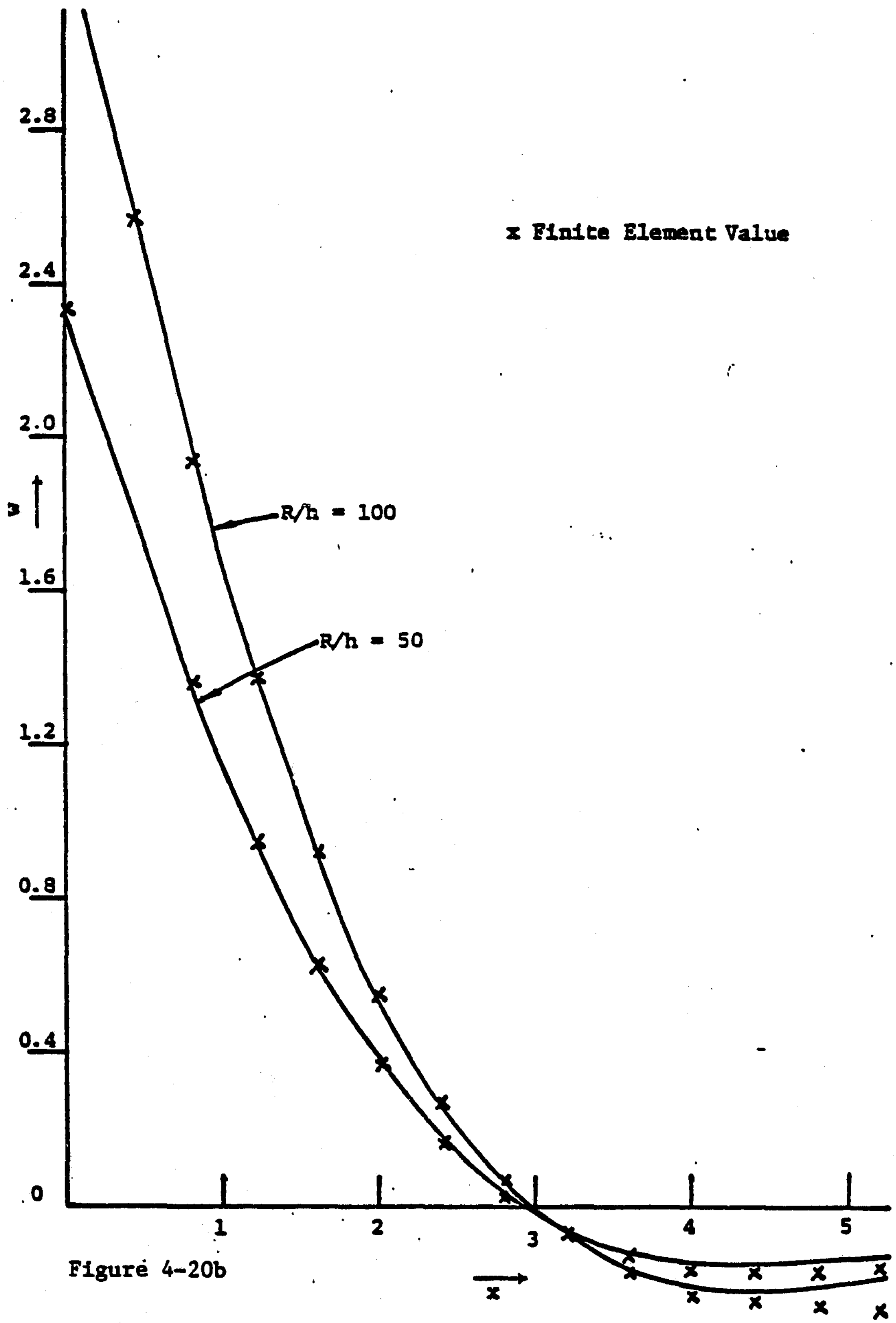

Figure 4-20b

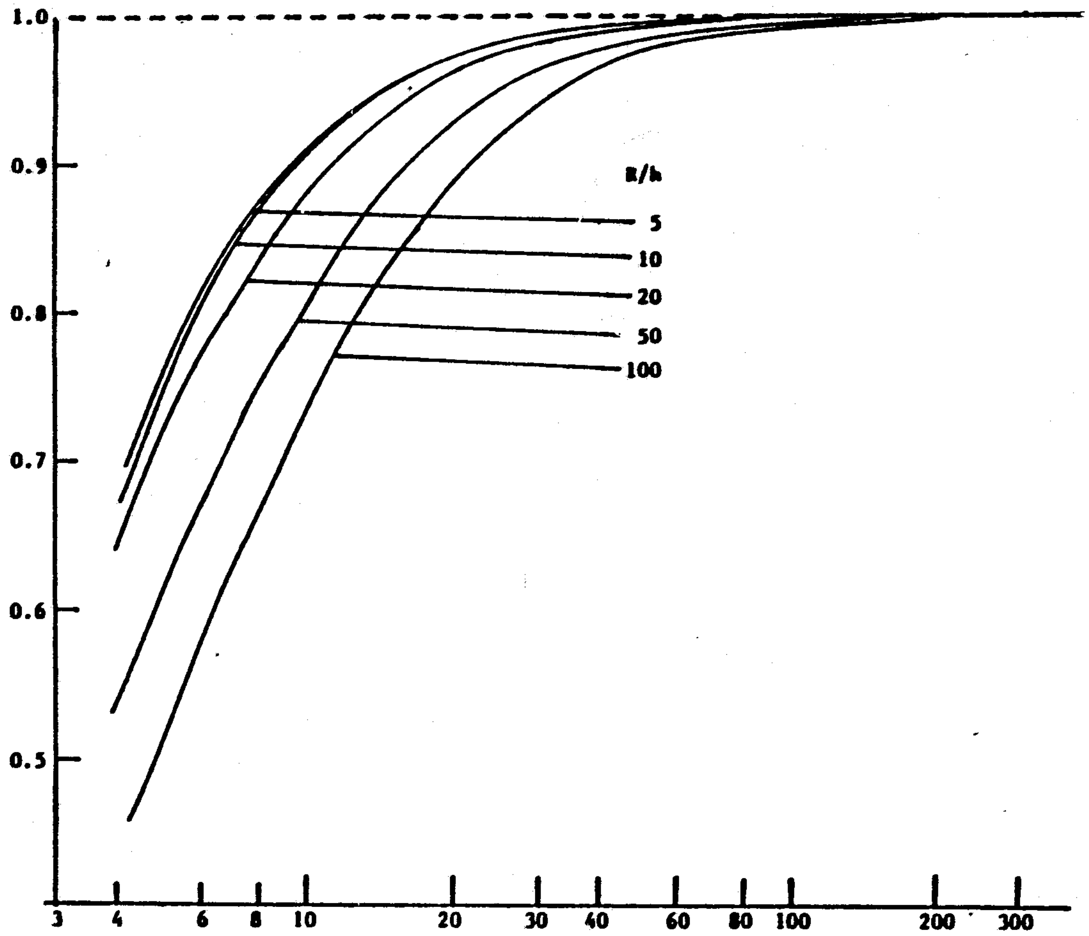

Figure 4-21 Comparison of Finite Element and Analytic Values of Radical Displacement

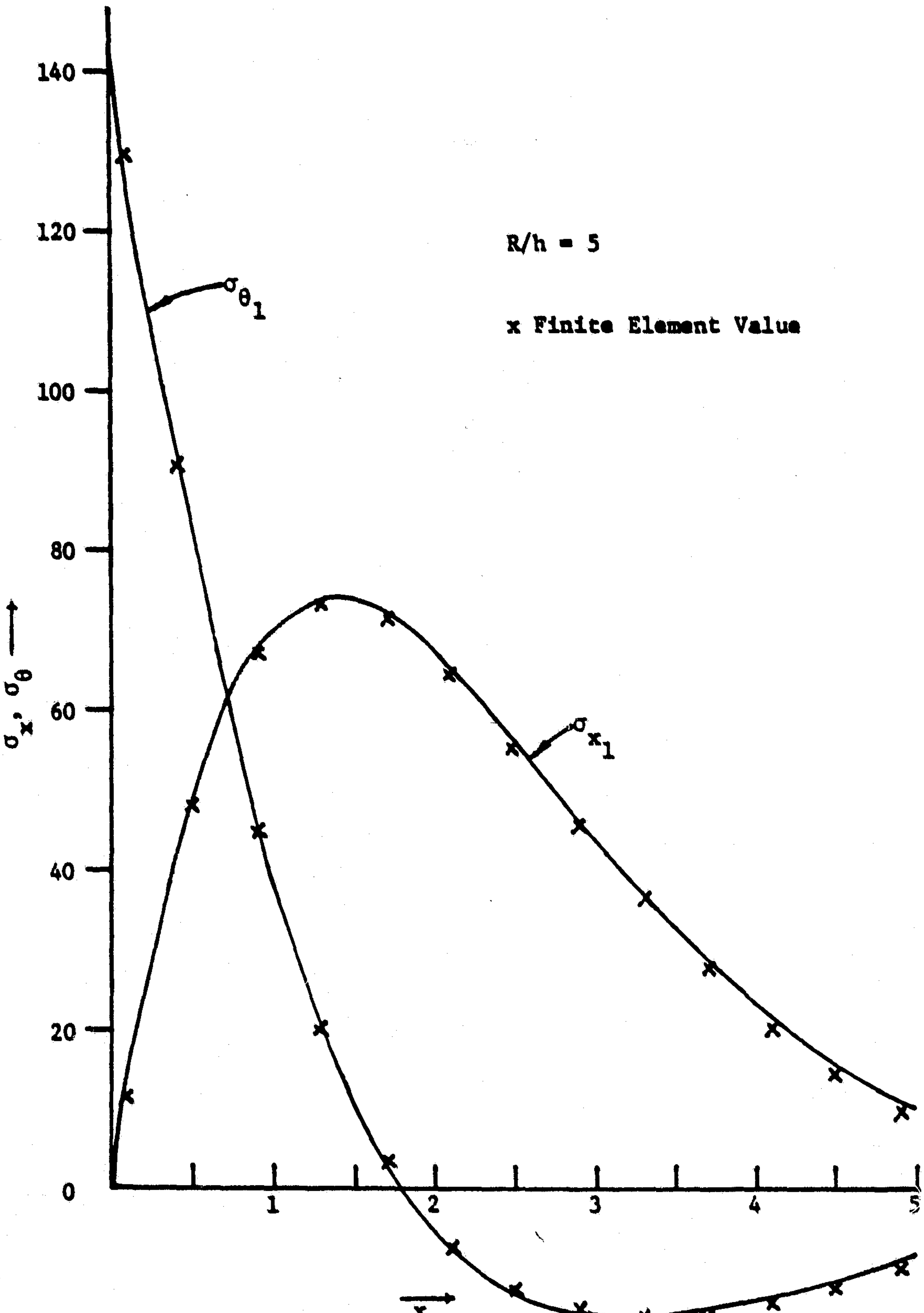

Figure 4-22a Comparison of Finite Element and Analytic Stress Distribution for a shell with R/h = 5. Top Surface

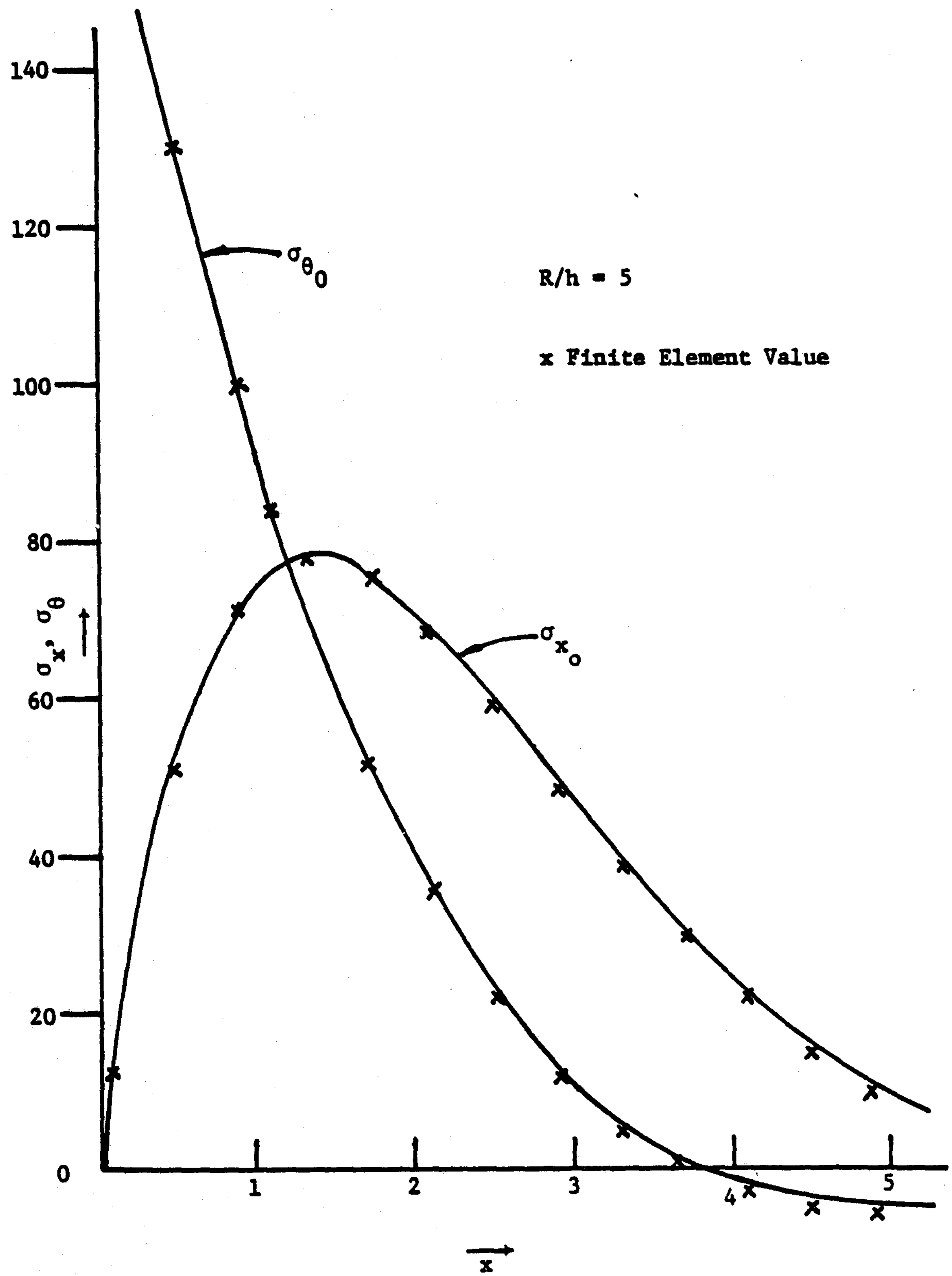

Figure 4-22b Comparison of Fintie Element and Analytic Stress Distribution for a Shell with R/h = 5. Bottom Surface

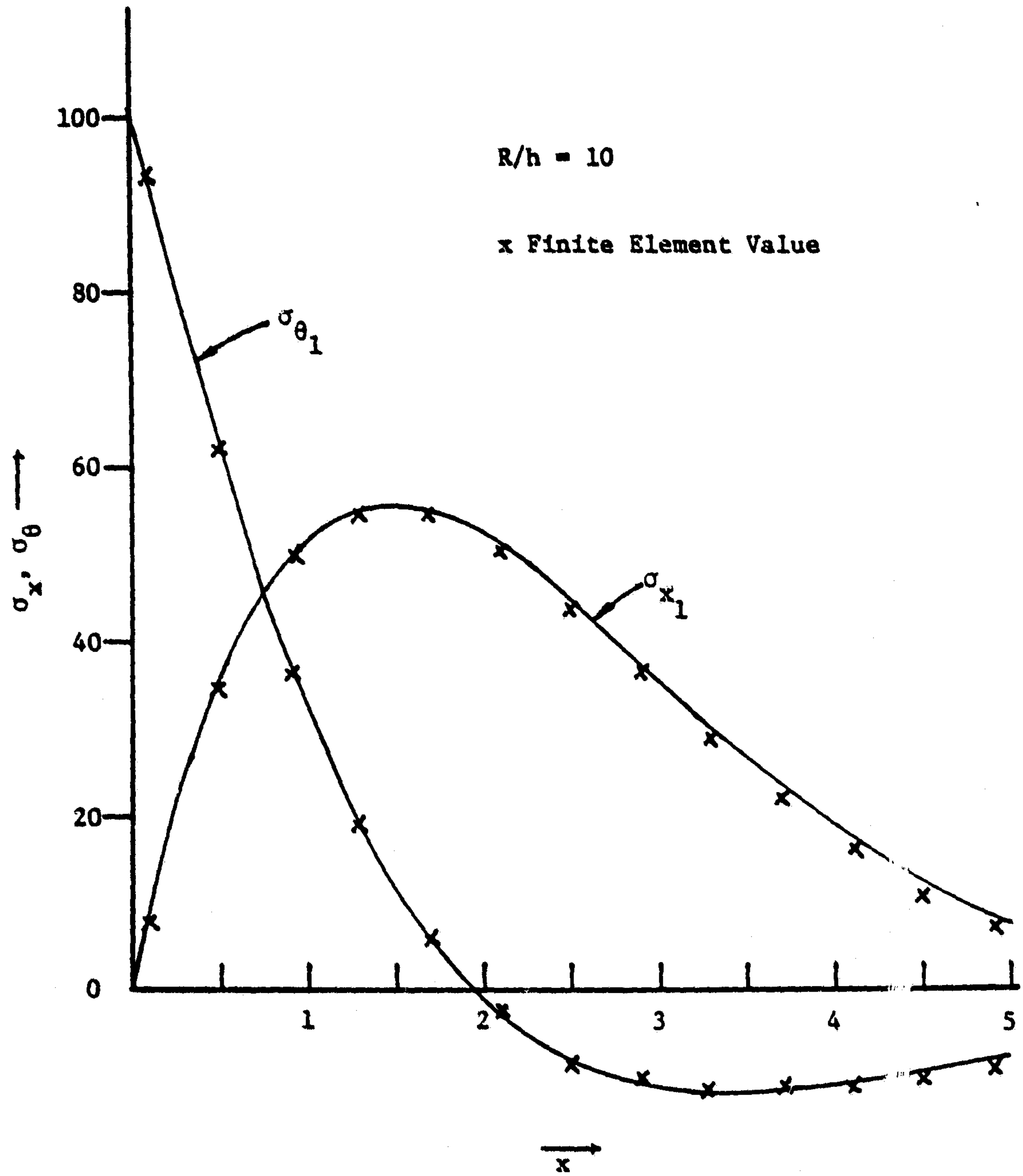

Figure 4-23a Comparison of Finite Element and Analytic Stress Distribution for a Shell with R/h= 10 Top Surface

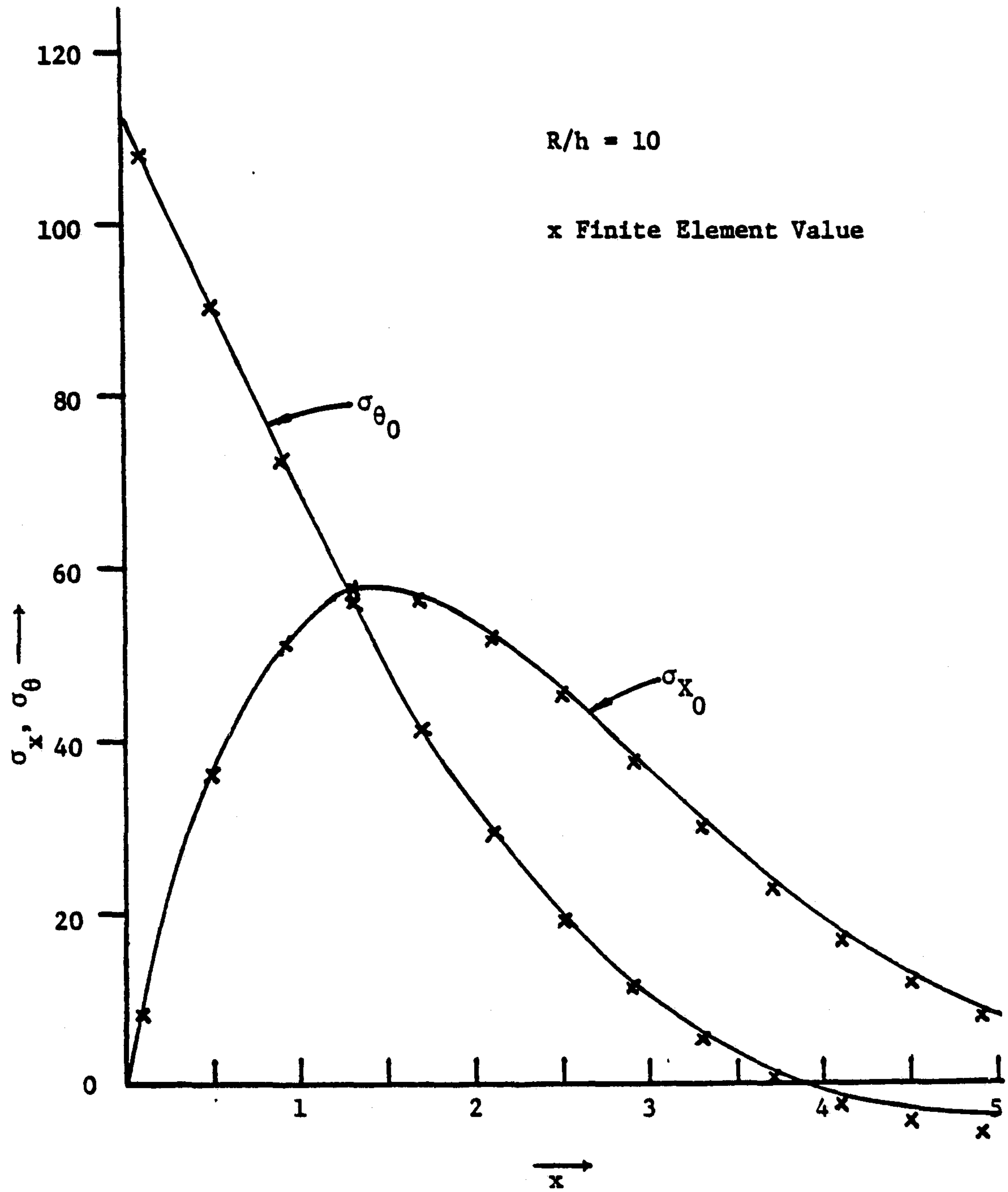

Figure 4-23b Comparison of Finite Element and Analytic Stress Distribution for a Shell with R/h=10 Bottom Surface

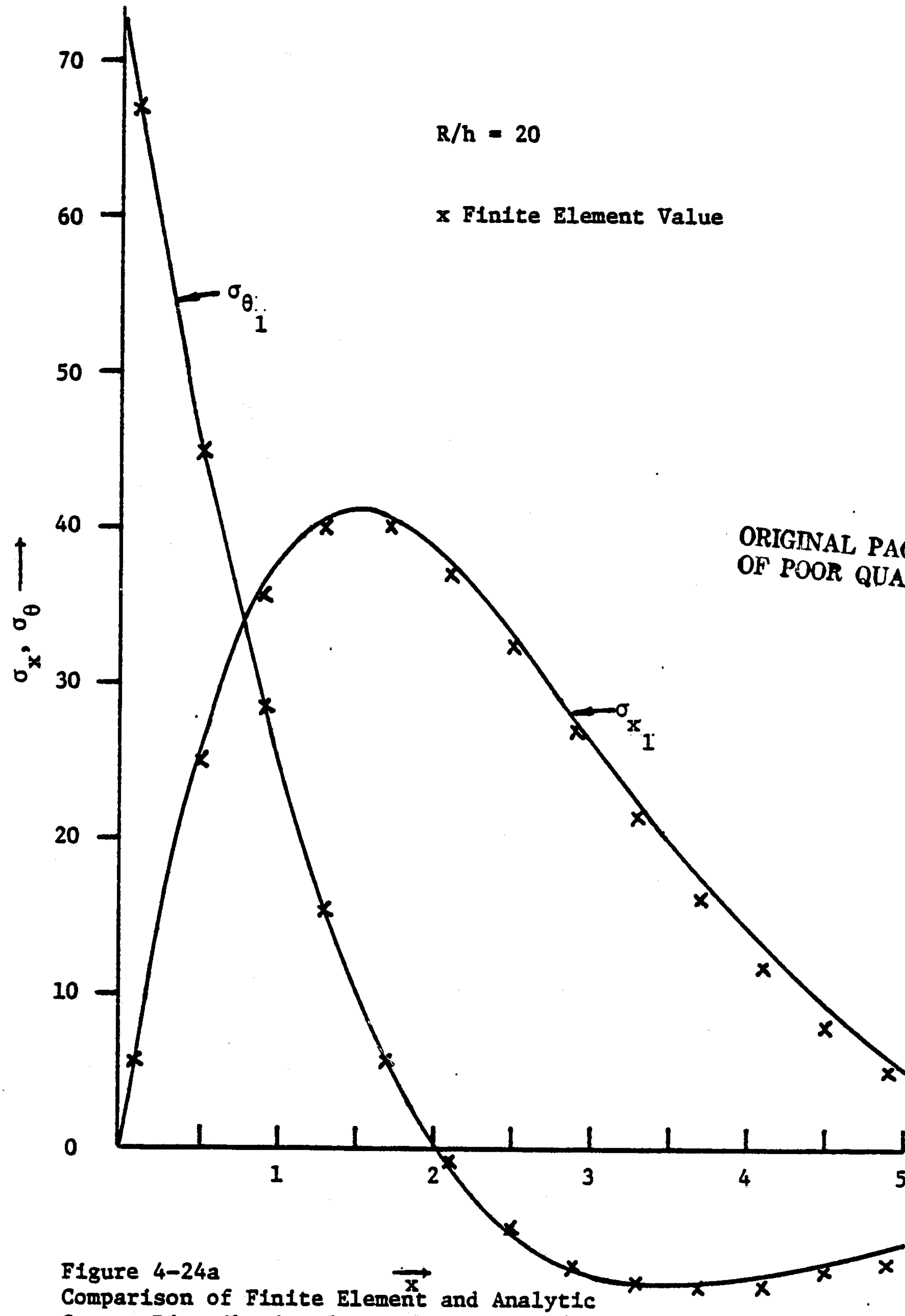

ORIGINAL PAGE IS OF POOR QUALITY

Figure 4-24a
Comparison of Finite Element and Analytic Stress Distribution for a Shell with R/h=20. Top Surface

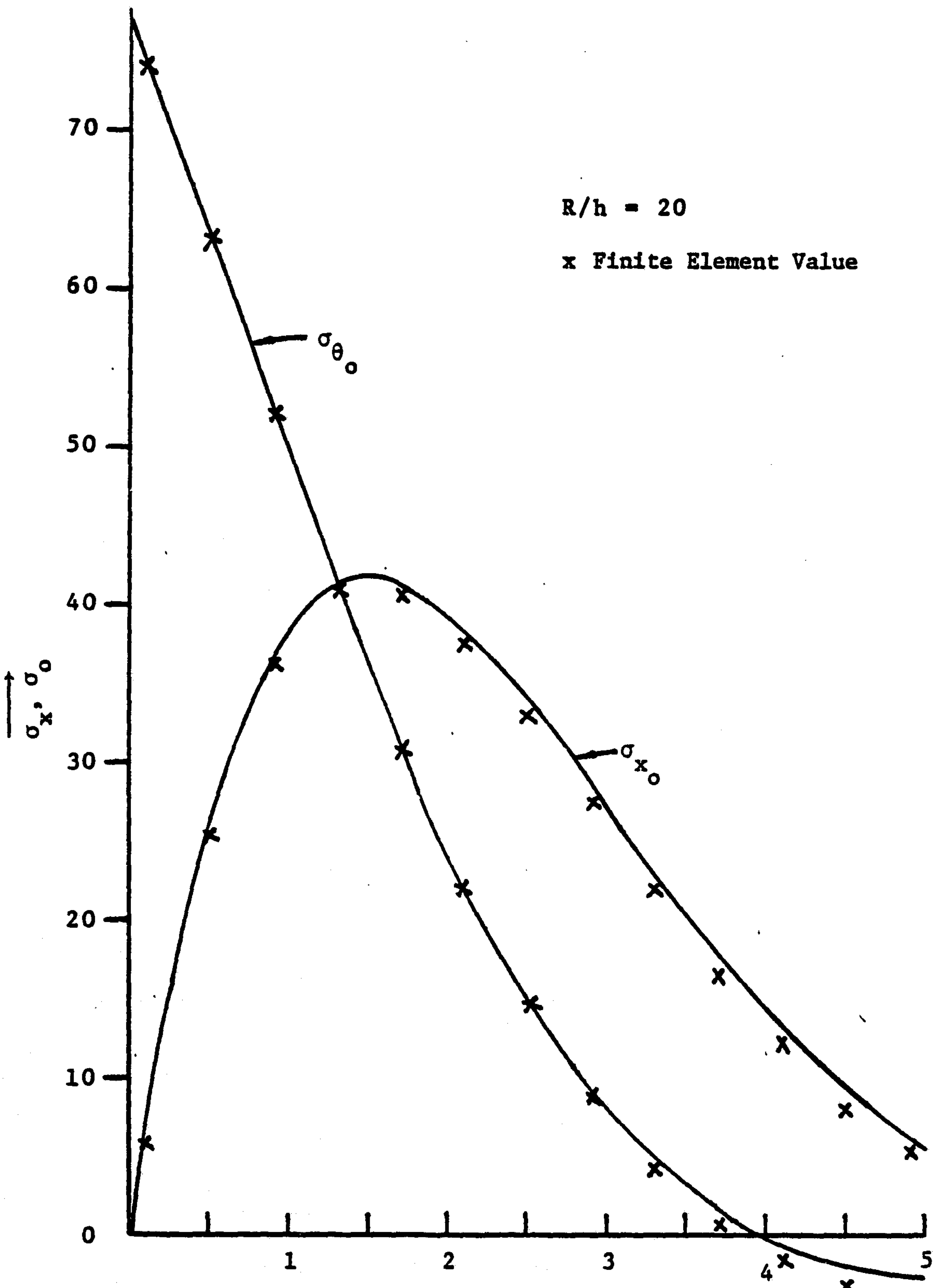

Figure 4-24b Comparison of Finite Element and Analytic Stress Distribution for a Shell with R/h=20. Bottom Surface

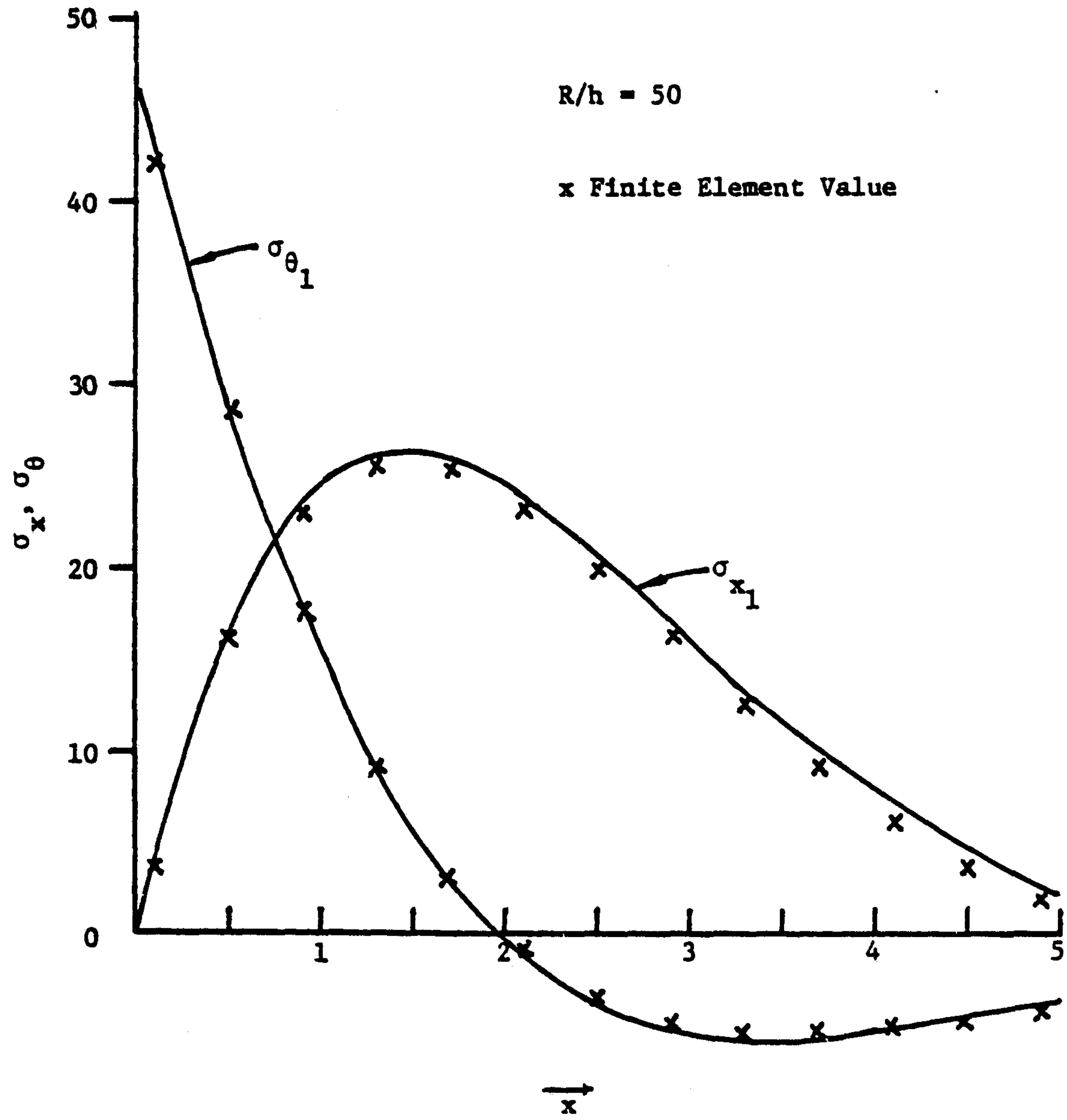

Figure 4-25a Comparison of Finite Element and Analytic Stress Distribution for a Shell with R/h=50. Top Surface

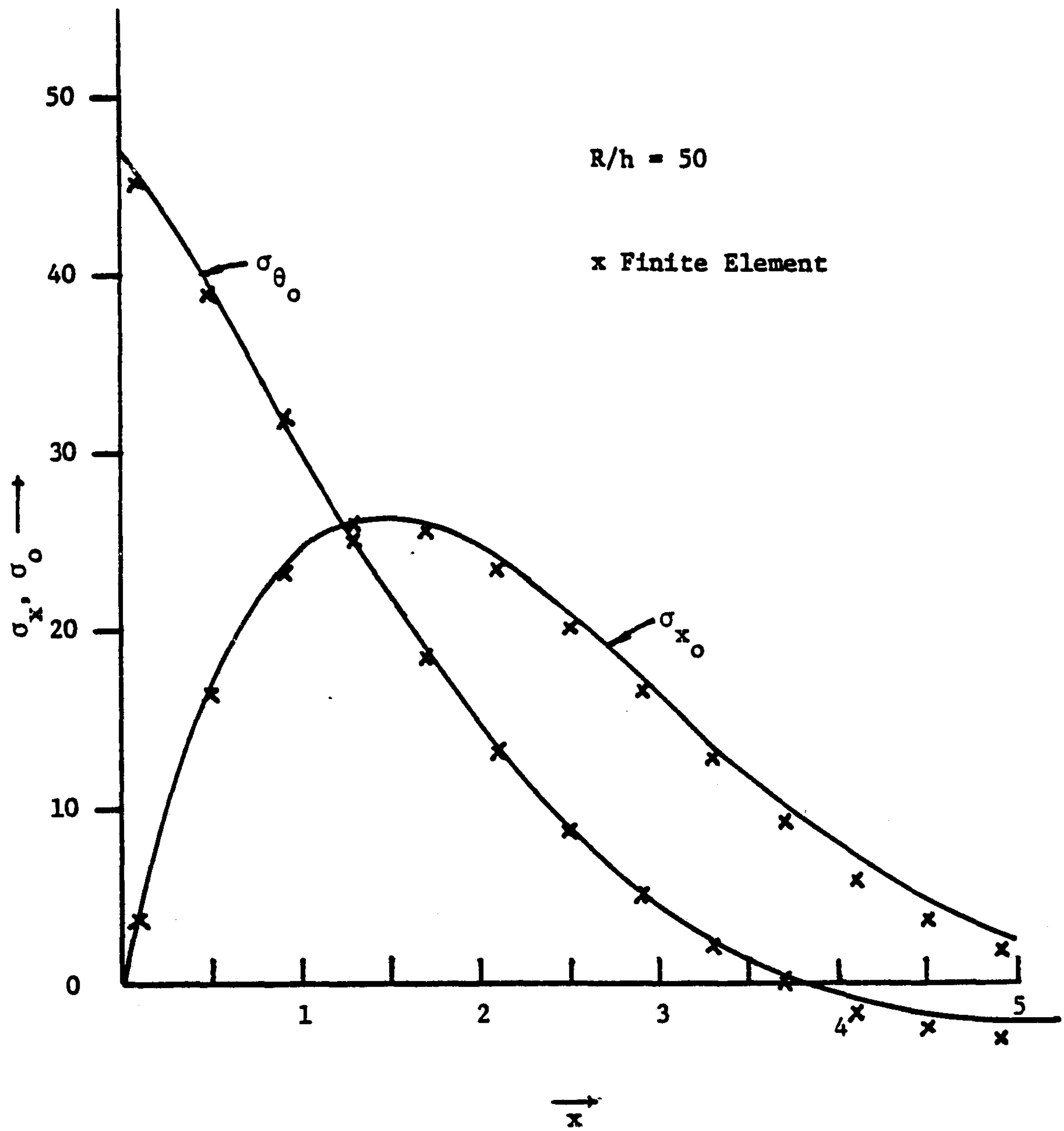

Figure 4-25b Comparison of Finite Element and Analytic Stress Distribution for a Shell with R/h=50 Bottom Surface

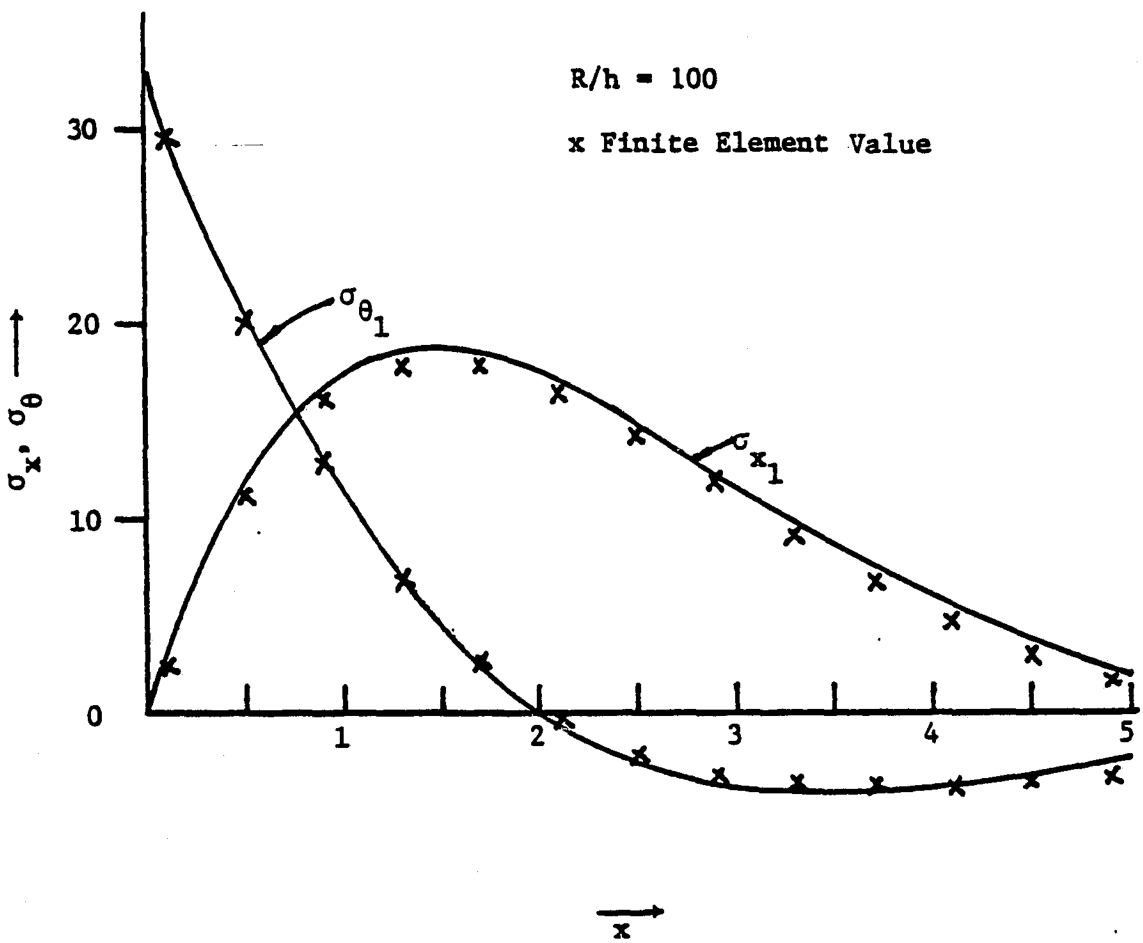

Figure 4-26a Comparison of Finite Element and Analytic Stress Distribution for a Shell with R/h=100 Top Surface

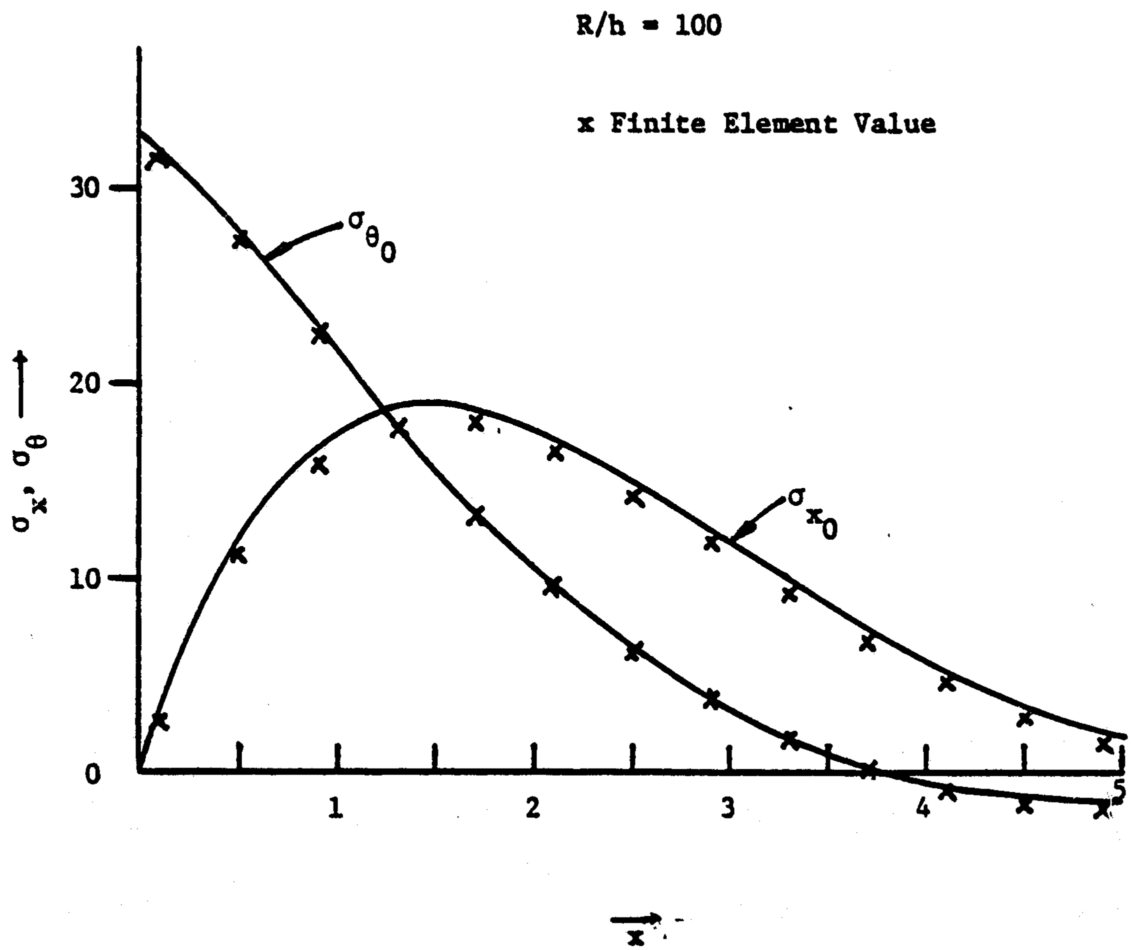

Figure 4-26b Comparison of Finite Element and Analytic Stress Distribution for a Shell with R/h=100 Bottom Surface

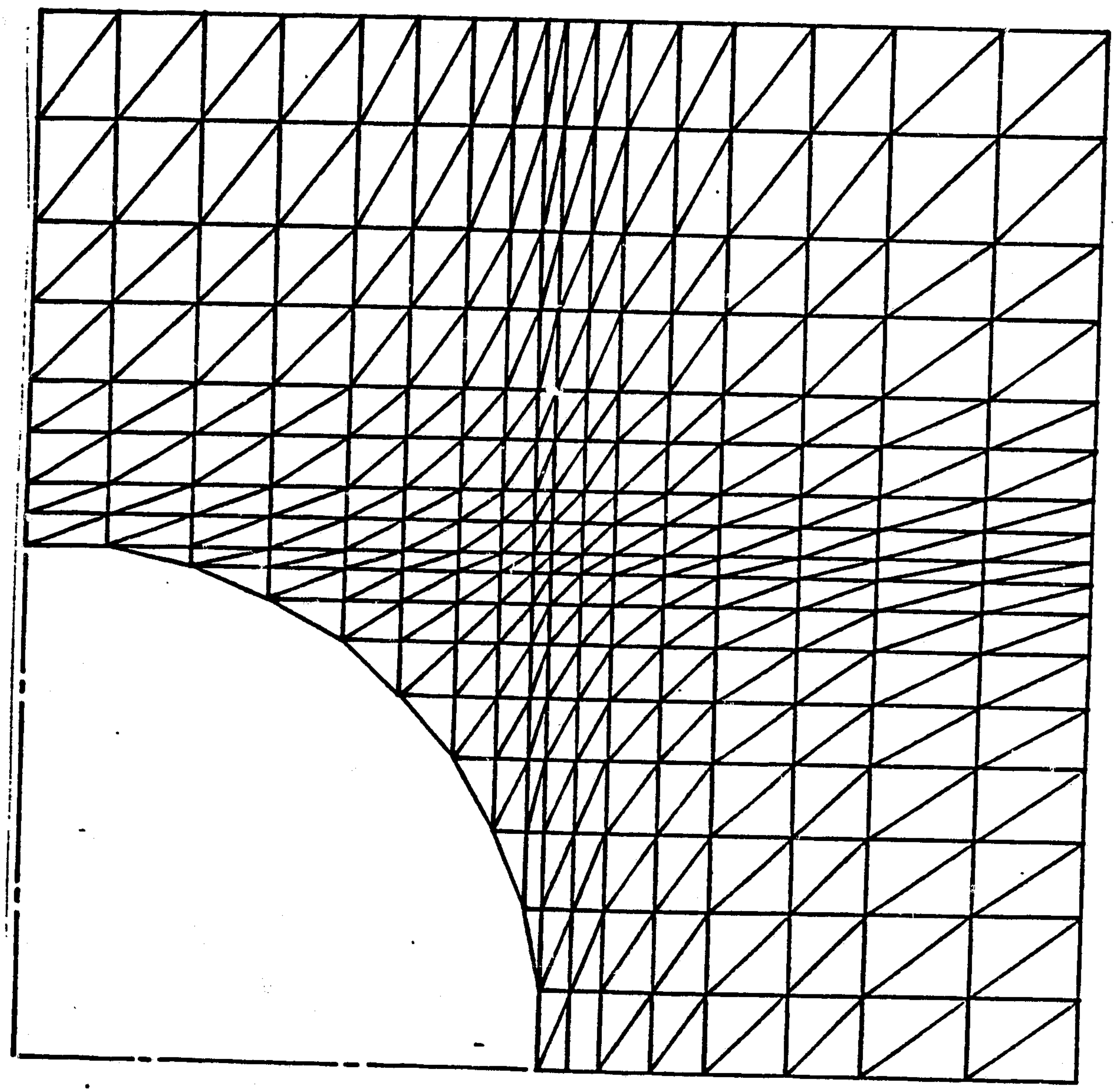

Figure 4-27 Finite Element Model for Curved Plate With a Circular Hole

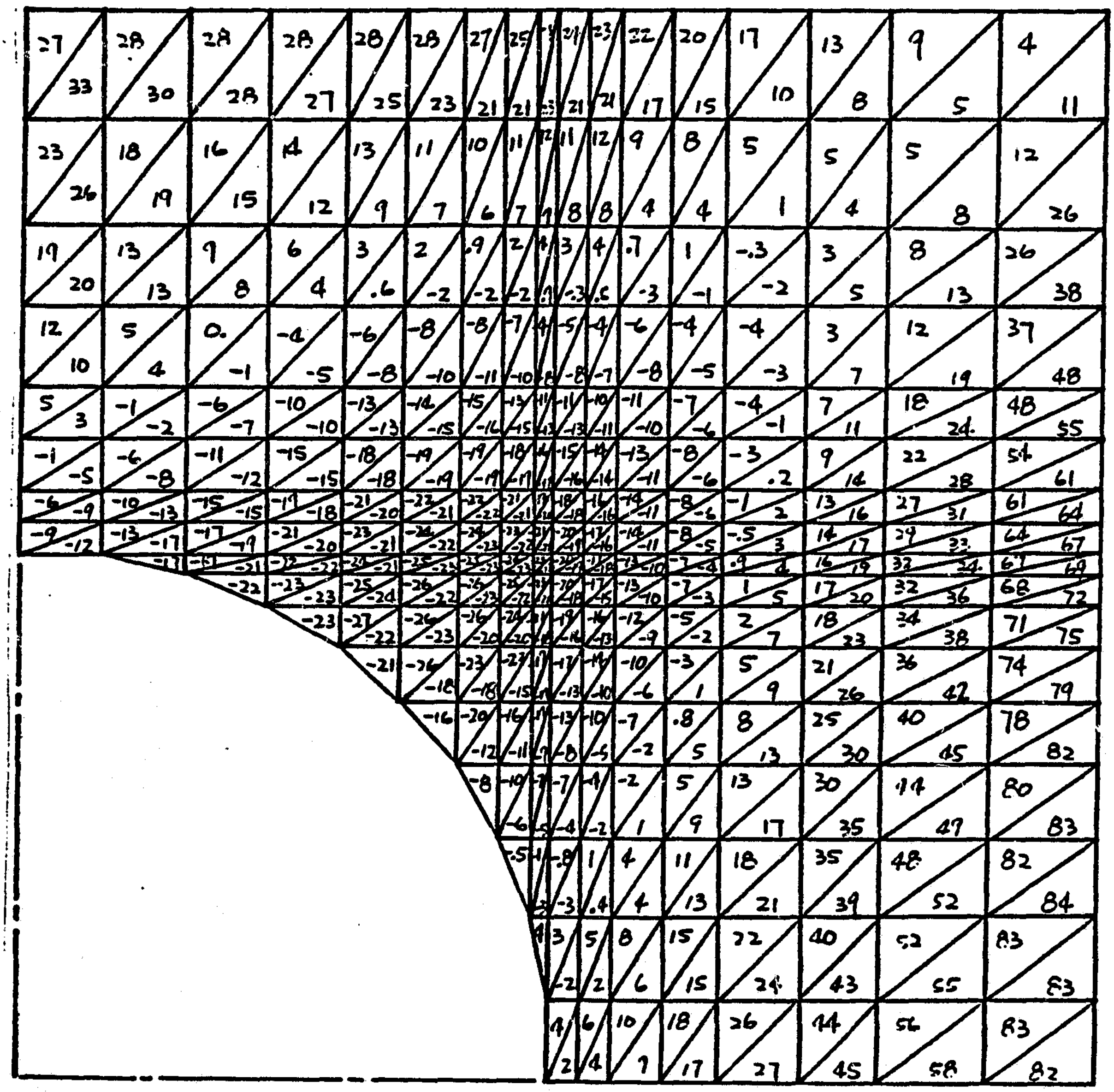

Figure 4-28a Inner Stress σ_{α_o} for Curved Plate with a Circular Hole

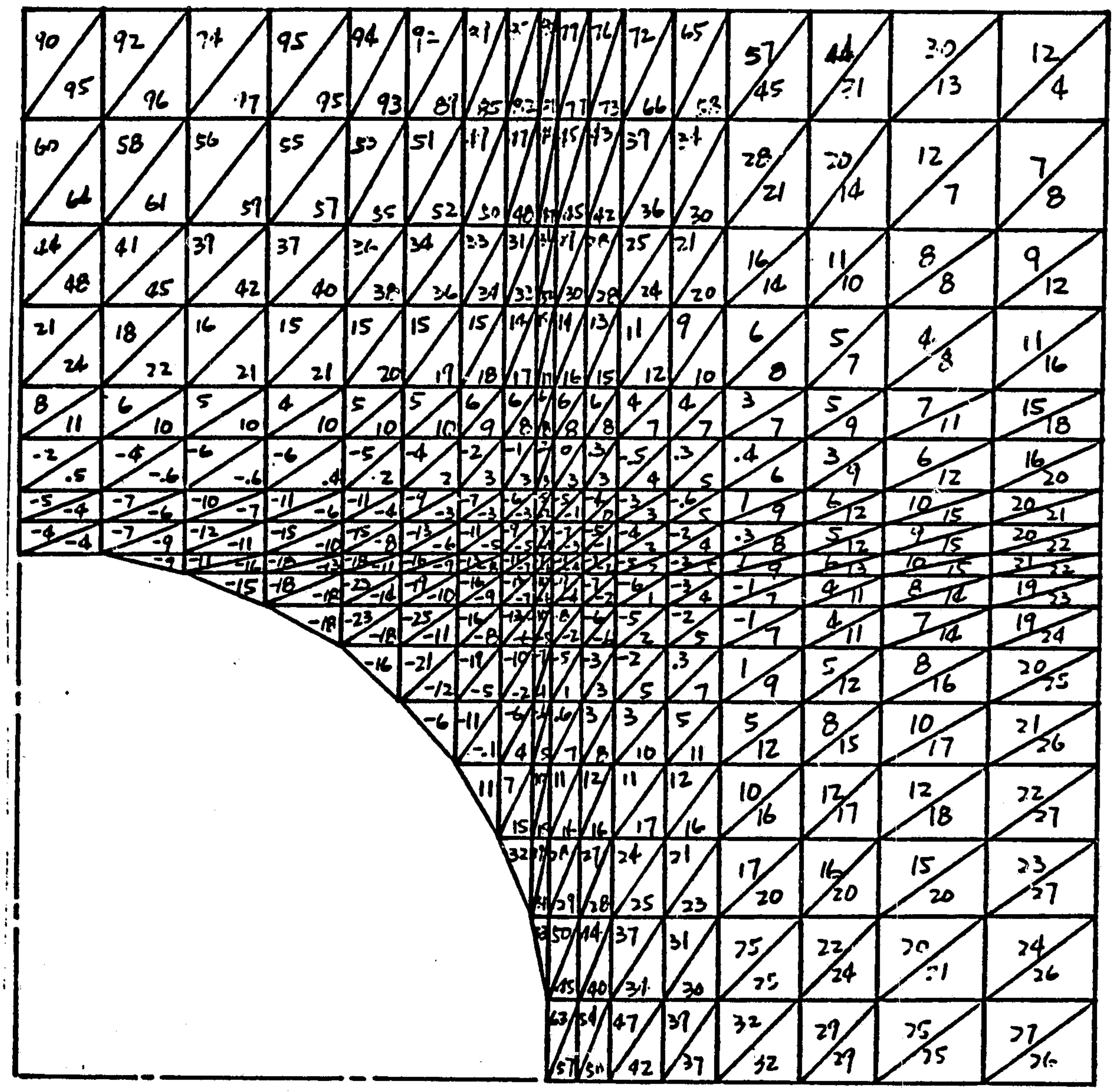

Figure 4-28b Inner Stress σ_{β_o} Distribution for Curved Plate with a Circular Hole

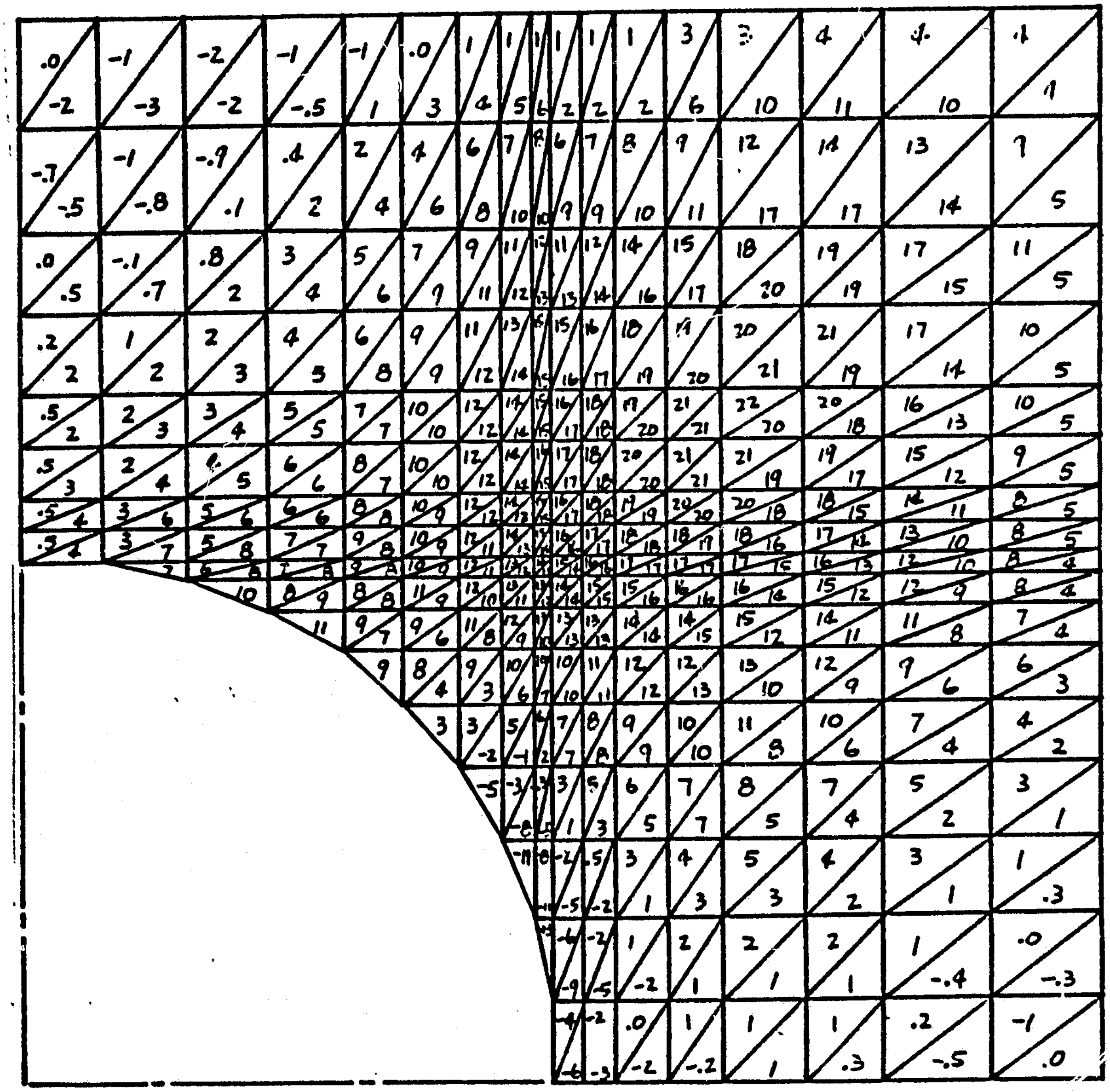

Figure 4-28c Inner Stress $\tau_{\alpha\beta_o}$ Distribution for Curved Plate with a Circular Hole

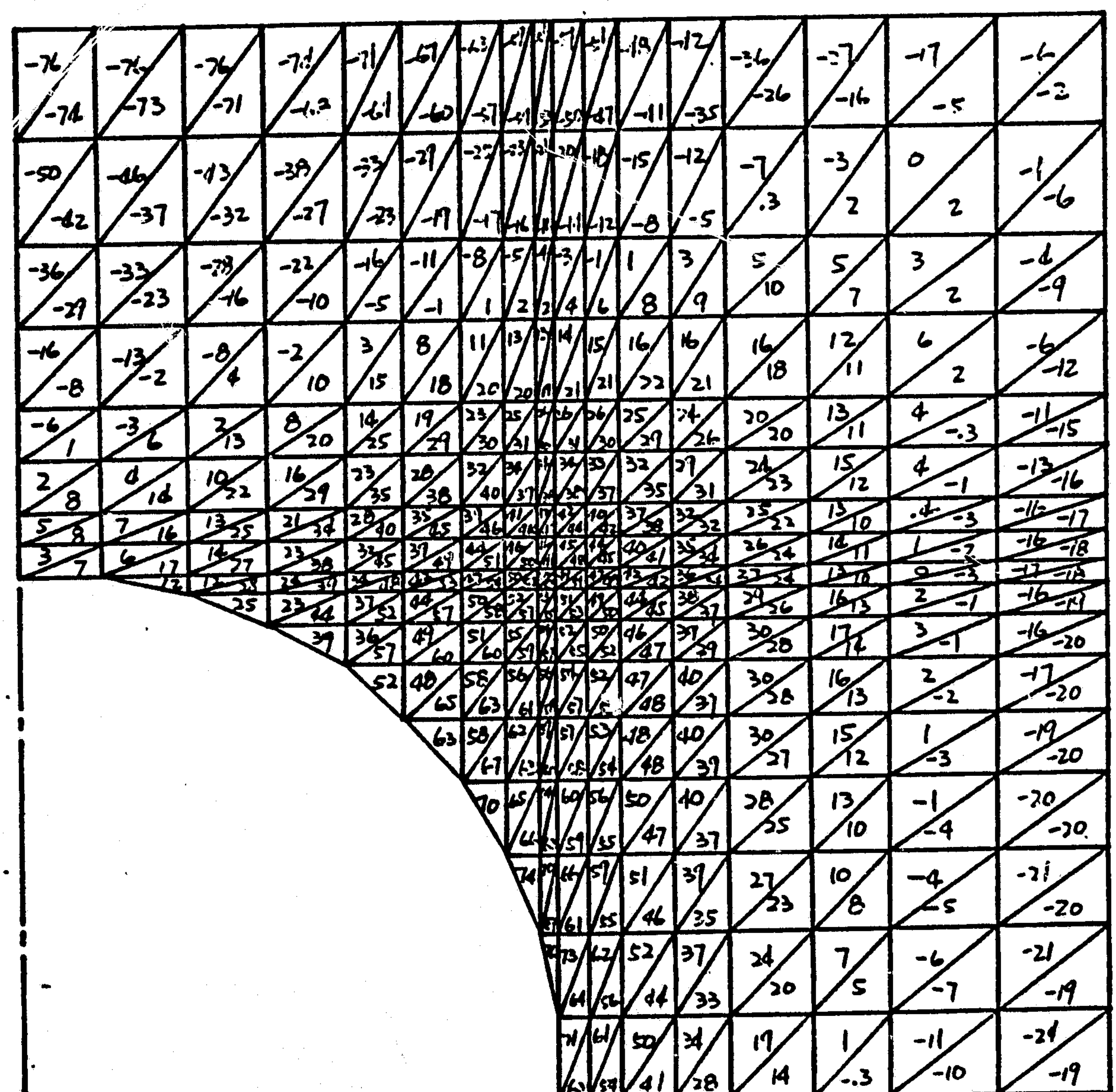

Figure 4-29a Outer Stress σ_{α_1} Distribution for Curved Plate with a Circular Hole

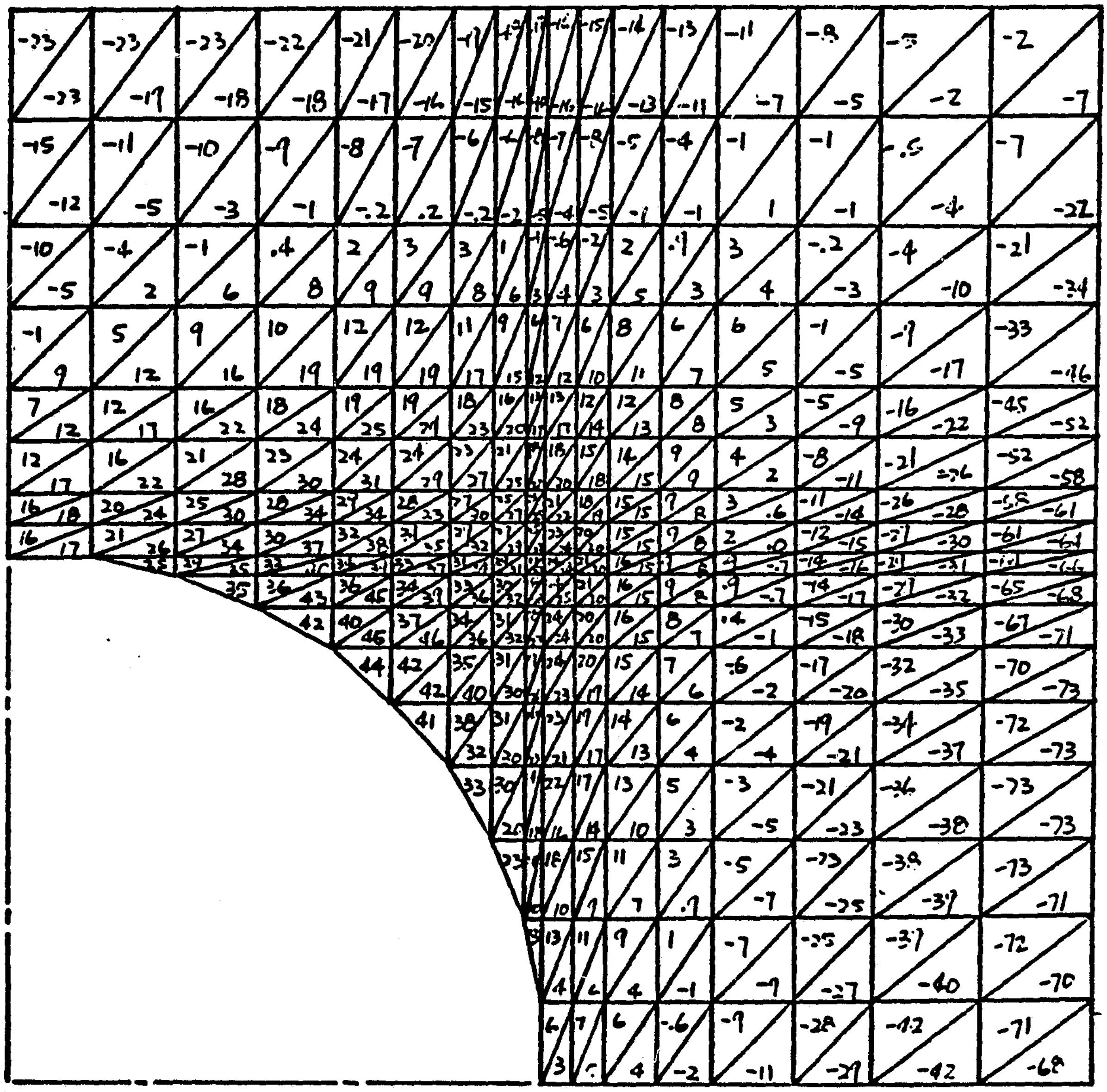

Figure 4-29b Outer Stress σ_{β_1} Distribution for Curved Plate with a Circular Hole

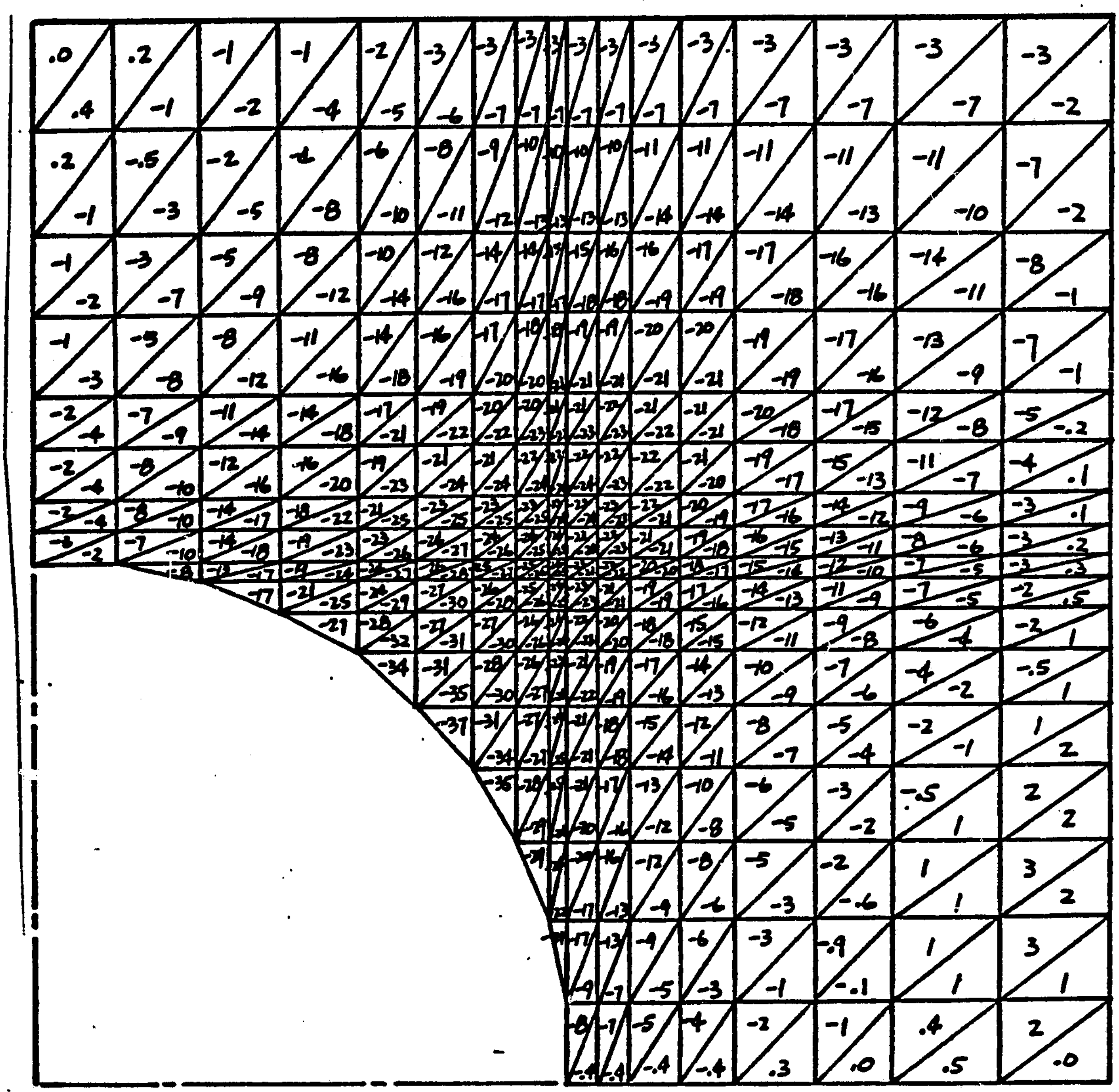

Figure 4-29c Outer Stress $\tau_{\alpha\beta_1}$ Distribution for Curved Plate with a Circular Hole

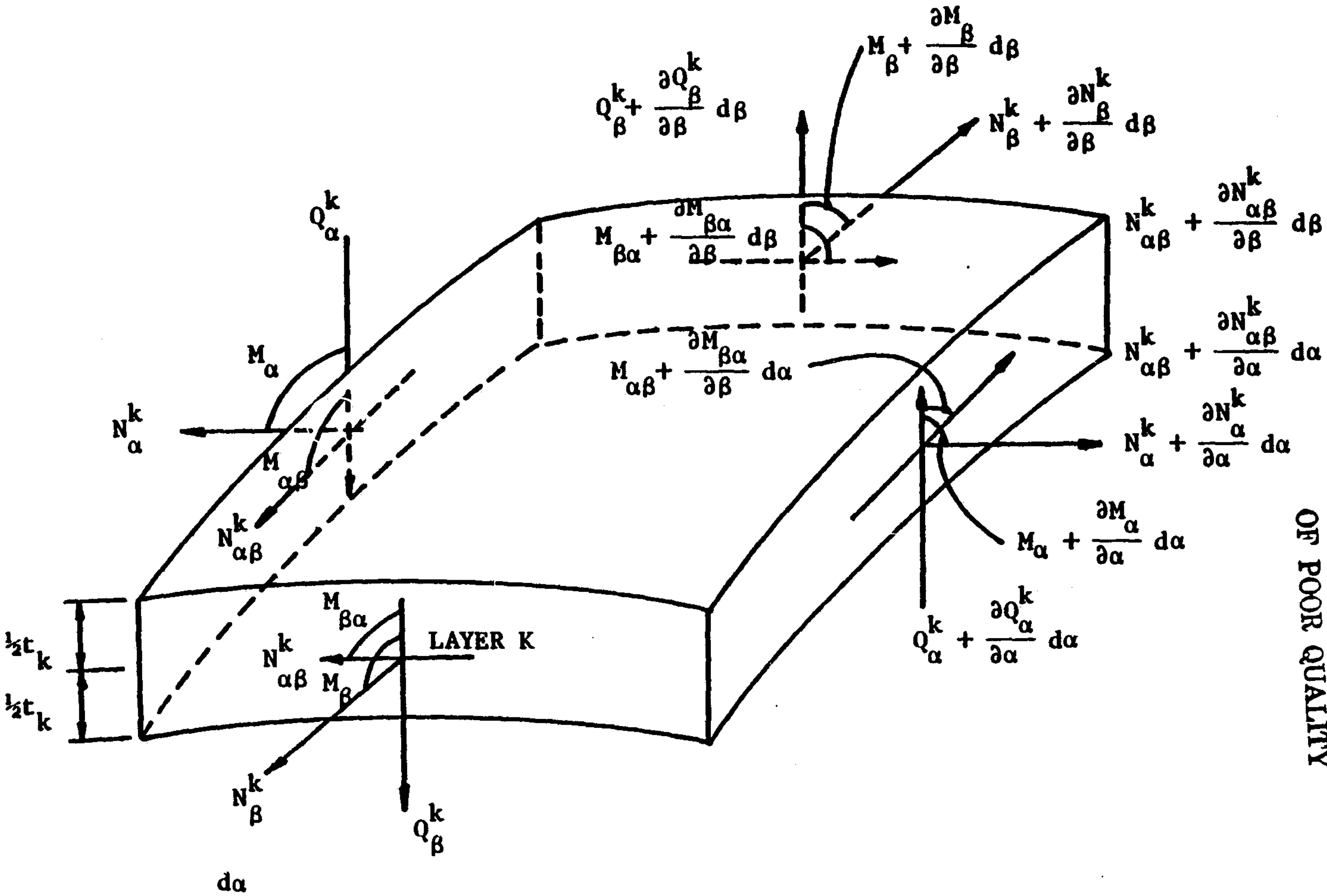

Figure D-1a Shell Element Loaded by Shear, Normal Stresses and Force, Moment Stress Resultants

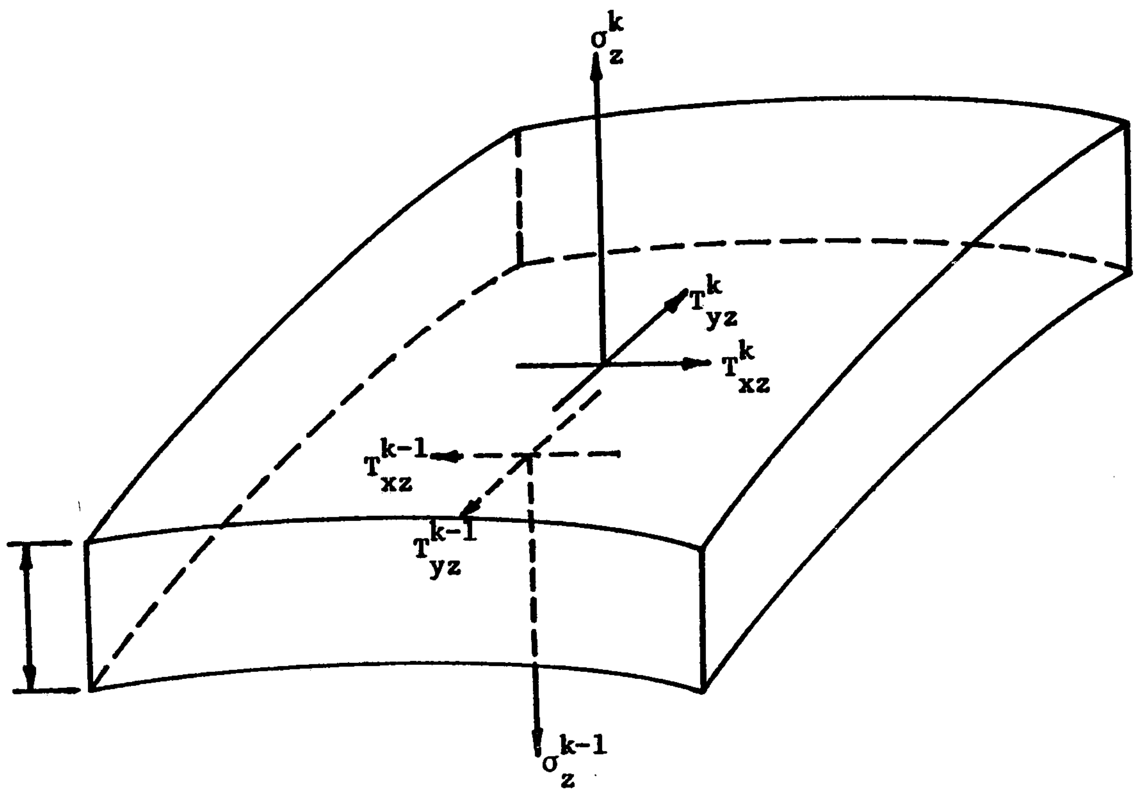

Figure D-1b Shell Element Loaded by Shear, Normal Stresses and Force, Moment Stress Resultants